B-1

Duplicate

research report

SC-4239(TR)
RESEARCH & DEVELOPMENT
M-3679 (Ed. 22) AEC Category
EFFECTS OF ATOMIC WEAPONS

BLAST LOADING OF STRUCTURES IN THE REGULAR REFLECTION AND LOW MACH-STEM REGIONS

J. P. Murtha - 5112

February 1959

Sandia Corporation
CONTRACTORS FOR U.S. ATOMIC ENERGY COMMISSION

LEGAL NOTICE

Printed in USA. Price ~~$2.25~~. Available from the Office of Technical Services, Department of Commerce, Washington 25, D. C.

SC-4239(TR)
RESEARCH & DEVELOPMENT
M-3679 (Ed. 22) AEC Category
EFFECTS OF ATOMIC WEAPONS

BLAST LOADING OF STRUCTURES IN THE REGULAR REFLECTION AND LOW MACH-STEM REGIONS

J. P. Murtha - 5112

ABSTRACT

An investigation was made of the blast loading on model structures in the regular reflection region and in the region where the height of the Mach stem varies from less than the structure height to several times the structure height. The three structure models employed were 2 x 2 feet in cross section, with lengths of 2, 4, and 18 feet. They were subjected to blast waves from 250-pound charges of TNT detonated at heights of 38, 64, and 90 feet above the surface. When scaled to nuclear burst, these conditions represent a 7-story building subjected to a 20-kt burst. They therefore constitute a situation involving multistory structures.

Variations from two-dimensional theory for predicting the pressure loading on the front surface were observed for small zenith angles while variation on the top surface was observed at large zenith angles. Shortening of the positive-pressure duration on the front surface was found to occur in the regular reflection and low Mach-stem regions. The measured times of occurrence for maximum average pressure on the rear face of the 2- x 2- x 18-foot target are in good agreement with times predicted.

ACKNOWLEDGMENT

It is difficult for the author to acknowledge all of the persons who contributed to this study. This results not only from the large number of persons involved but also from the lapse of several years since the project began. However the association of some persons with this project cannot go unmentioned. The project was originally planned by Mr. L. J. Vortman and he has guided it throughout its course. The field work was carried out by the Coyote Canyon Section under the direction of Mr. D. G. Palmer, and the many calculations necessary were performed principally by Miss Dorothy Delap and Mrs. Kay Walker. Finally, many fruitful conversations with Dr. J. D. Shreve and Dr. M. L. Merritt must be acknowledged.

TABLE OF CONTENTS

LIST OF ILLUSTRATIONS

LIST OF ILLUSTRATIONS (Cont)

LIST OF ILLUSTRATIONS (Cont)

LIST OF TABLES

LIST OF SYMBOLS

α	Zenith angle
α_A	Apparent zenith angles as determined from the space-time-of-arrival data
β	Ground baffle separation angle
D	Horizontal distance from ground zero to the target front face
h	Height of target (2.0 feet in all cases)
h_m	Height of Mach stem-target interception
H or HOB	Height of burst
L	Target length
LM	Low Mach stem $\left(\frac{h_m}{h} < 1\right)$
P_o	Ambient pressure
p	Shock overpressure reflected at the ground as measured by gauge in a ground baffle
p_m	Peak shock overpressure reflected at the ground as measured by gauge in a ground baffle
p_i	Incident shock overpressure before arrival at ground plane
p_{im}	Peak incident shock overpressure before arrival at ground plane
t_+	Duration of positive phase of the incident wave
p_1	Average pressure on front surface at time equal to t_1
t_1	Front-surface transit time of the incident wave
p_2	Maximum average pressure on front face
t_2	Assumed time at which maximum average pressure occurs on the front target surface ($t_2 = 2t_1$)

t_{fm}	Measured time from arrival of incident wave to maximum average pressure on the front face as determined from the average pressure time plots
p_4	Average pressure on top surface at t_4
t_4	Transit time of incident wave across top surface
p_b	Maximum average pressure on back surface
t_b	Time from arrival of incident wave at back face until p_b occurs
t_f	Duration of positive pressure on front surface
t_r	Duration of positive pressure on back surface
U	Velocity of incident shock wave
W	Weight of the TNT charge in pounds
I_f	Front-surface positive phase total impulse
I_t	Top-surface positive phase total impulse
I_b	Back-surface positive phase total impulse
ξ	$\frac{p_{im} + P_o}{P_o}$

CH I -- INTRODUCTION

Objective

Most experimental work on the blast loading of structures has been done in the region of Mach reflection. It has usually been assumed that the shock front which strikes a target structure consists of a single shock front, that it is essentially plane in the region of the structure, that the shock front approaches the target as a vertical front, and that the height of the Mach stem is at least twice the height of the target structure. These conditions exist for low heights of burst throughout the regions of heavy, moderate, and light damage, but only throughout the region of light damage for high heights of burst. There is reason to suspect that most structures resist blast pressures within the region of regular reflection better than corresponding pressure levels in the region of Mach reflection.[1] Therefore, a need exists for detailed knowledge of blast loading on target structures within the region of regular reflection. The object of this experiment was to contribute to that knowledge and, in addition, learn more of loading in the region where the height of the Mach stem is close to the height of the structure.

Armour Research Foundation has developed a method of predicting blast loading on the various surfaces of two-dimensional solid targets in the region of regular reflection[2] and has conducted shock tube investigations to compare results obtained by the prediction method with the average pressure-time pressure loading observed on various target surfaces.[3] Shock-tube observations were limited to the diffraction phase and angles of incidence (zenith angles) of 20 and 45 degrees with an incident shock strength $(\xi)^*$ of 1.33 were studied. The agreement between shock-tube observations and predictions was satisfactory, especially for the front surface.

---

* $\xi = \frac{P_{im} + P_o}{P_o}$

In later shock-tube investigations by Armour Research Foundation[4] 3- and 4-story two-dimensional models were studied at angles of incidence with the shock front of 20 and 0 degrees, respectively. The target models used in this test series were hollow blocks with simulated window openings, and were quite different from the models used in the test reported here. Therefore, the results of the two tests cannot be compared.

The zenith angle (α) is defined either as the angle between the path of the incident shock and a vertical line through the burst point, or the angle between the ground and a plane tangent to the incident shock front.

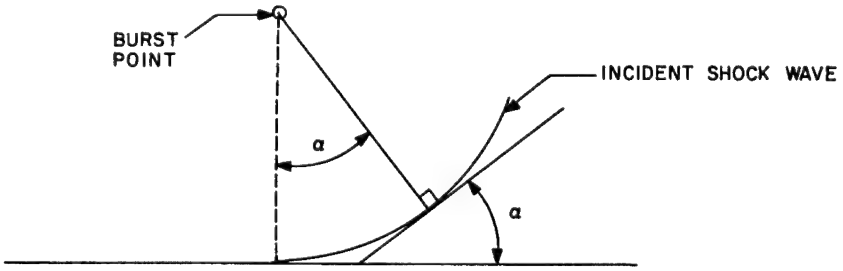

Scaling

In this experiment, spherical TNT charges weighing 250 pounds and target structures 2 feet high were used. Scaled to sea level, these are equivalent to about a 3-story structure for a 1-kt weapon or a 7-story building for a 20-kt weapon. No means were available for lifting charges larger than 250 pounds or higher than 100 feet, and the type of instrumentation used made it undesirable to use a smaller structure. It would have been more satisfactory to scale to a 1- to 3-story structure for a weapon of 20 kt or larger.

Hudson[5] has shown that, particularly in HE diffraction experiments, the positive pressure duration on the front wall of a structure can be less than that of the incident blast wave. He defines this shortening in terms of positive phase duration on the front of a structure divided by positive phase duration of the incident wave (t_f/t_+) and has calculated its relation to the spatial duration (Ut_+) of the incident wave and the height (h), or half-length (L/2) of the structure. Figure 1 shows a comparison of Hudson's calculations with experimental Mach region data. While the calculations assume that the wave strikes normal to the front of a wall, the effect of duration shortening is not expected to be greater for a structure located in the region of regular reflection and may be somewhat less. The range of Ut_+/h for these experiments is also given in Figure 1.

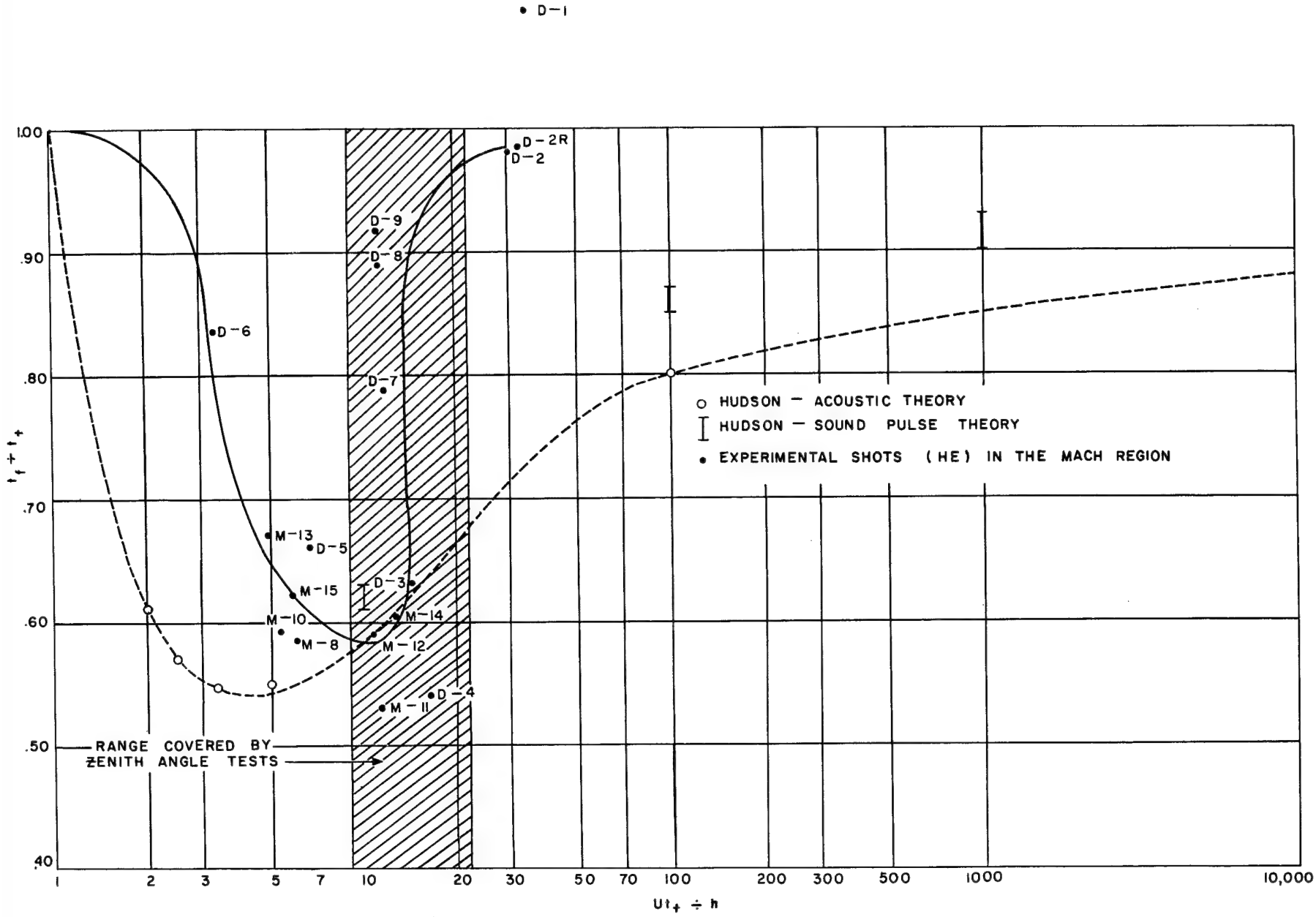

Figure 1. Theoretical and experimental duration shortening effects

Table Ia shows, for the heights of burst and zenith angles used, the preshot predictions of expected peak overpressures and positive-phase durations for the conditions of the tests. These expected pressures and durations were predicted from raw data which, when subsequently refined, were reported in WT-520[6] and SC-3858(TR).[7] The predictions were used in this experiment to determine gauge calibration steps and recording times. Table Ib gives the same information scaled to 1 kt at sea level. Since only about 50 percent of the total energy in a nuclear explosion causes blast, in scaling it has been assumed that 1/2 kt of TNT is equivalent to 1 kt of nuclear radiochemical yield.

To make the experiment more realistic, heights of burst were chosen to give overpressures comparable to similar full-scale conditions. Lower heights of burst were not used because high pressures would place structures in the region of "over-kill", and because overpressures would be beyond the capacity of the gauges on hand.

TABLE I

Scaling 250 Pounds of TNT at Coyote Canyon to 1 kt at Sea Level

(a)

250 Pounds at an Elevation of 6000 Feet Above Sea Level

Zenith angle (deg)	0	15	30	45	60	67.5	75	0	15	30	45	60	67.5	75
HOB (ft)	Peak overpressure (psi)							Positive duration (msec)						
38	60	54	37	22	12	6.6	3.5	8.3	9.5	11.4	14.6	16	18	24
64	21	16	12	8.3	4.8	3.4	1.9	12.7	14.6	16.5	18.7	20	22.5	25
90	11.5	8.6	6.5	4.8	3	2	1	19.1	20.3	21.6	23.5	24	25	26

(b)

1 kt at Sea Level

Zenith angle (deg)	0	15	30	45	60	67.5	75	0	15	30	45	60	67.5	75
HOB (ft)	Peak overpressures (psi)							Positive duration (msec)						
565	74	58	40	25	15	8.7	4.3	145	160	170	193	230	260	320
950	22	17	13	9.6	5.5	3.0	2.5	191	215	242	262	305	344	410
1335	11	9.6	7.5	5.5	3.6	2.2	1.2	250	265	295	322	365	385	420

CH II -- EXPERIMENTAL PROCEDURE

High-Explosive Charges

The high-explosive charges were solid cast TNT spheres 20-1/4 inches in diameter with a nominal weight of 256 pounds. With the exception of the addition of an automatic hoisting mechanism, the method of suspension was that described in Reference 6.

Gauge and Recording System

Variable-reluctance, Bourdon-type, air-pressure gauges manufactured by Wiancko Engineering Company were used as end instruments. The sensing element of the gauge is a flat, twisted Bourdon tube, 0.65 inch long, which acts in torsion, imparting a rotation to a vane attached to the sealed end. The vane forms the armature of a variable-reluctance sytem comprised of an E-core and two E-coils. Mechanical angular displacement of the armature changes the reluctance of the magnetic loops of the E-core and results in the modulation of the carrier current flowing through the E-coils. Variations in applied pressure are thus translated into electrical signals which are amplified and recorded. For this series of experiments, the gauge was repackaged[8] into a small unit to simplify the locating of gauges close to each other and to isolate the vibration of the metal target from the gauge mechanically.

The recording system is exactly as recorded in Appendix A of Reference 4. It may be briefly described as follows: a 20-kc carrier system is fed to the gauge, which modulates the carrier to the degree determined by the impressed air pressure. The modulated signal is in turn rectified, filtered free of the 20-kc carrier signal, and fed to a high-frequency string galvanometer in a standard Consolidated Engineering Corporation oscillographic recorder, which makes a permanent pressure-time record on photosensitive film or paper.

Target Layout and Measurements

The layout of the target area is shown in Figures 2 and 3. The target structures (2 x 2 feet in cross section) were located at horizontal distances (D) from ground zero determined by two principal variables: height of burst (H) and zenith angle (α). These variables are specified for each shot in Table II.

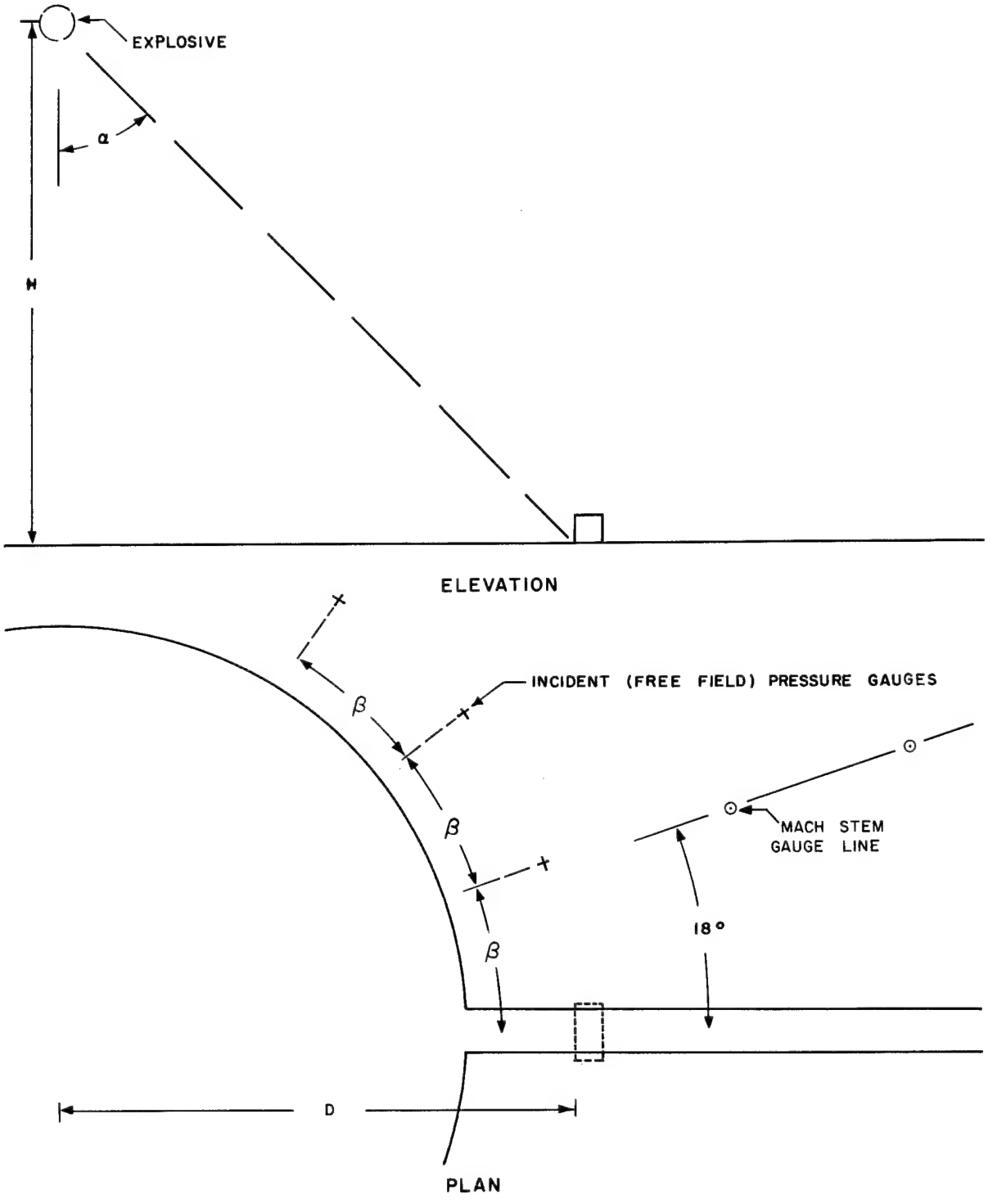

Figure 2. Schematic target layout

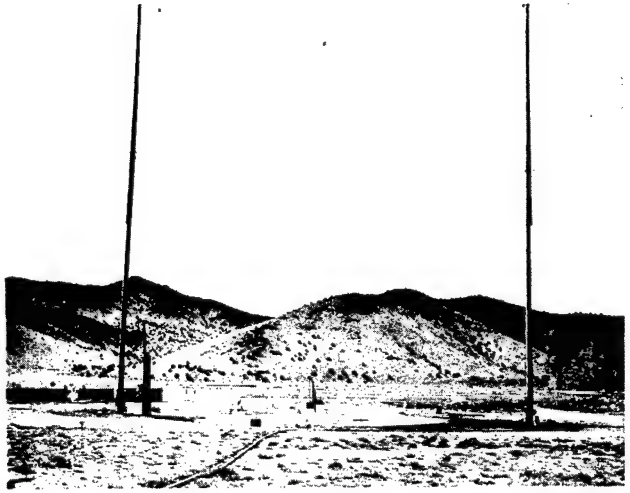

Figure 3. The target layout

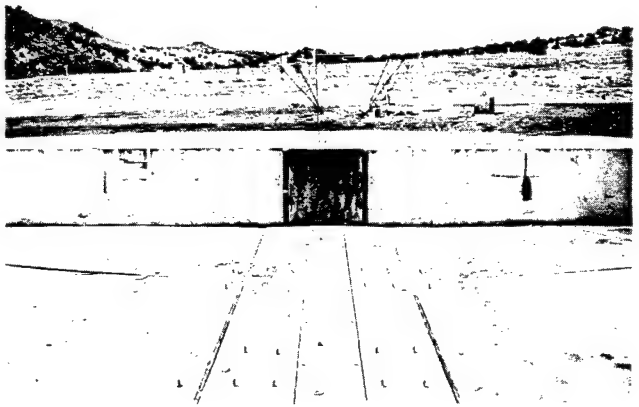

Figure 4. The 18-foot target structure

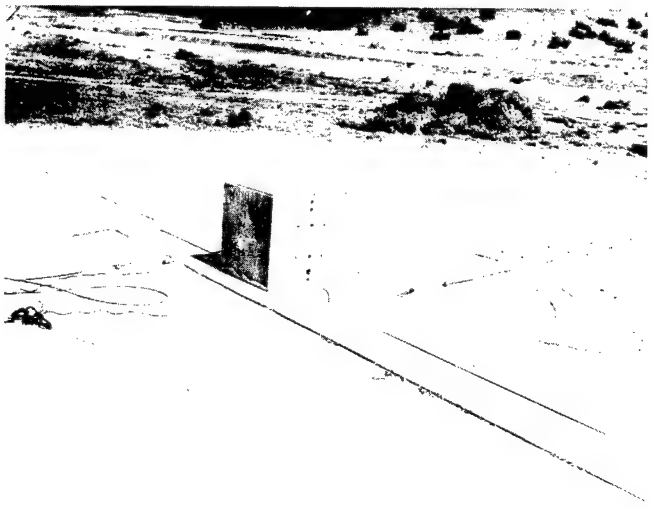

Figure 7. The 2-foot target structure

Figure 8. The 4-foot target structure

In experiments of the effect of two- and three-dimensional loading, Hudson[9] found that end effects are insignificant for targets located normal to the blast and in the Mach reflection region. In zenith-angle experiments, target structures with three dimensions (2 x 2 x 2 feet, 2 x 2 x 4 feet, and 2 x 2 x 18 feet)* were used to check end effects in the region of regular reflection. The 18-foot target was selected because it was sufficiently long to assure two-dimensionality of the 2- x 2-foot cross section (Figures 4 and 5). Gauge positions on the centerline of the 2-foot and 4-foot structures are shown in Figures 6, 7, 8, and 9. In addition, the 4-foot structures had a series of gauges located 4-1/2 inches from one end (except Nos. 18, 19, and 22, on which the distance was 3-1/2 inches) and placed as shown in Figure 8. These gauges were located so as to show differences in loading between the centerline and the near end area of target faces.

The incident (free-field) pressure for each target was measured by three gauges in ground baffles. When the target was directly beneath the charge, these gauges were located 3 feet in front of, and 2 and 4 feet in back of the target. For other positions of the target, the gauges were located at the same ground distance as the front of the target, with an angular separation to prevent arrival of reflections from the target at the nearest ground baffle gauge before the end of the positive phase of the incident shock. The angles of separation (β) (see Figure 2) of the ground baffle gauges for each target position are given in Table II.

Operation Log

Table III gives pertinent information for each shot. Occasionally, the conditions under which a shot was fired resulted in a failure of some portion of the recording system. It was necessary to repeat such shots. (Repetitions are shown in Table III by the letter R following the shot number. Second repetitions are designated RR.).

*Since the cross section is the same for all models, they will be referred to as the 2-, 4-, and 18-foot models in the following pages.

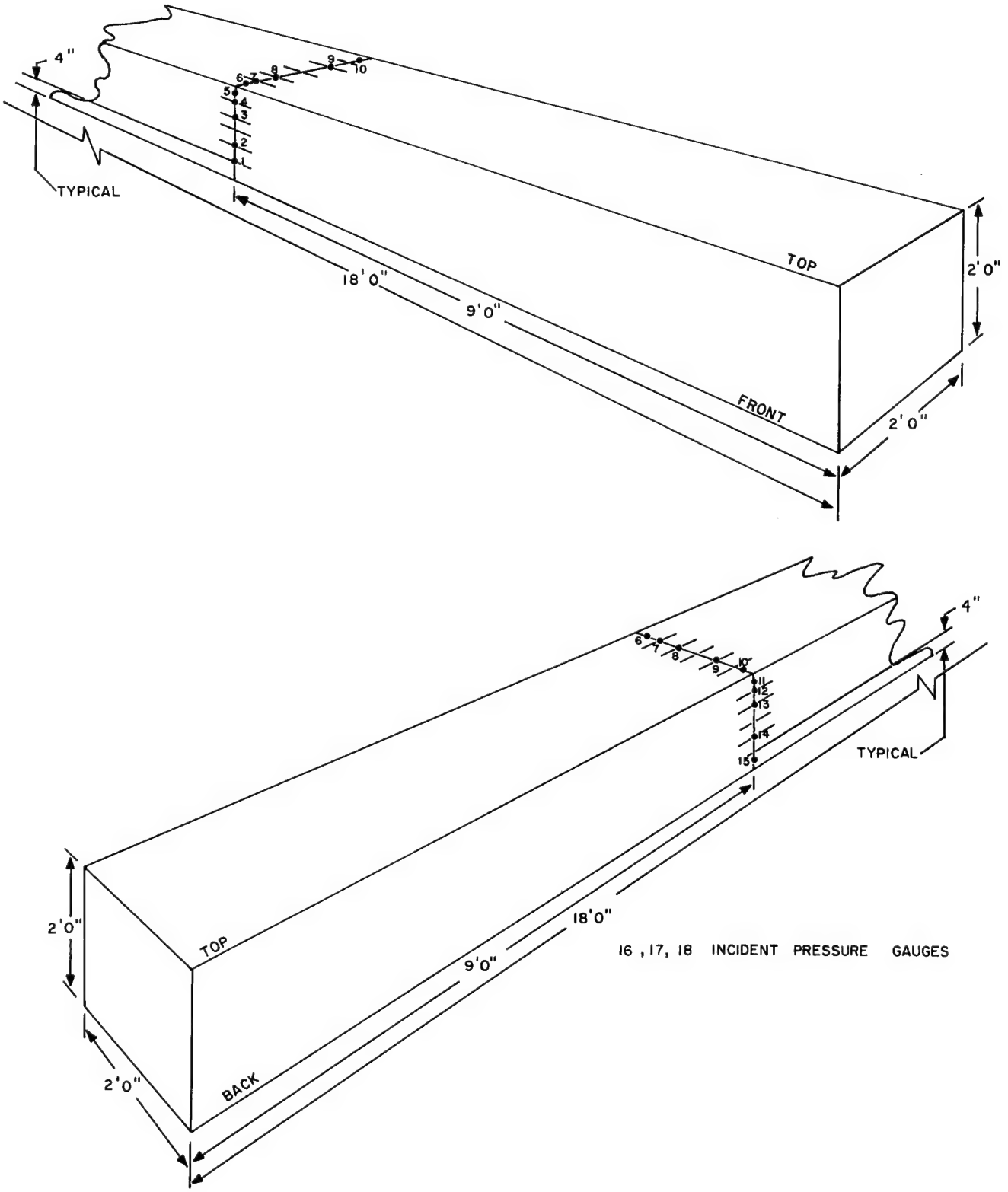

Figure 5. Gauge locations on the 18-foot target structure

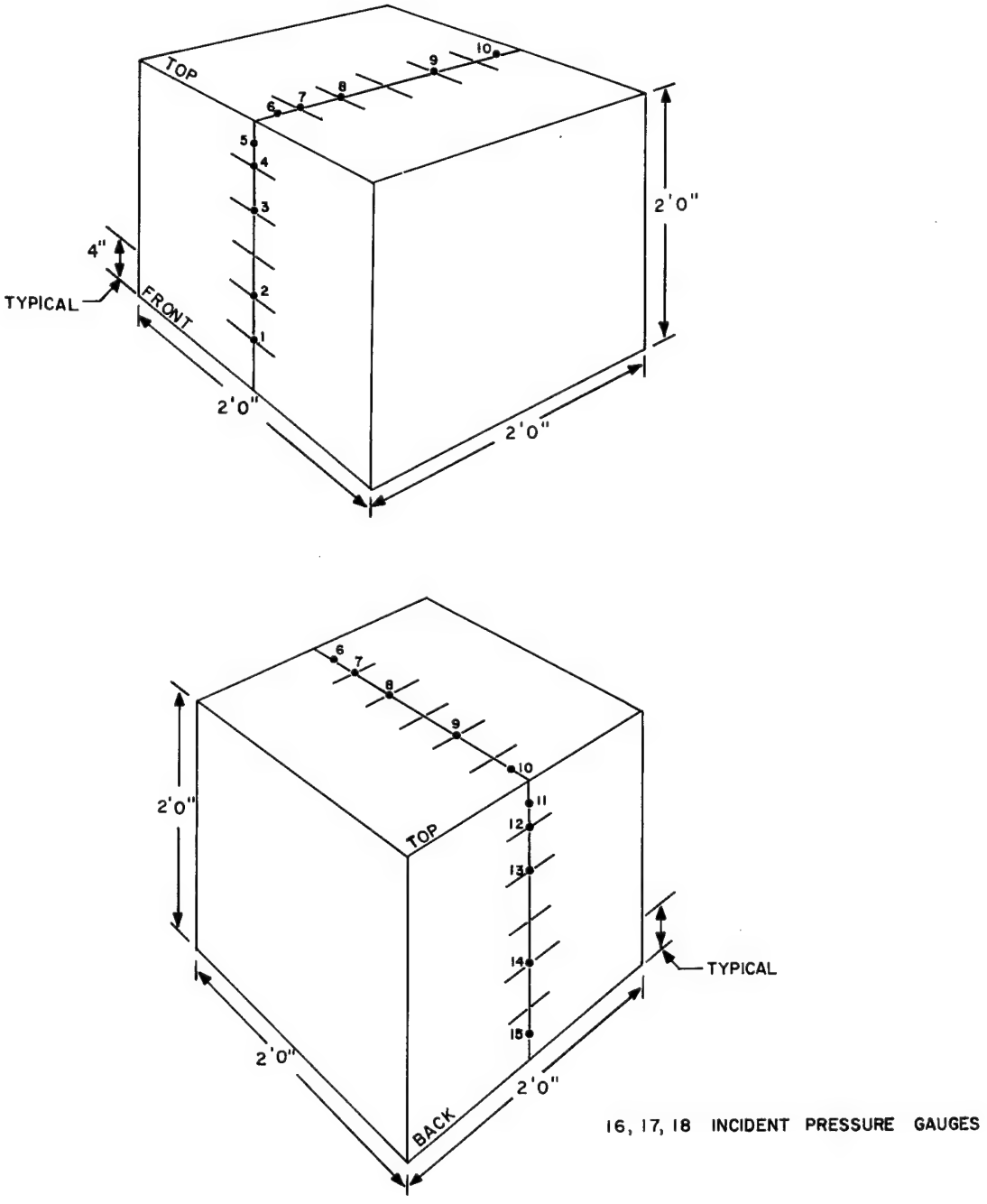

Figure 6. Gauge locations on the 2-foot target structure

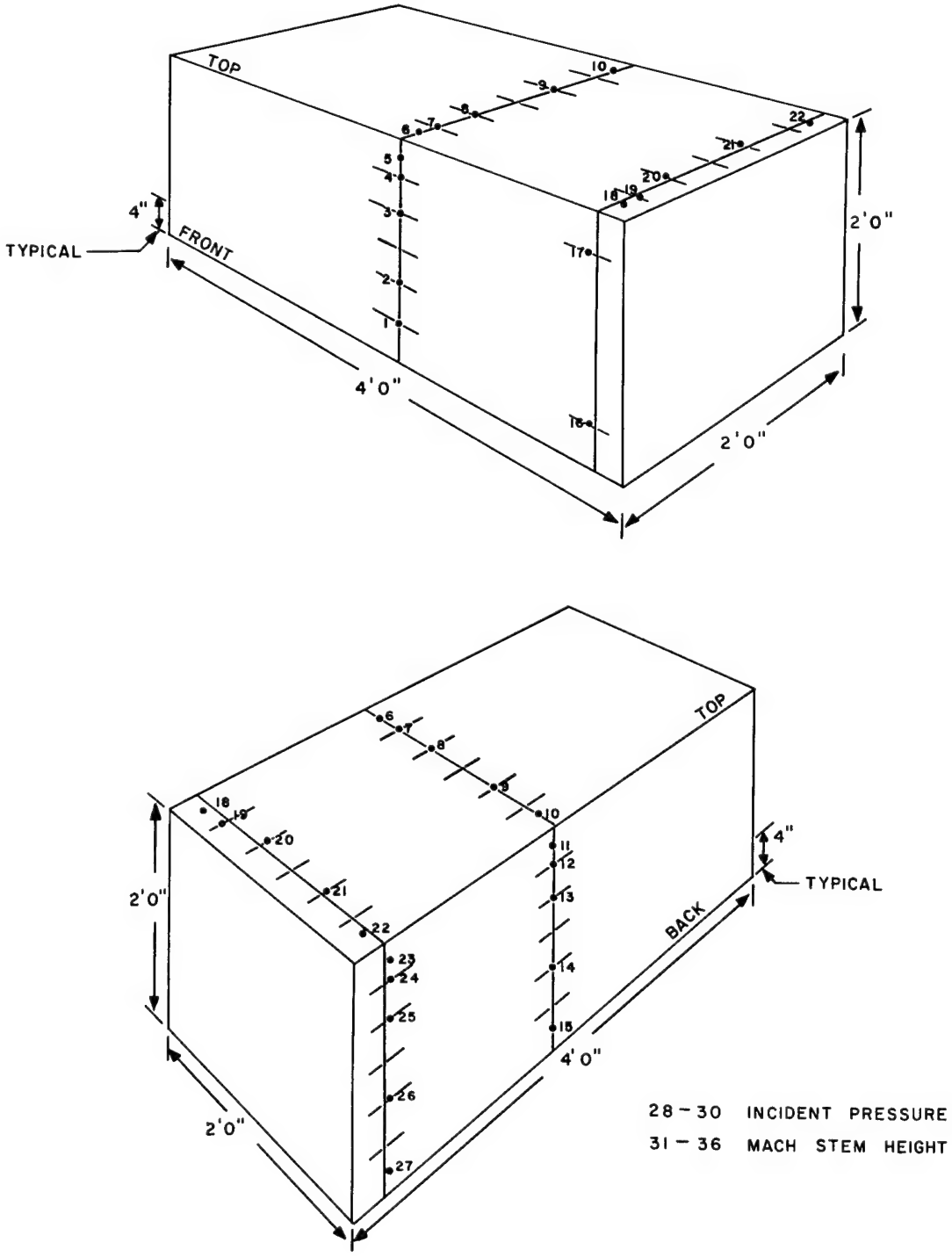

Figure 9. Gauge locations on the 4-foot target structure

TABLE II

Major Variables for Shots in the Series

Shot No.	Structure length	Zenith angle	Height H	Ground dist. D	Ground baffle separation angle (β)^{o}
1	4	0	38	0	180
2	4	0	64	0	180
3	4	15	38	10	30
4	4	15	64	17	30
5	4	30	38	22	30
6	4	30	64	37	21
7	4	45	38	38	19
8	4	45	64	64	13
9	4	60	38	66	13
10	4	67.5	38	92	10
11	4	75	38	142	8
12	18	0	64	0	180
	2	30	64	37	21
13	18	0	38	0	180
	2	45	38	38	19
14	18	0	90	0	180
	2	30	90	52	18
15	18	15	38	10	30
	2	60	38	66	13
16	18	15	64	17	30
	2	45	64	64	13
17	18	30	38	22	30
	2	67.5	38	92	10
18	18	30	64	37	21
	2	0	64	0	180
19	18	45	38	38	19
	2	75	38	142	8
20	18	30	90	52	18
	2	45	90	90	11
21	18	45	64	64	13
	2	15	64	17	30
22	18	60	38	66	13
	2	0	38	0	30
23	18	45	90	90	11
	2	0	90	0	180
24	18	67.5	38	92	10
	2	15	38	10	30
25	18	75	38	142	8
	2	30	38	22	30
26	18	64^{o}40'	38	80	11
27	4	15	64	17	30
	18	66^{o}20'	64	146	6

TABLE III

Operations Log

Shot No.	Date fired	P_o (lbs/sq in)	Relative humidity (%)	Temperature (^oF)	Wind velocity (est mph)	Weight (lbs)
Z-1	4-2-54	11.98	8	72	10	252.5
Z-2	4-8-54	11.93	22	72	0	250
Z-3	4-14-54	11.81	8	71	20-30	250
Z-4	4-16-54	11.99	7	75	5-10	252
Z-5	4-20-54	11.91	7	78	15	250
Z-6	4-22-54	11.82	24	80	0	252
Z-7	4-23-54	11.87	>10	78	15	252
Z-7R	4-30-54	11.71	30	62	20-25	252
Z-6R	5-3-54	11.95	16	69	0	252
Z-3R	5-5-54	11.82	26	77	0	252
Z-8	5-28-54	11.84	20	73	7	256
Z-9	6-2-54	11.89	18	76	25	256
Z-10	6-8-54	11.84	12	82	11	256
Z-10R	6-10-54	11.87	11	82	12	256
Z-12	6-15-54	11.87	13	82	10	256
Z-13	6-16-54	11.86	8	81	10-15	256
Z-18	6-17-54	11.84	10	90	Calm	252
Z-22	6-24-54	11.91	32	85	Calm	252
Z-21	7-1-54	11.95	20	85	6	256
Z-16	7-2-54	11.99	39	82	Calm	256
Z-15	7-6-54	11.91	16	89	7	256
Z-11	12-27-55	11.62	64	52	3	256
Z-11R	12-29-55	11.72	60	54	Calm	256
Z-20	1-19-56	11.59	66	48	12	256
Z-14	1-23-57	11.94	29	55	8	256
Z-23	1-25-57	11.91	24	55	9	256
Z-10RR	1-31-57	11.91	12	52	12	256
Z-9R	2-7-57	11.98	28	62	Calm	256
Z-19	2-14-57	11.90	20	71	6	256
Z-25	2-19-57	11.89	38	55	Calm	256
Z-17	2-21-57	11.91	42	59	Calm	256
Z-24	2-26-57	11.99	28	63	Calm	256
Z-26	2-28-57	11.92	32	61	Calm	256
Z-27	2-28-57	11.93	42	54	Calm	256
Z-13R	3-5-57	11.88	34	55	Calm	256

CH III -- MACH-STEM HEIGHT

To study loading in the region of formation of the Mach stem and in the region where the Mach stem was close to the height of the target, it was necessary to determine the height of the Mach stem as a function of distance from ground zero. For this purpose, six Wiancko pressure gauges modified to give arrival times only were located at six different heights at seven stations (Figure 10). It was planned to use only four stations for any one shot (Table IV) The line of these gauges was 18 degrees from the base line on which the targets were located.

TABLE IV

Mach-Stem Gauge Locations

Horizontal distance from ground zero (ft)	Gauge heights (ft)	Shot No.
52	1, 2, 3, 4, 5, 6	1, 7, 9
66	1, 2, 3, 4, 5, 6	1, 3, 7, 8, 9, 10
77	1, 2, 3, 4, 5, 6	1, 3, 7, 8, 9, 10
92	1, 2, 4, 6, 7, 8	1, 2, 3, 4, 5, 6, 7, 8, 9, 10
107	1, 2, 4, 6, 7, 8	2, 3, 4, 5, 6, 8, 10
125	2, 4, 6, 8, 9, 10	2, 4, 5, 6
142	2, 4, 6, 8, 9, 10	2, 4, 5, 6

The original plan was to measure the height of Mach stem on only the first ten shots and then to assume that the path of the triple point on the subsequent shots was the same as for a shot of corresponding height of burst among the first ten shots. From the first ten shots, the measured path of the triple point was as shown in Figure 11. When these data were scaled to 1 pound of TNT at sea level, their lack of agreement with other published results was considerable (Figure 12). Because the target structure was resting on a concrete "sidewalk" (Figure 9), while the line of Mach-stem gauges was located over irregular, poorly compacted earth, it was doubtful if the Mach-stem height measured by the gauges was the same as the

Figure 10. Gauge array used to determine Mach-stem height

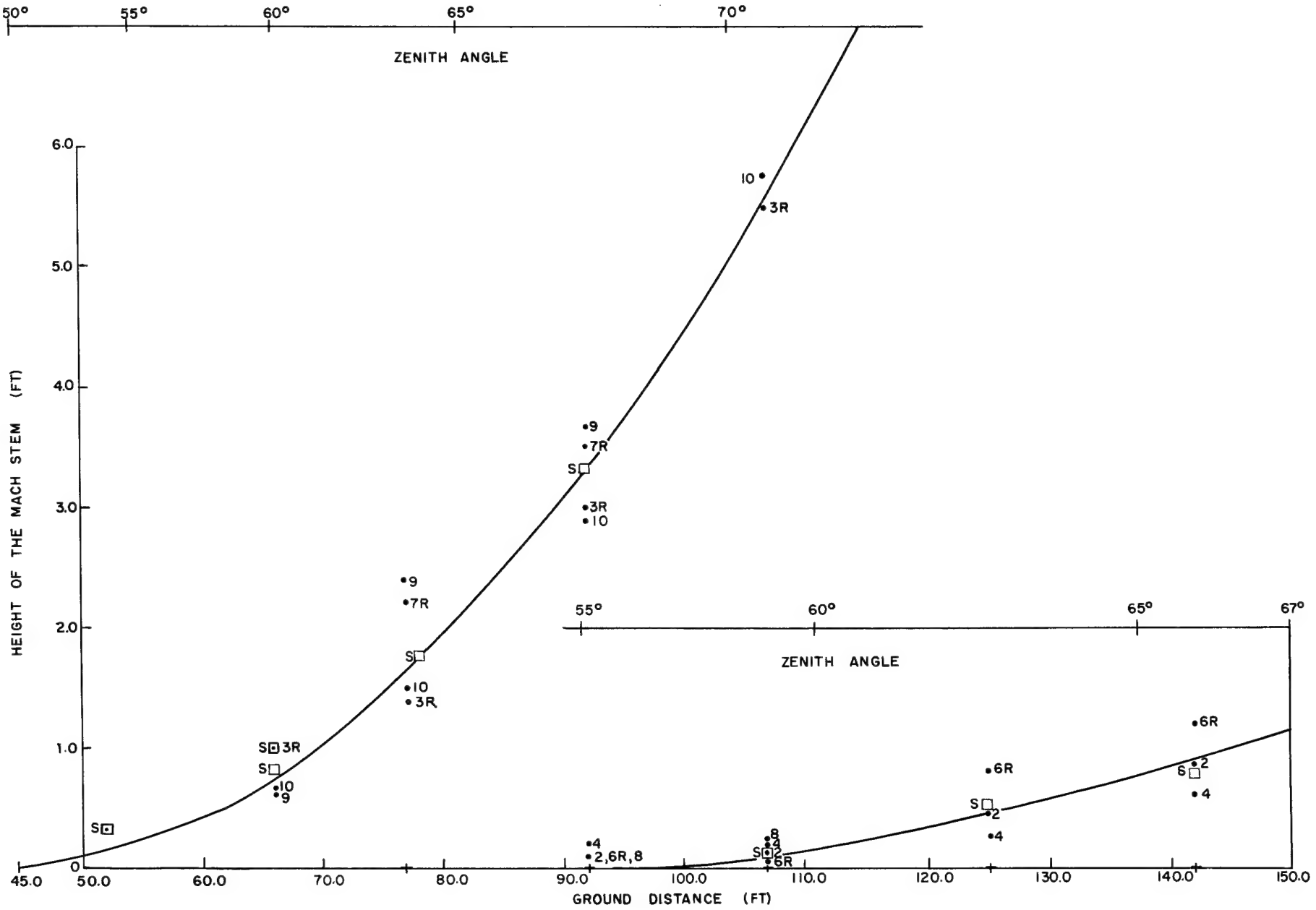

Figure 11. Measured path of the triple point

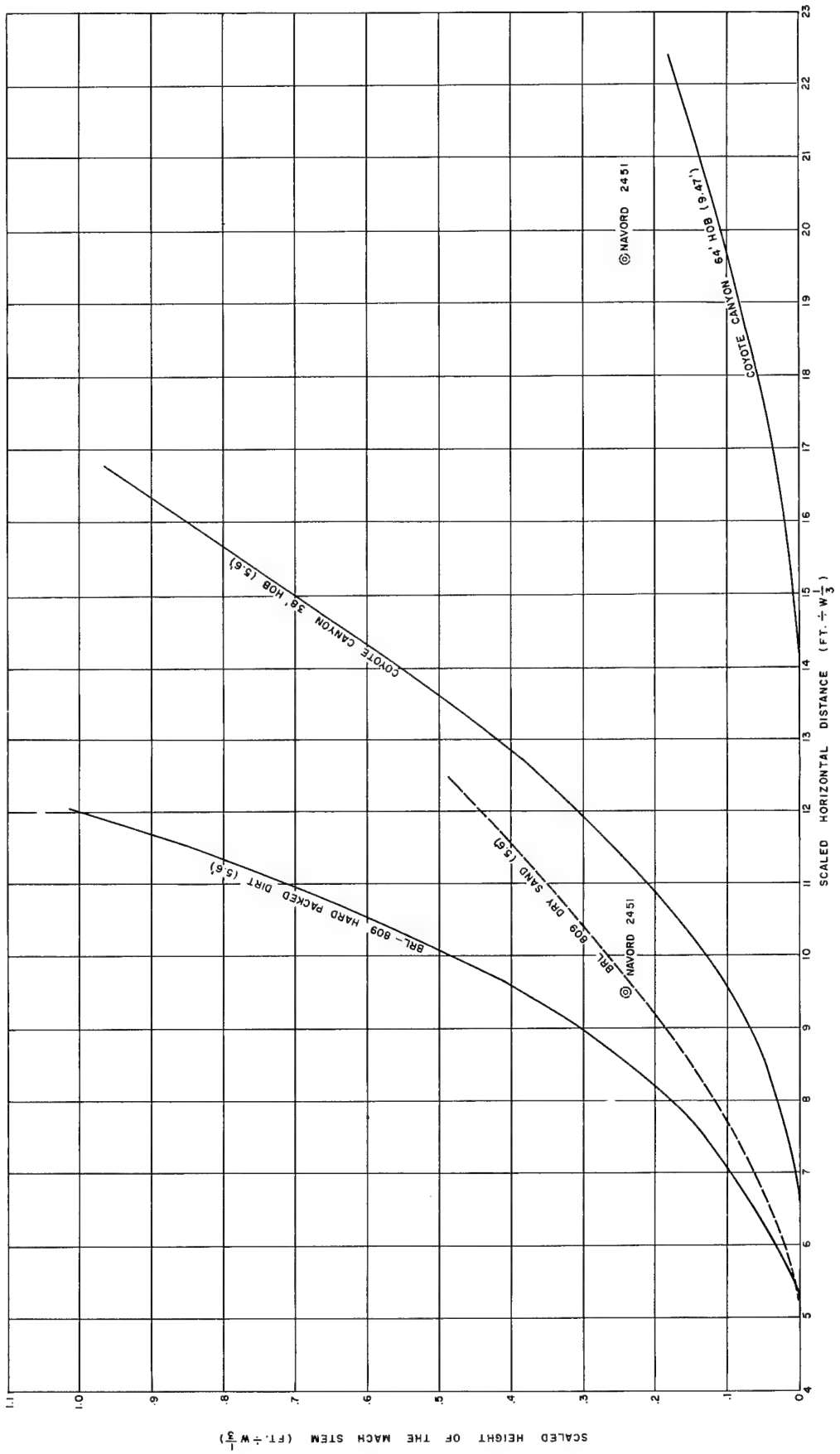

Figure 12. Comparison of Mach-stem data scaled to 1 pound TNT at sea level

stem height at the structure location. For this reason, seven Mach-stem gauge stations were moved to a line at the edge of the concrete "sidewalk", and charges were fired at 38 feet and at 64 feet. The results of these two shots are designated in Figure 11 by S. Since there was no essential disagreement between the stem heights of these two special shots and those fired earlier, it was concluded there were no major differences in Mach-stem height versus distance along the concrete "sidewalk" and a line 18 degrees from it, in spite of the lack of agreement with other published data.

CH IV -- BLAST LOADING OF TARGET SURFACES IN THE REGULAR REFLECTION REGION

Free-Field Pressure Measurements

The quantities used to correlate data from the various shots are the angle between the shock front and ground surface (α), and the free-field peak overpressure (p_m) at the same ground range as the targets. On each shot, three ground baffle gauges were used to record pressure-time. They were located as described in Chapter II. The free-field peak overpressure data are summarized on Figure 13, which shows the relationship between peak overpressure and distance for each burst height used. For comparison purposes, Figure 13 also shows curves from Dr. Shreve's tests, [5] which employed similar TNT charges. The bend of the curve at 0 horizontal distance is attributed to the inability of the gauges to respond to the reflected pressures. This is supported by the calculated reflected pressures shown in Figure 13.

Target Surface-Pressure Measurements

The 15 pressure-time records obtained from the target centerline gauges were used to construct pressure profiles on the target cross section at successive time increments. From these pressure profiles, the average pressure acting at the centerline on each of the three target surfaces at specific times was computed. The time interval used in the average-pressure computation was 0.5 millisecond in the first few milliseconds of the positive phase and 1.0 millisecond for the remainder of the positive phase. The resultant average pressure-time curves represent the average pressure acting on a particular surface (front, top, or back) as a function of time. A number of these curves are shown in Appendix A.

The centerline pressure-time records were also used to determine the time of arrival of the blast wave at the gauge points on the target. The time that the incident wave arrived at various points of the front and top surfaces being known, the position of the shock front in space can be determined at the target. The angle of the intersection of the shock front and the ground surface should equal the zenith angle if the wave front is truly spherical. In practice, however,

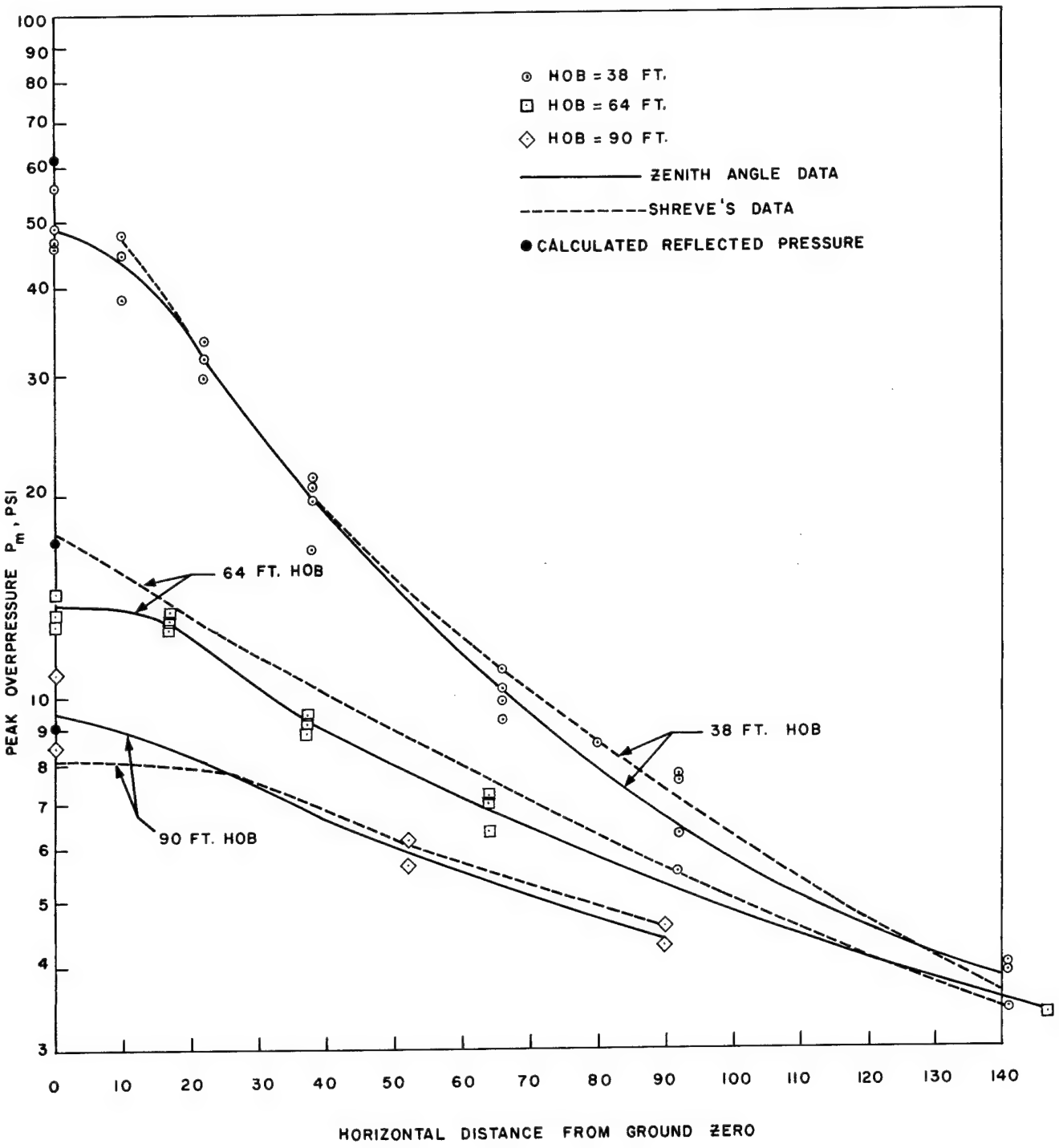

Figure 13. Overpressure-distance relationship for three heights of burst used

this angle of intersection differs by a few degrees from the zenith angle defined by the geometric relation of the target to the burst point. The angle of intersection of the shock front and any horizontal surface as determined from arrival-time data is termed the apparent zenith angle (α_A). An example of the procedure used to determine the apparent zenith angle is shown in Figure 14. Figure 14a shows the time of arrival of the incident blast wave at the various gauge points. Figure 14b was constructed from Figure 14a and shows the location of the incident wave front at 15.200 msec and 15.690 msec imposed on the target cross section for shot 17. The apparent zenith angle was determined to be 36 degrees as compared to an actual zenith angle of 30 degrees. The space-time-of-arrival plots, illustrated in Figure 14a, were also used to determine the transit time of the incident wave across the front, top, and back surfaces of the target.

For zenith angles less than about 45 degrees, a Mach stem forms on the front face. The velocity of the shock down the front face would be increased by virtue of the Mach stem and would lead to an overestimation of the value of the apparent zenith angle. The overestimation averages about 5 degrees (Table V).

Since the pressure gauges do not respond with sufficient rapidity to measure the initial peak pressure, it was necessary to extrapolate the pressure-time records in order to obtain the best estimate of the peak pressures. For the ground baffle gauges used to measure the incident pressure, each of the three records was extrapolated to the time of arrival, and the three values were then averaged to obtain the free-field pressure at the target range. To obtain the peak pressure on the target surfaces, a different procedure was used. For the top surface, the average pressure-time curves were extrapolated to a time corresponding to the transit time of the wave across the top surface. For the front surface, the average pressure-time curves were extrapolated to a time equal to twice the transit time of the wave down the front surface. No extrapolations were made on the back surface except for $\alpha = 0^o$. The validity of these extrapolations is discussed in subsequent paragraphs. The transit times used in the above extrapolations were those determined from the space-time-of-arrival plots (see Figure 14a). The process of extrapolating the average pressure-time curves is comparable to extrapolating each individual pressure-time record before constructing the pressure profiles. These extrapolations are shown in the figures of Appendix A.

Target Front-Surface Loading

The average pressure on the front face of the targets reaches a peak value (p_2) at a time when the reflected wave has traversed the front face. The time (t_2) when p_2 occurs was

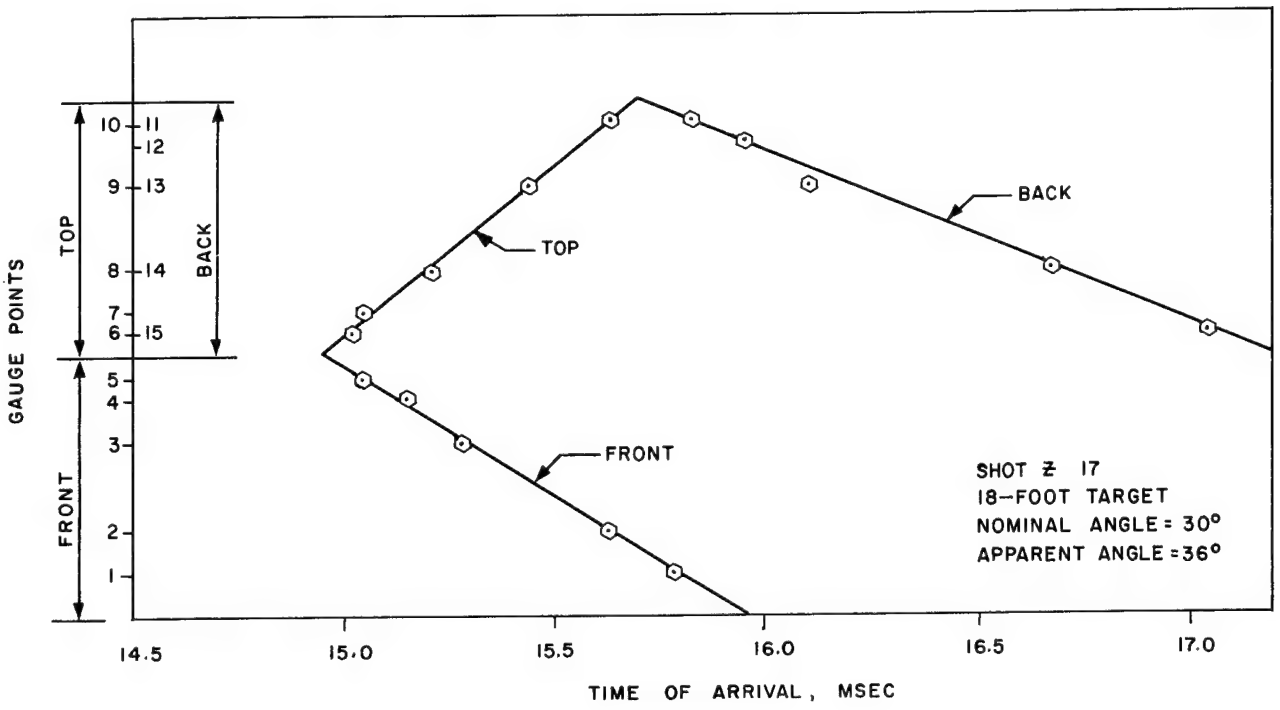

A) SPACE—TIME—OF—ARRIVAL PLOT

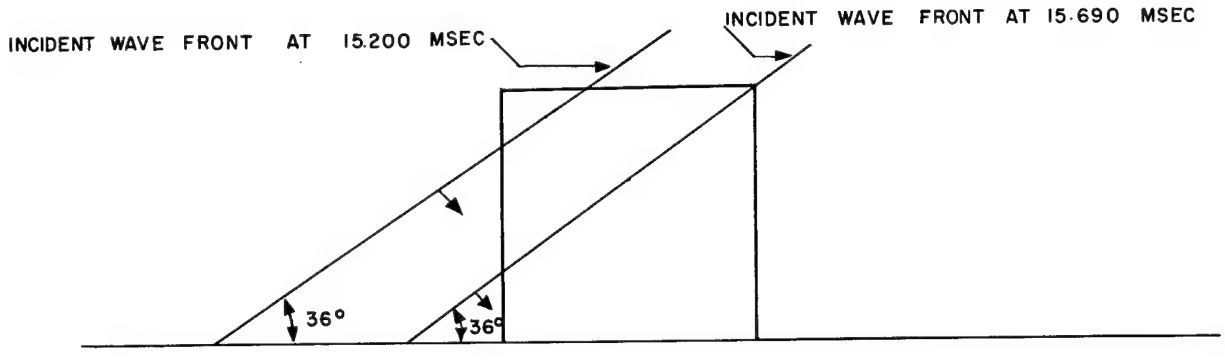

B) LOCATION OF THE INCIDENT SHOCK FRONT AT 15.200 AND 15.690 MSEC

Figure 14. Determination of apparent zenith angle from space-time-of-arrival data

TABLE V

Summary of Zenith Actual and Apparent Angles

Z No.	Row	HOB	Length (ft)	Actual angle (deg)	Apparent angle (deg)	Difference Appr. - Act.
1	C	38	4	0	9	9
	E	38	4	0	20	20
2	C	64	4	0	13	-13
	E	64	4	0	4	-4
3R	C	38	4	15	21	6
	E	38	4	15	19.5	4.5
4	C	64	4	15	16	+1
	E	64	4	15	14	-1
5	C	38	4	30	34	4
	E	38	4	30	36	6
6R	C	64	4	30	37.5	7.5
	E	64	4	30	37.5	7.5
7	C	38	4	45	58	13
7R	C	38	4	45	45	0
	E	38	4	45	50.5	5.5
8	C	64	4	45	52	7
	E	64	4	45	45	0
9	C	38	4	60	59	-1
	E	38	4	60	51.5	-8.5
9R	C	38	4	60	60.3	0.3
	E	38	4	60	60.3	0.3
10R	C	38	4	67.5	90	MS
	E	38	4	67.5	90	MS
10RR	C	38	4	67.5	90	MS
	E	38	4	67.5	90	MS

TABLE V (Cont)

Z No.	Row	HOB	Length (ft)	Actual angle (deg)	Apparent angle (deg)	Difference Appr. - Act.
11R	C	38	4	75	90	MS
	E	38	4	75	90	MS
12	C	64	18	0	4.5	4.5
	C	64	2	30	47	17
13	C	38	18	0	0.7	0.7
	C	38	2	45	51	6
13R	C	38	18	0	7.0	7
	C	38	2	45	51.5	6.5
14	C	90	18	0	5	5
	C	90	2	30	37	7
15	C	38	18	15	14	-1
	C	38	2	60	48	-12
16	C	64	18	15	21.5	6.5
	C	64	2	45	47	2
17	C	38	18	30	36	6
	C	38	2	67.5	90	MS
18	C	64	2	0	0.5	0.5
	C	64	18	30	32.5	2.5
19	C	38	18	45	50	5
	C	38	2	75	90	MS
20	C	90	18	30	36.7	6.7
	C	90	2	45	41	-4
21	C	64	2	15	21.3	6.3
	C	64	18	45	49	4
22	C	38	2	0	1.5	1.5
	C	38	18	60	60.5	MS
23	C	90	2	0	9.5	9.5
	C	90	18	45	48	3
24	C	38	2	15	18.5	3.5
	C	38	18	67.5	90	MS
25	C	38	2	30	37.5	7.5
	C	38	18	75	90	MS
26	C	38	18	$64^{o}40'$	90	MS
27	C	64	4	15	22	7
	C	64	18	$66^{o}20'$	75.5	$9^{o}10'$

determined by doubling the travel time of the incident wave down the target front as determined from the time-of-arrival plots. Since the gauge was not able to measure this peak pressure, it was determined by extrapolating the average pressure-time curve back to t_2. Table VI compares t_2 as determined from the arrival times with the time from arrival of the blast wave to the maximum of the average pressure on the front surface (t_{fm}) for all 18-foot targets in the regular reflection region. This table shows that with few exceptions the measured peak average pressure occurs within 0.5 millisecond (the calculation interval) of t_2 as determined from arrival-time plots, thus the minor differences are inherent in the procedure used for reducing the data.

The relationships between front-surface pressure ratios (p_2/p_m) and apparent zenith angles (α_A) are shown in Figures 15, 16, and 17. Figure 15 shows the front-surface pressure ratio and zenith-angle relationship for 2-, 4-, and 18-foot targets exposed to a burst at a 38-foot height. Figure 16 presents a similar analysis for the 64-foot burst height. It must be emphasized that these curves show the ratio p_2/p_m (p_m = average peak incident overpressure) for targets at various ground ranges for a fixed burst height, not for a constant shock strength. Essentially the curves in Figures 15 and 16 show the effect of the target length on the front-surface pressure ratio. Figure 17 shows the relationships between p_2/p_m and the apparent zenith angle for the separate target lengths and various heights of burst and, therefore, the effect of different overpressures upon the front-surface pressure ratio for constant target dimensions. One would expect Figure 17 to show the transition from $\frac{p_2}{p_m} = 1$ to $\frac{p_2}{p}$ = reflection factor at the angle where the Mach stem is equal to the height of the target, as in general it does. Most unusual is the apparent dip in the vicinity of 15 degrees.

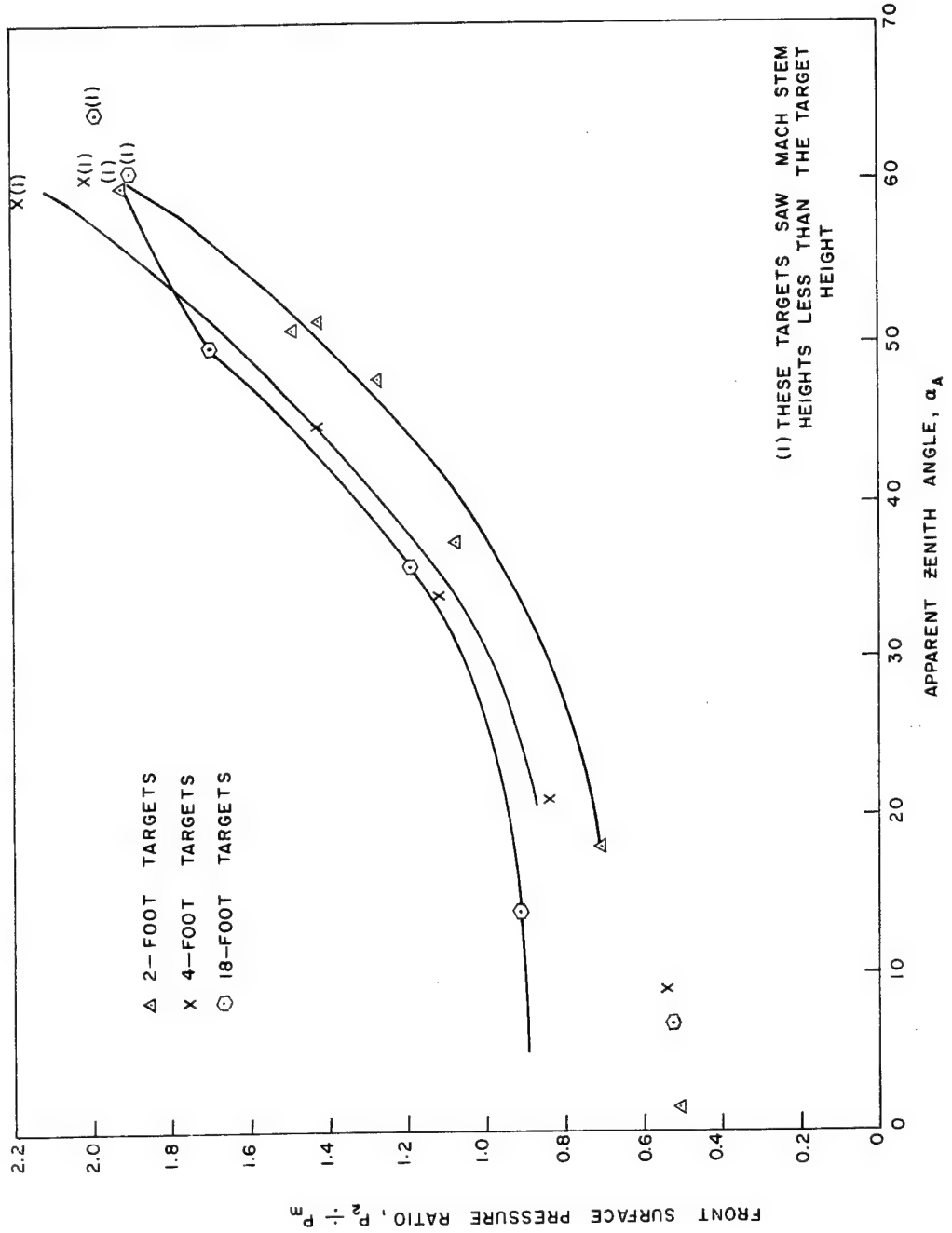

Figure 15. Relationship between front-surface pressure ratio, p_2/p, and the apparent zenith angle, α_A, for a height of burst of 38 feet.

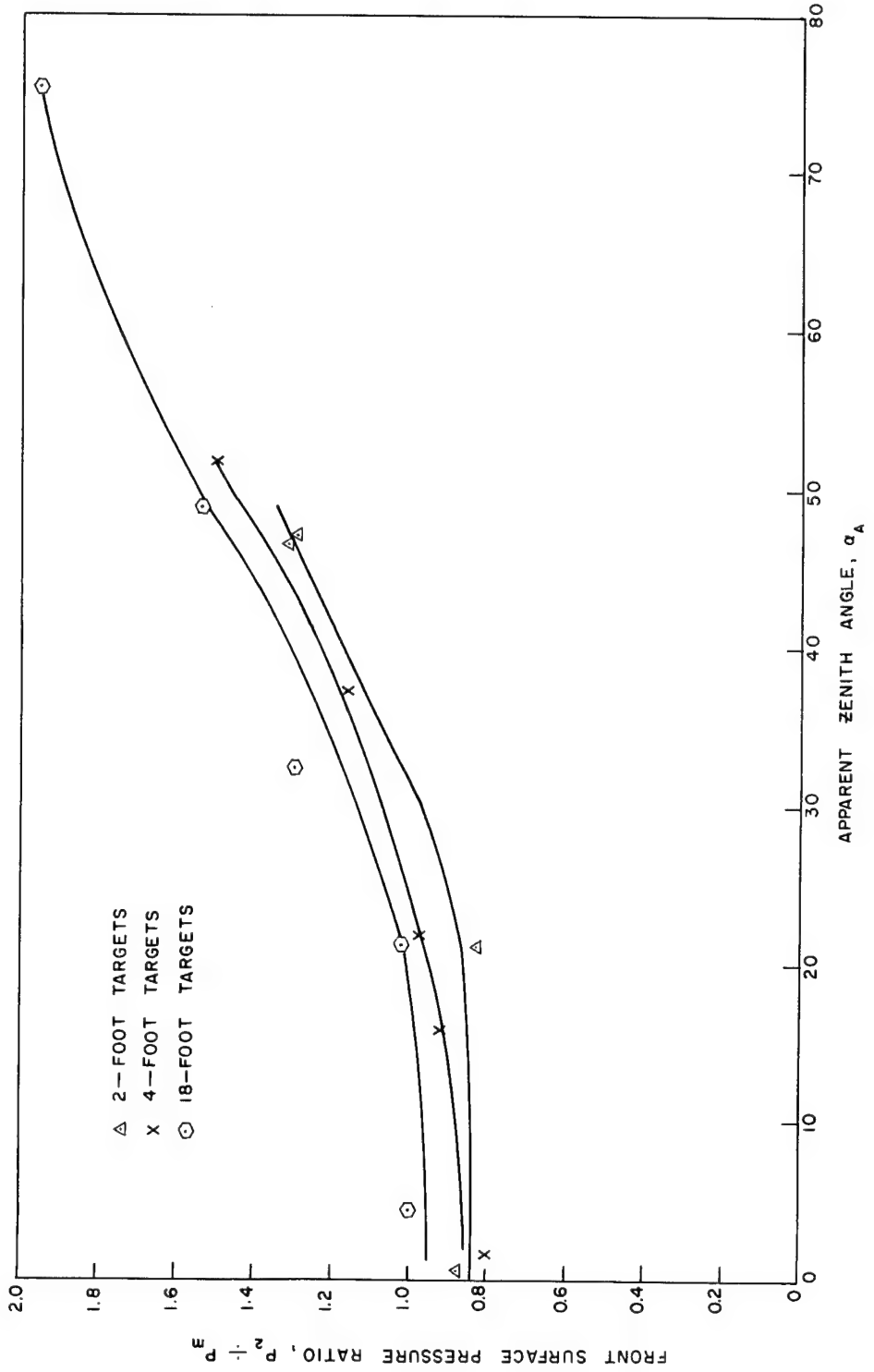

Figure 16. Relationship between front-surface pressure ratio, p_2/p, and the apparent zenith angle, α_A, for a height of burst of 64 feet

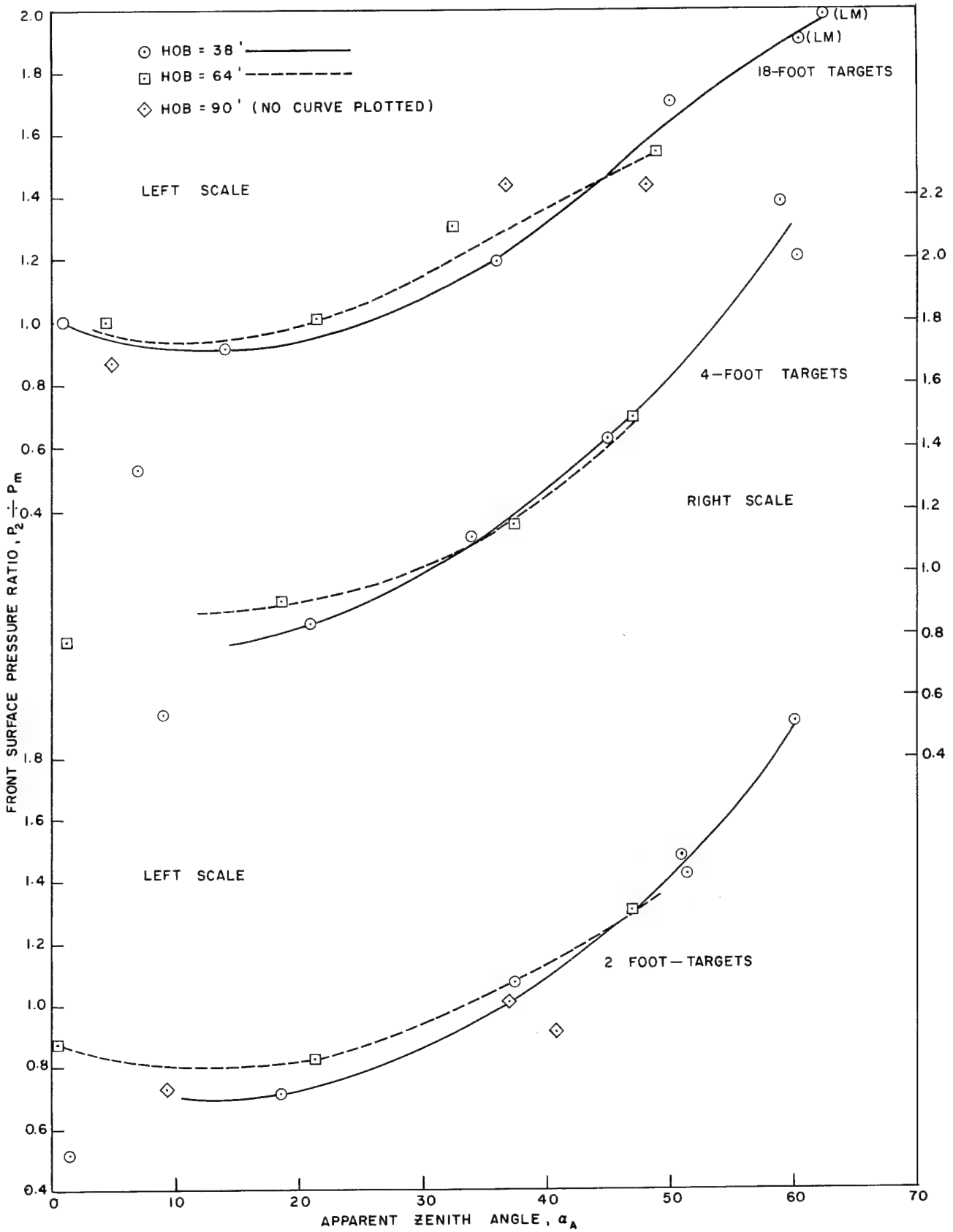

Figure 17. Relationship between front-surface pressure ratio, p_2/p, and the apparent zenith angle, α_A, for various target lengths

TABLE VI

Comparison of t_2 and t_{fm} for 18-Foot Targets

Shot	t_2* (milliseconds)	t_{fm}** (milliseconds)	$t_{fm} - t_2$ (milliseconds)
12	3.30	3.70	+0.40
13	1.91	1.98	+0.07
13R	2.32	2.30	-0.02
14	3.28	3.52	+0.24
15	2.25	2.40	+0.15
16	2.64	3.30	+0.66
17	2.02	2.50	+0.48
18	2.44	2.67	+0.23
19	1.95	2.20	+0.25
20	2.69	3.20	+0.51
21	1.84	2.21	+0.37
22	1.05	1.12	+0.07
23	2.44	2.70	+0.26
27	0.93	4.75	-0.28

*t_2 is the assumed time of maximum average pressure on the front surface. It was determined from the time-of-arrival plots.

**t_{fm} is the time of maximum average pressure on the front surface as read from the average pressure-time curve for the front surface.

Target Top-Surface Loading

The average pressure on the top surface reaches an initial maximum value (p_4) at a time (t_4) equal to the transit time of the incident wave across the top surface. As in the case of the front surface, time-of-arrival plots were used to determine t_4. The general shape of the top-surface average pressure-time curve after the initial maximum value is reached depends principally upon the zenith angle, or rather on the arrival of the reflected wave at the top surface. For targets near ground zero and thus for small zenith angles, the average pressure on the top surface decays rapidly following p_4. The reflected wave moving up the front surface for small zenith angles reaches the target top with a higher pressure than exists on the top and therefore produces a second but inferior maximum. Examples of this condition are the top-surface average pressure-time plots in Figures A-1, A-2, and A-3 of Appendix A. As the target is moved away from ground zero, the time between the occurrence of top-surface initial maximum pressure (p_4) and the arrival of the reflected wave decreases. Eventually the second maximum gives way to an interval of nearly constant or slightly decreasing top-surface pressure behind the peak pressure, p_4. An example of this condition is shown in Figure A-4. At large zenith angles, the reflected wave arrives on the top surface shortly after or even before the initial peak pressure occurs. In this case, the top-surface average pressure-time curve is characterized by a gradual decay subsequent to the time p_4 occurs.

The treatment of the top-surface data is similar to that of the front-surface data, in that initial-peak average pressure (p_4) was obtained by extrapolating to the top-surface transit time determined from the time-of-arrival plots. In a few cases at zenith angles of about 45 degrees or greater, p_4 was produced solely by the incident wave; however, the reflected wave arrived so soon thereafter that extrapolation was not possible. In these cases, usually the highest recorded pressure was used.

Figure 18 shows the relationships between the top-surface pressure ratio (p_4/p_m) and the apparent zenith angle for the three target lengths and a burst height of 38 feet. Figure 19 is a similar plot for a burst height of 64 feet. These two figures show the effect of target length on the top-surface pressure ratio.

There exists several anomalies in the top-surface data shown in Figures 18 and 19. The data for shot Z-25 (Figure 18) for the 2-foot target located at a nominal zenith angle of 30 degrees indicated an apparent zenith angle of 37.5 degrees and $p_4/p = 0.78$. The peak overpressure for this shot is compatible with data from other shots with targets in the same range, and the space-time-of-arrival plot is smooth. Even so, the pressure ratios on the front, top, and possibly the rear surface seem high when compared with data from nearby

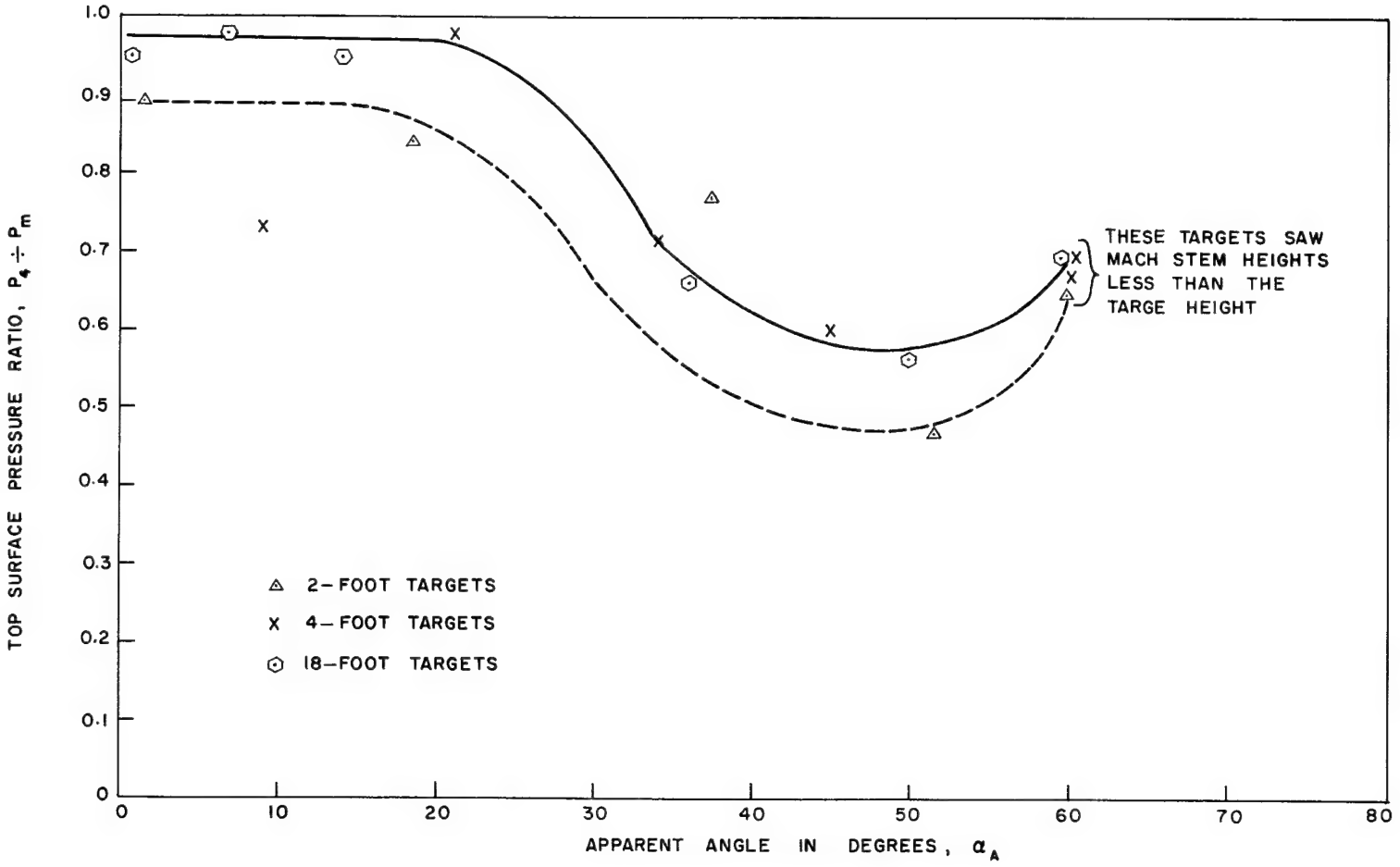

Figure 18. Relationship between top-surface pressure ratio, p_4/p, and the apparent zenith angle, α_A, for a 38-foot height of burst

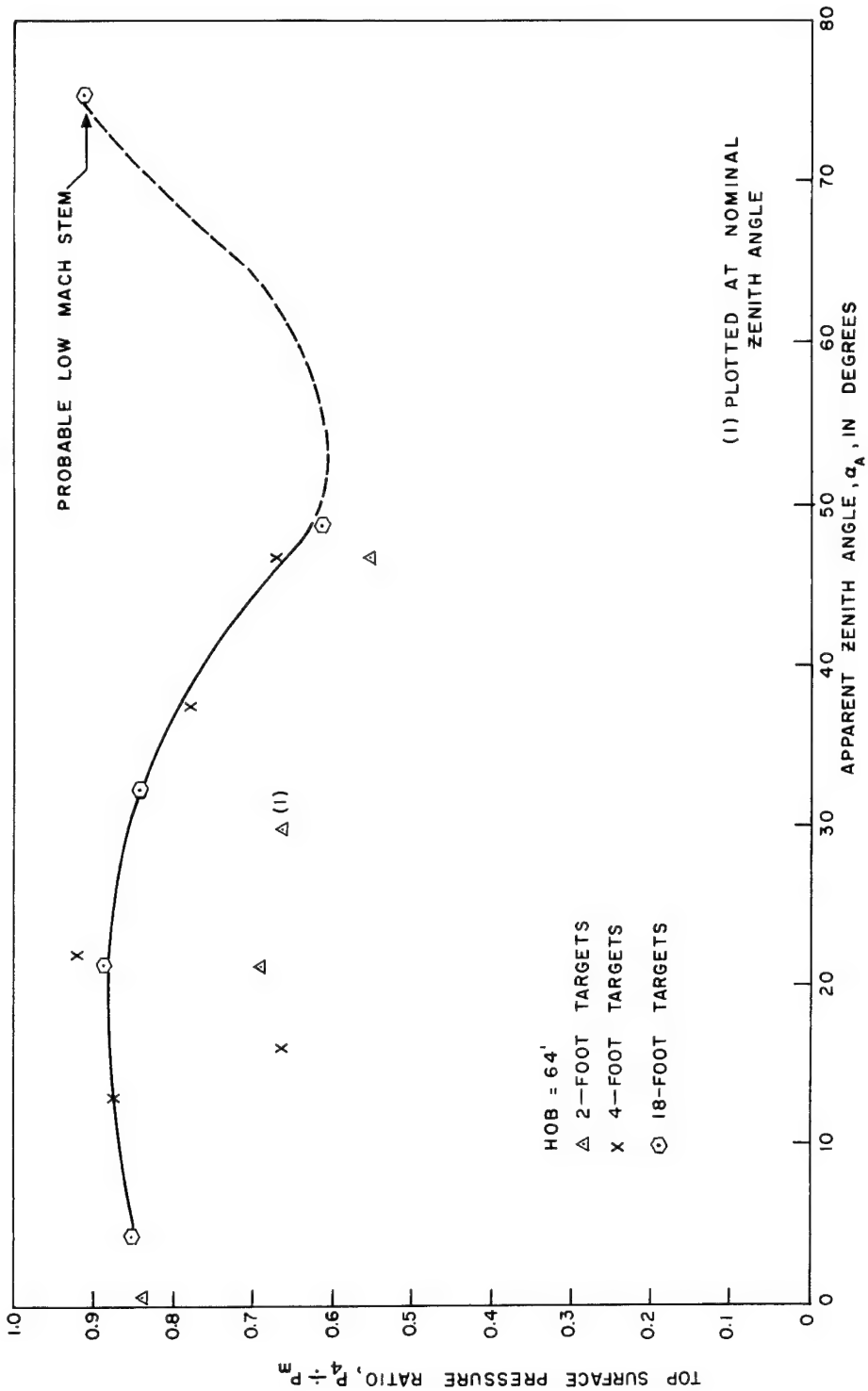

Figure 19. Relationship between top-surface pressure ratio, p_4/p, and apparent zenith angle, α_A, for a 64-foot height of burst[4]

angles (see Figures 15, 18, and 21). For this reason p_4/p Z-25 was essentially ignored in data smoothing.

On Figure 19 it is noted that one shot (Z-12) was plotted at the nominal zenith angle. Use of the nominal zenith angle was necessary since the time-of-arrival data were erratic for the 2-foot target. One of the top-surface gauges on this target was also erratic, resulting in the low value of p_4/p. The 4-foot target at α_A = 16 degrees is shot Z-4 on Figure 19. One of the top-surface gauges appears erratic. No reason is apparent for the low value of p_4/p for shot Z-21, which used a 2-foot target at α_A = 21.3 as shown on Figure 19.

Figure 20 shows the relationship between the ratio p_4/p_m and the apparent zenith angle for the various heights of burst. Again, the curves shown are for targets at various ground ranges from a fixed height of burst -- not for a constant shock strength. However, for any angle, p_4/p_m can be obtained for two or three shock strengths, depending on the availability of 90 feet height-of-burst data from this figure.

The most interesting thing to be gained from Figures 18 to 20 is the dip which is maximum at a zenith angle of 45 degrees. The dip is due to a decrease in p_4 caused by the rarefaction wave which forms very close behind the reflected shock wave as it crosses the top. The rarefaction wave follows most closely behind the reflected wave at approximately 45 degrees and hence decreases p_4 more than for the other angles.

Target Back-Surface Loading

The pressure-time loading of the back surface was handled somewhat differently than that of the front and top surfaces. Times of maximum pressure on the back surface, as calculated by the Armour Research Foundation prediction method, were not thought to be as reliable as for the other surface. Consequently, it was desirable to investigate the time of maximum pressure as well as the magnitude of the maximum pressure itself. The values presented herein for the back-surface maximum average pressure (p_b) are the peak pressures read directly from the average pressure-time curves for this surface. No extrapolation has been made except for those targets with a nominal zenith angle of 0 degree.

The relationships between the back-surface pressure ratio (p_b/p_m) and the apparent zenith angle are given in Figures 21 and 22 for burst heights of 38 and 64 feet, respectively. Each of these figures shows the effect of the three target lengths on the back-surface pressure ratio. However, only the individual data points for the 2-foot targets are shown since the scatter in the available data for this length precludes any implication of functional relationship. Those data points labeled LM are for targets situated where Mach-stem heights less than the target height existed.

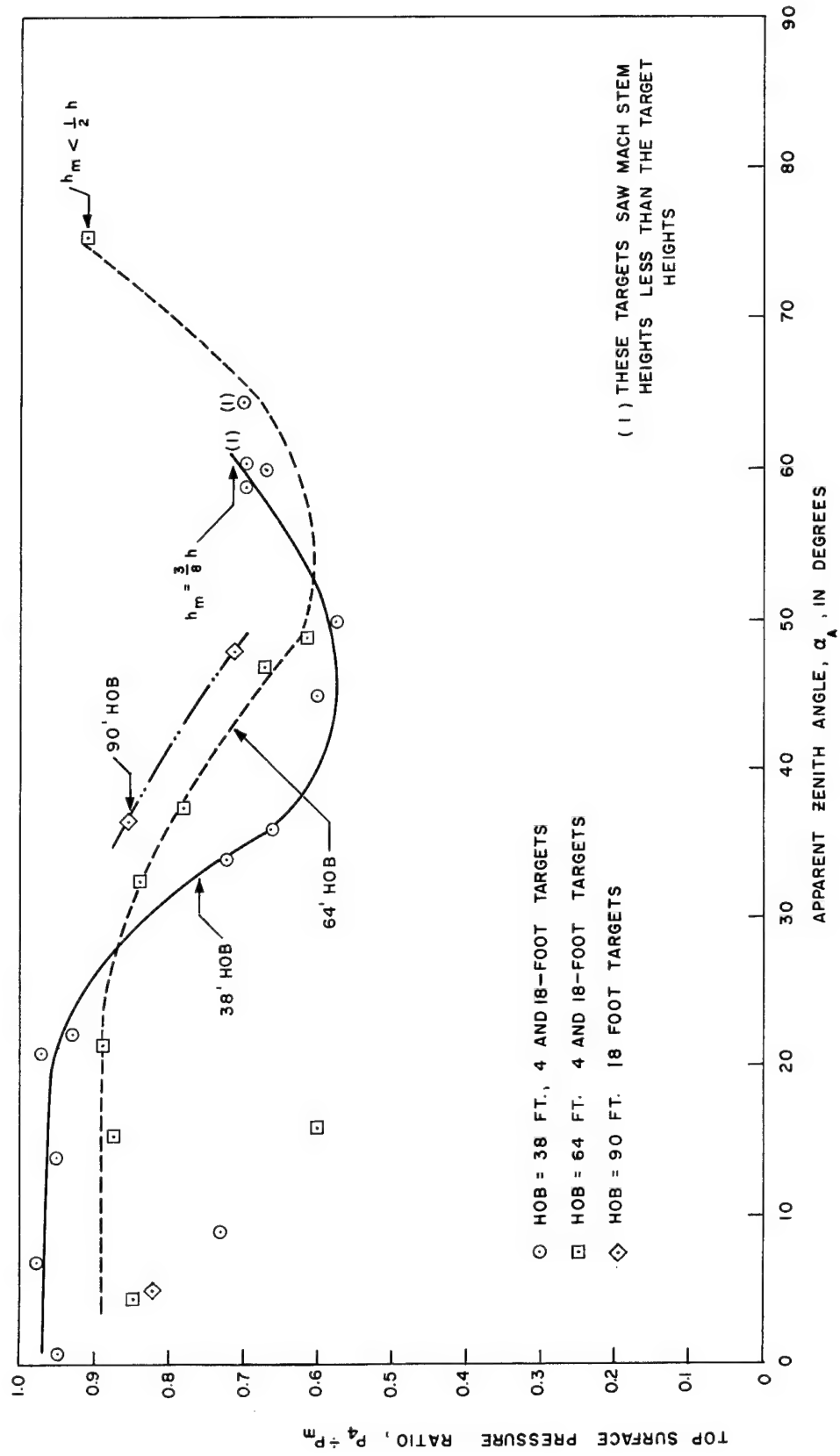

Figure 20. Relationship between top-surface pressure ratio, p_4/p, and apparent zenith angle, α_A, for various heights of burst

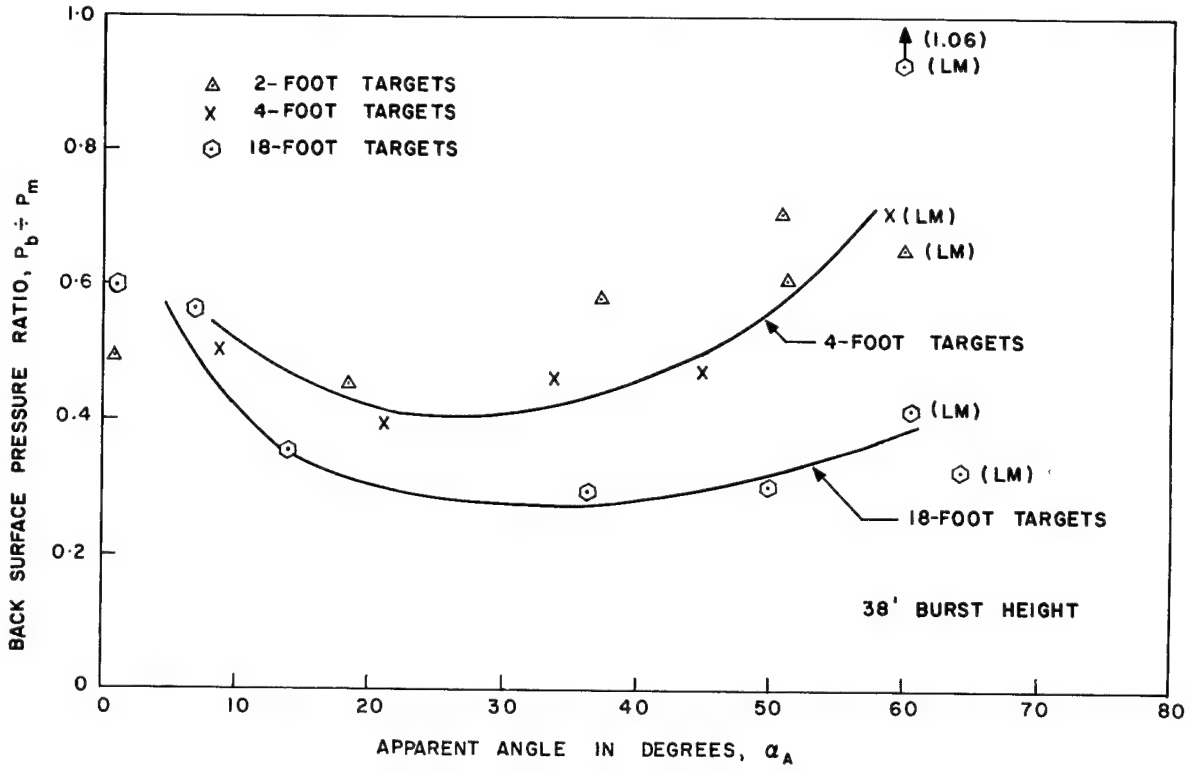

Figure 21. Relationship between back-surface pressure ratio, p_b/p, and apparent zenith angle, α_A, for a 38-foot burst height

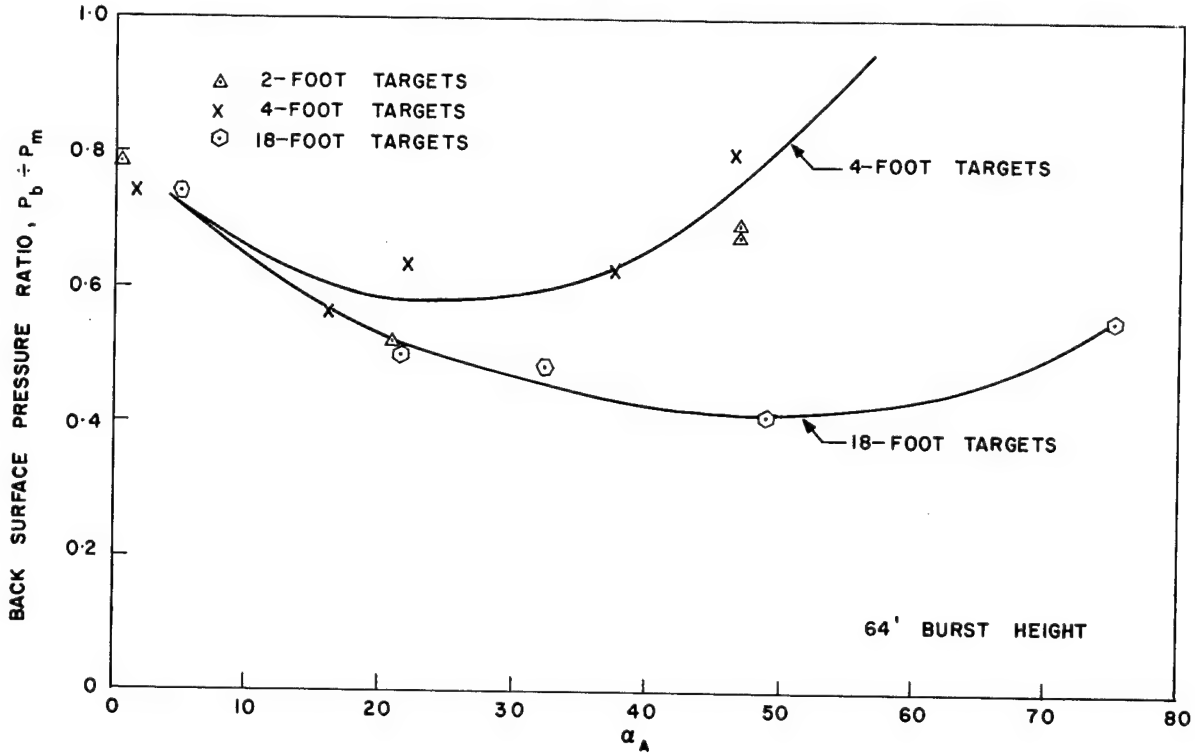

Figure 22. Relationship between back-surface pressure ratio, p_b/p, and apparent zenith angle, α_A, for a 64-foot burst height

Curves in Figures 23 and 24 show effects of apparent zenith angles for various heights of burst and hence shock strengths on the back-surface pressure ratios for 18- and 4-foot targets respectively. Inconsistencies in the back-surface data for the 2-foot targets make such a curve for this target length impractical. Figures 23 and 24 present the data for burst heights of 38 feet, and also 90 feet where available. The maximum pressure data for targets other than the 18-foot target lack consistency for the rear surface. However, the effects of target length and overpressure are indicated.

The time difference (t_b) between the arrival of the incident wave at the rear edge of the top surface and the occurrence of maximum pressure on the rear surface was determined from the average pressure-time plots. The ratio, t_b/t_1 is in the front-surface transit time and the apparent angles of incidence were studied to determine the effect of target length, peak overpressure, and zenith angle on t_b.

The relationships between t_b/t_1, and the apparent zenith angle for the burst height and various target lengths are shown in Figures 25, 26, and 27. Two points, shot Z-22, and Z-27, appear erratic on Figure 25. However, the average pressure-time plots for these two back surfaces have several maxima; the value of t_b used is the time to occurrence of the absolute maximum average pressure, which is not the first maximum for either shot. More important is that t_1 which decreases gradually with increasing zenith angle goes rapidly to zero between the point where the Mach stem forms and the point at which it reaches a height equal to that of the target.

Figure 28, a reproduction of the curves shown in Figures 25, 26, and 27, shows the effect of target length on the ratio t_b/t_1. The target data shown on Figure 28 are for the 64-foot burst height.

Since the data indicate that the pressure ratio for the back surface is more dependent on target size than for the front or top surface, it was of interest to examine the average back pressure-time pulse for various target lengths, subject to free-field conditions which are as similar as the data permit. Consequently, plots were constructed in which the average pressure on the back face divided by the peak overpressure was plotted as a function of time. Figures 29, 30, and 31 show the plots for various target lengths and for nominal zenith angles of 15, 30, and 45 degrees, respectively, and for a 38-foot height of burst. These plots indicate that for the conditions studied, the pulse shapes are similar for angles of 15 degrees and less. For larger angles, the 18-foot or two dimensional target experiences a similar pulse in the initial and final stages, but a more rounded midstage with a lower amplitude than either the 4-foot or 2-foot targets. Similarly, the amplitude of the 4-foot target is less than that of the 2-foot target.

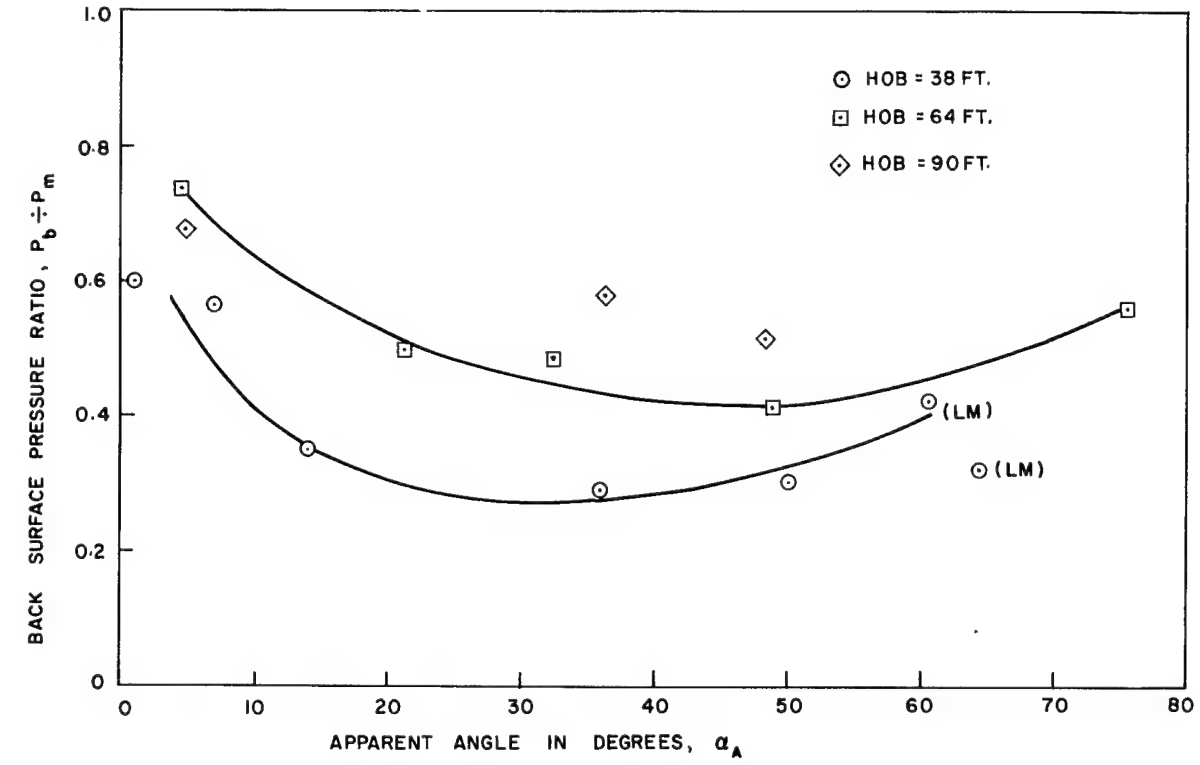

Figure 23. Effect of burst height on back-surface pressure ratio for 18-foot targets

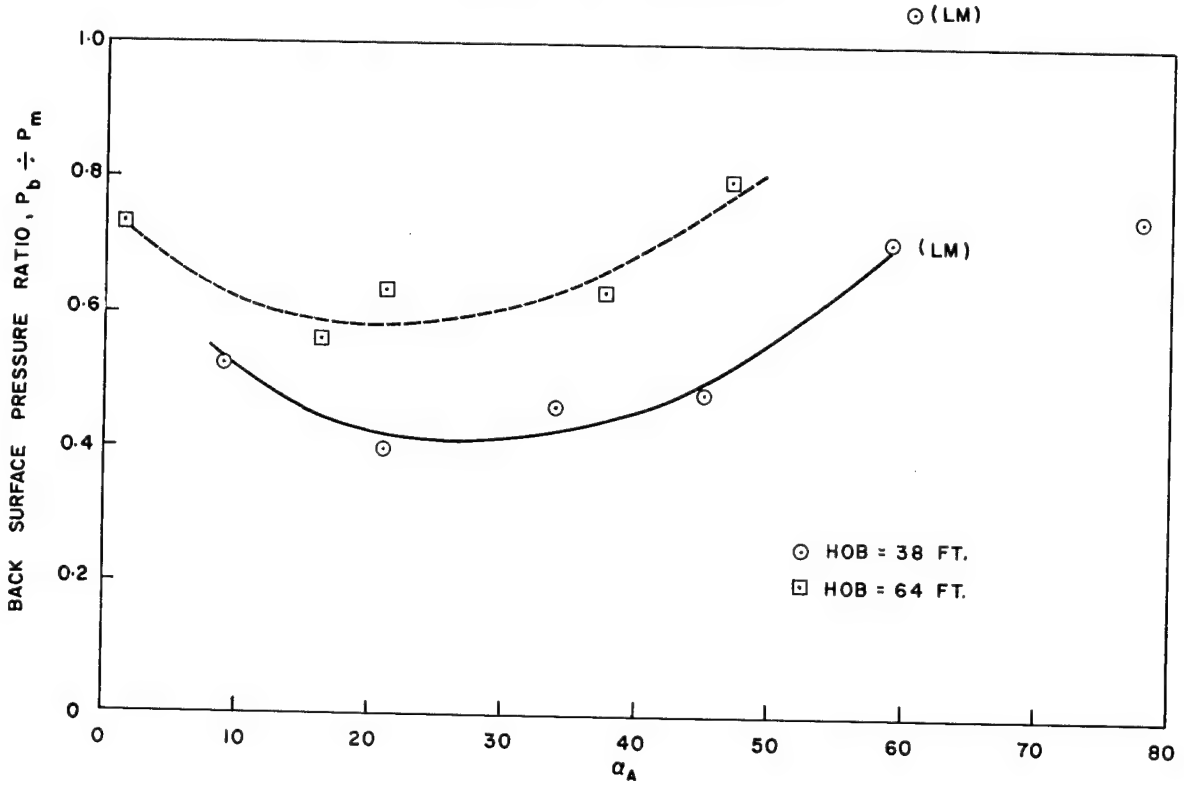

Figure 24. Effect of burst height on back-surface pressure ratio for 4-foot targets

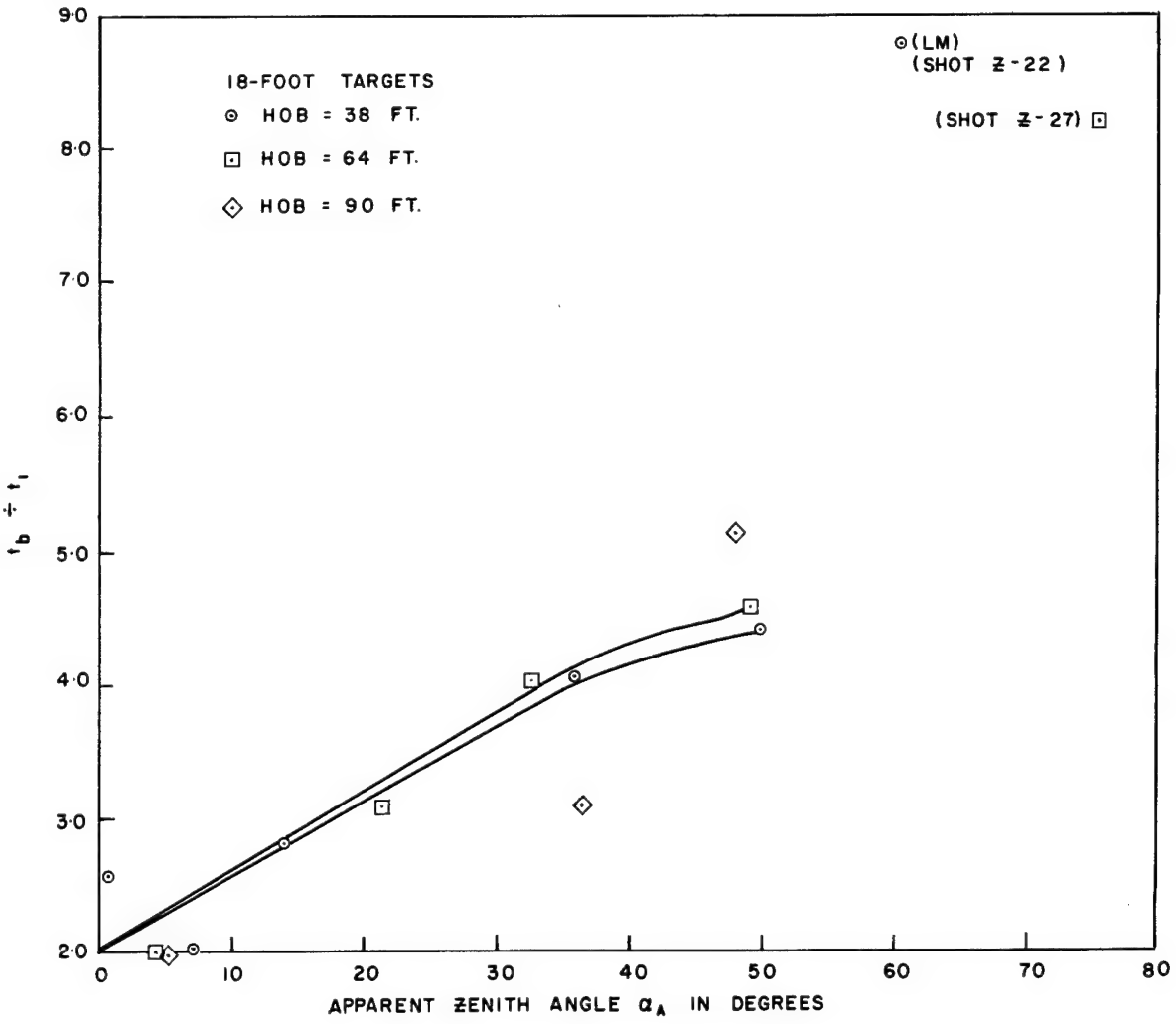

Figure 25. Relationship between t_b/t_1, and apparent zenith angle, α_A, for 18-foot targets

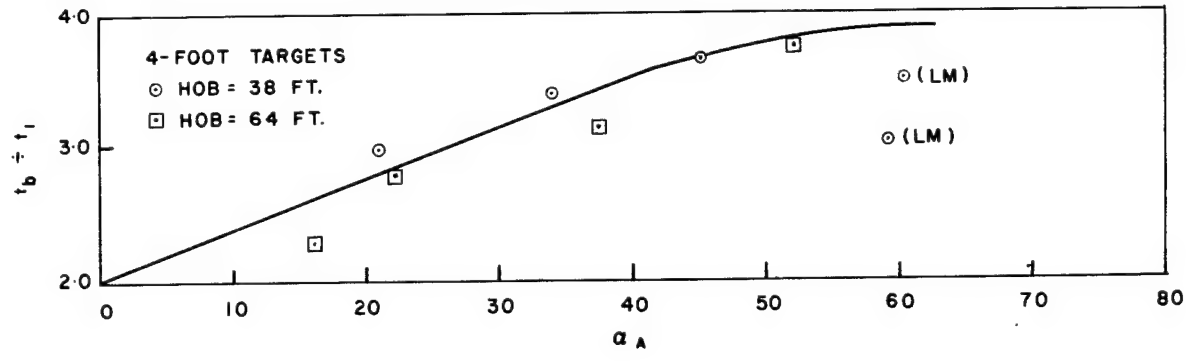

Figure 26. Relationship between t_b/t_1 and apparent zenith angle, α_A, for 4-foot targets

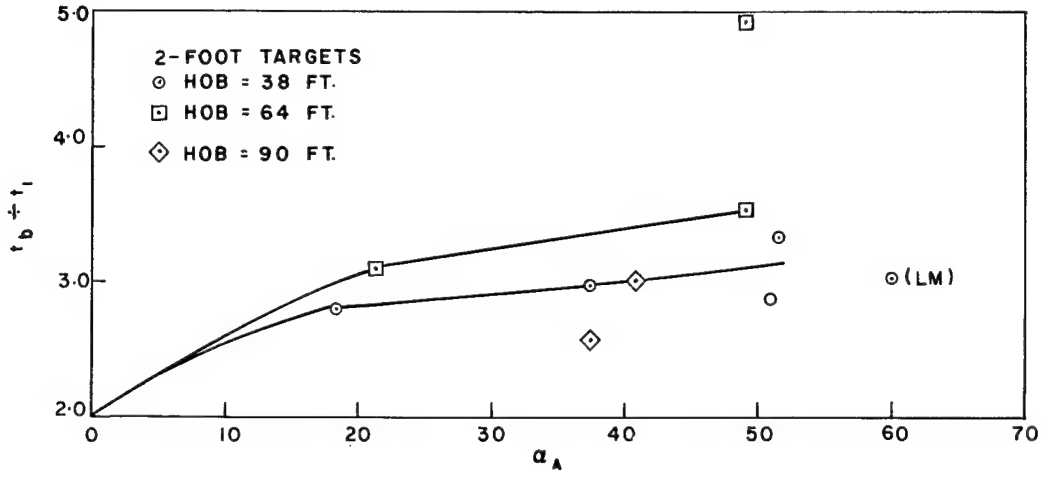

Figure 27. Relationship between t_b/t_1 and apparent zenith angle, α_A, for 2-foot targets

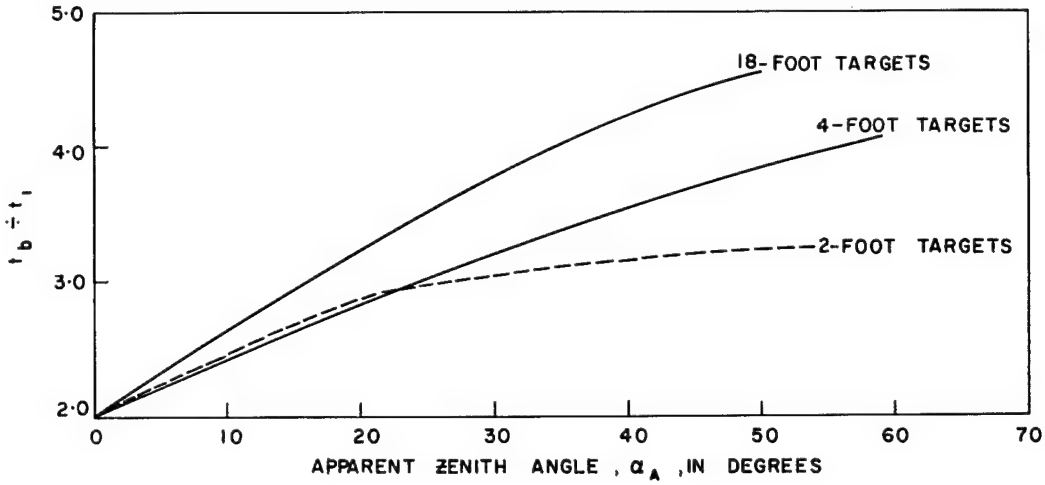

Figure 28. Effect of target length on t_b/t_1 at 64-foot burst height

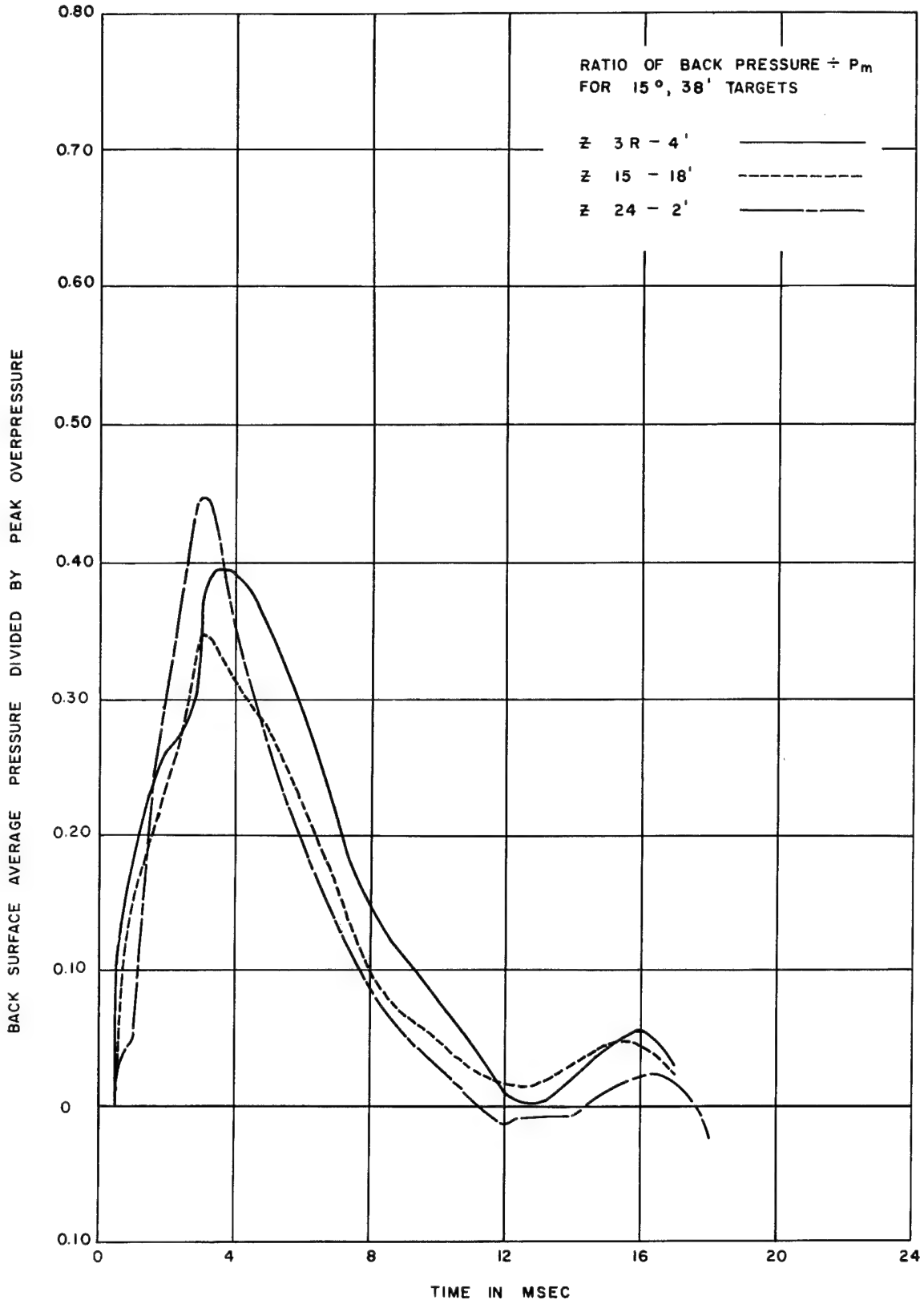

Figure 29. Comparison of back-surface pulse shapes at α = 15 degrees, 38 feet

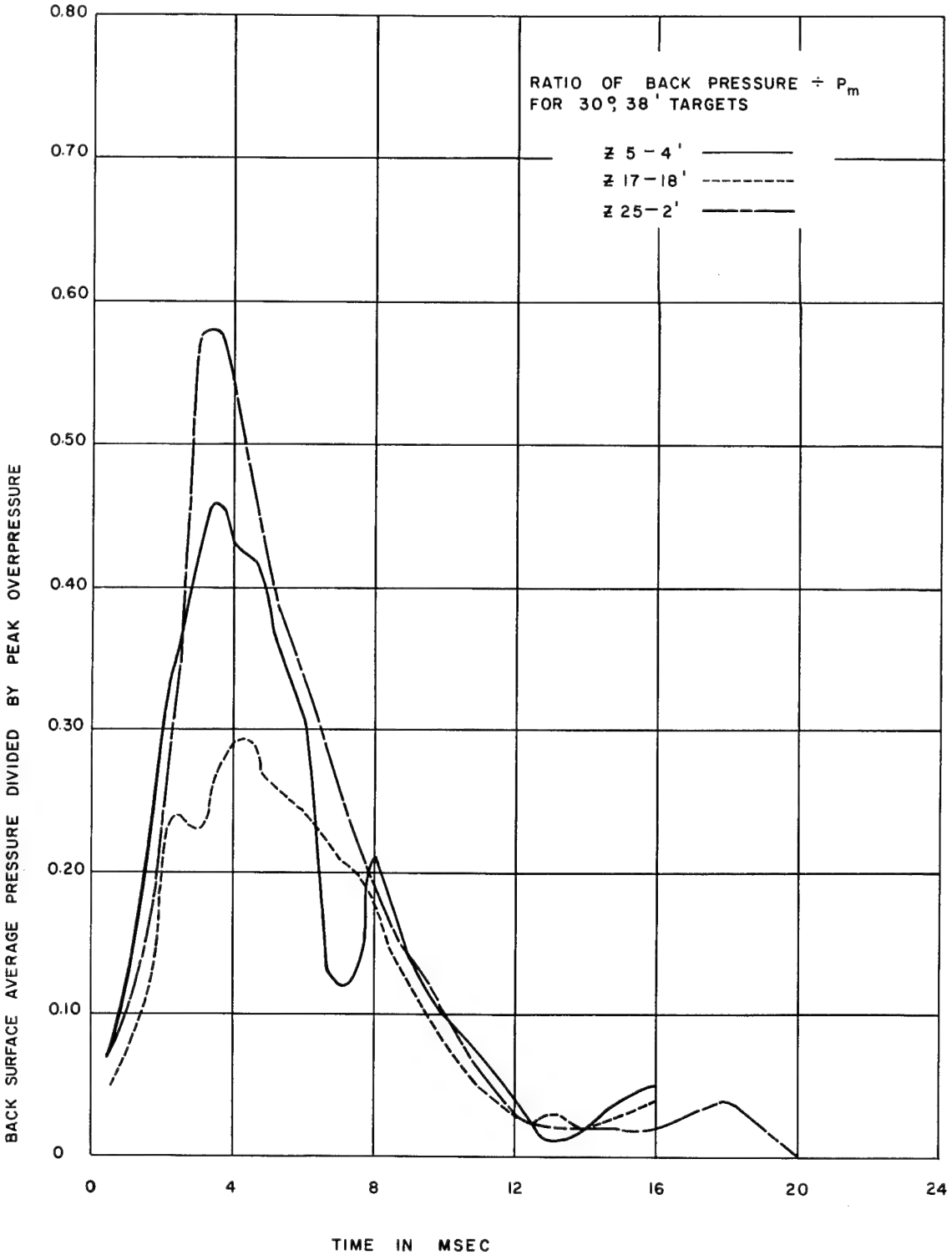

Figure 30. Comparison of back-surface pulse shapes at α = 30 degrees, 38 feet

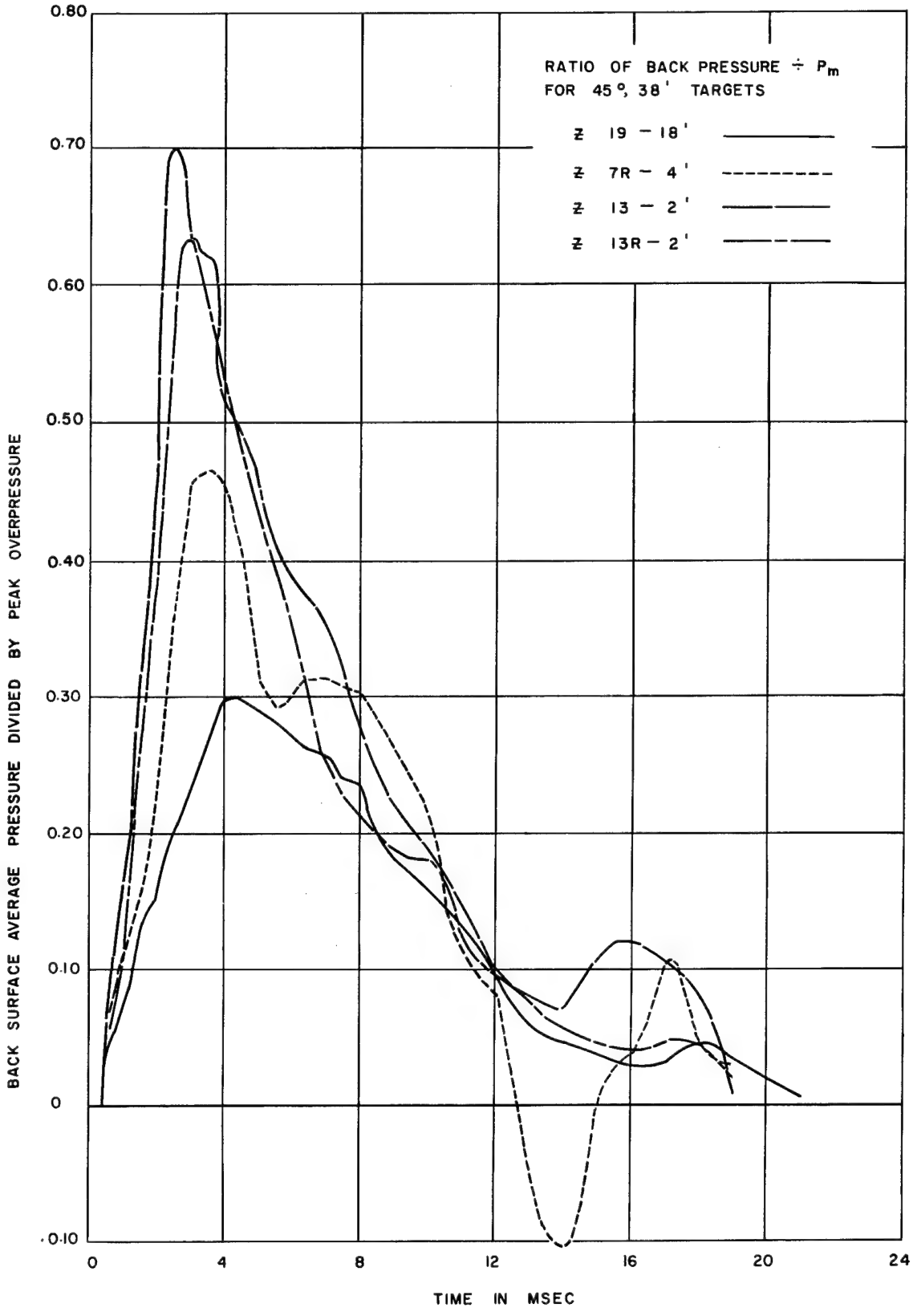

Figure 31. Comparison of back-surface pulse shapes at α = 45 degrees, 38 feet

Comparison with Theory

Procedures for predicting the average pressure-time loading on the various target surfaces for the regular reflection region are presented in Appendix A to Reference 1, and the theoretical calculations which follow were made using this method. These procedures are based principally on theoretical considerations at the shock front. Figure 32 summarizes the average pressure-time curves resulting from these theoretical considerations.

It is expected a priori that average pressures on the various target surfaces in these tests will be less than that predicted by theoretical considerations as a result of pressure decay occurring during the time necessary for the blast wave to transit a given surface. Further, these tests represent what is probably the lower limit of interest with respect to yield when scaled to nuclear detonations, while the assumptions upon which the theoretical considerations are based result in predictions that represent the opposite limit. It is therefore necessary that the tests reported herein be placed in proper perspective by some quantitative measure related to pressure decay during the transit of the blast wave over a given surface. Since the free-stream pressure decays behind the shock front in a somewhat regular fashion, the ratios t_1/t_+ and t_4/t_+ (t_+ = positive phase duration) are used to correlate these tests with theoretical predictions.

In comparing the results of these tests with theory, pressures p_1 and p_2 are the relevant pressures on the front face. Since the gauge response was not rapid enough to determine p_1, only the extrapolated values for p_2 are available for this purpose. Table VII summarizes all data for the front surface of the 18-foot targets in the regular reflection region. In this table the calculated and measured values of p_2 are tabulated in columns 5 and 6 respectively. The ratios of both to the measured maximum free-field pressure (p_m) are shown in columns 7 and 8. The difference between columns 7 and 8, shown in column 9, is a measure of the agreement between the measured and calculated values. Since both values are normalized to the measured peak overpressure (p_m), the difference cannot be due to inability of the gauges to respond to the peak pressure. Rather, it is probably due either to the fact that p_2 (measured) is an average of the values of five gauges during one transit time, or to an overestimate in the calculation of p_2. The ratio of front-surface transit time (t_1) to the positive phase duration in the free stream (t_+) is listed in column 11. The pressures listed in column 10 are the maximum pressures occurring on gauge No. 1 which was the gauge nearest the re-entrant corner of the front face (see Figure 4). Gauge No. 1 was located 4 inches above the horizontal and recorded the reflected pressure at a time approximately equal to t_1.

Comparison of the maximum pressure measured at gauge No. 1 and the calculated value of p_2 indicates that reflected pressures comparable with those predicted by theory occur in the re-entrant corner. However, comparison of the measured and calculated values of p_2 indicates that for the values of t_1/t_+ and shock strength used in these experiments, the rapid decay

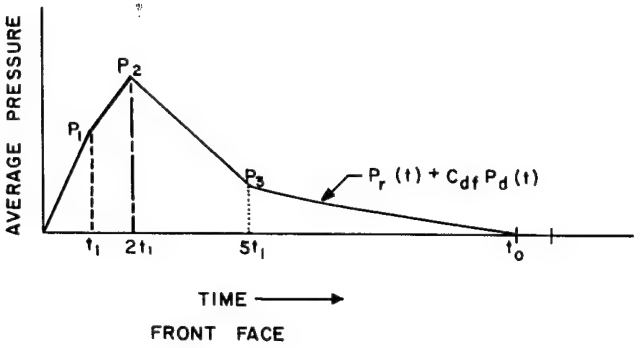

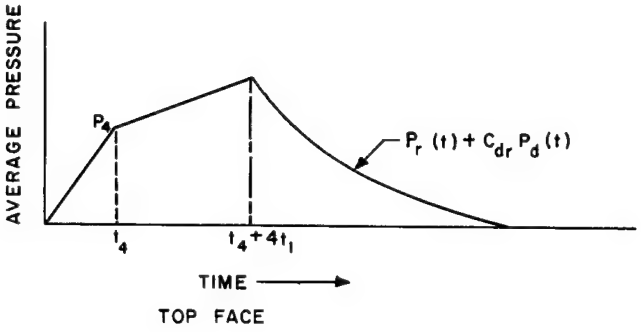

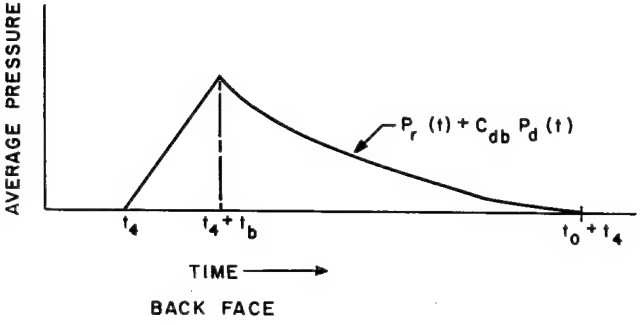

$$P_1 = P_m \left[\left(1 - \frac{\alpha}{90}\right) + \left(\frac{6+8\xi}{6+\xi}\right)\left(\frac{\alpha}{90}\right)\right]$$

$$P_2 = \frac{3}{4} P_r'' + \frac{1}{4} P_1$$

WHERE

$$P_r'' = P_m \left[\frac{\xi(\xi'\xi'^*)^{\frac{3}{2}} - 1}{\xi - 1}\right]$$

$$\xi = \frac{P_m + P_o}{P_o}$$

$$\xi' = \frac{P + P_o}{P_m + P_o}$$

$$\xi'^* = \frac{\alpha}{90}(\xi - 1) + 1$$

$$P_4 = P_m \left[\left(\frac{\alpha}{90}\right) + \left(1 - \frac{\alpha}{90}\right)\left(\frac{6+8\xi}{6+\xi}\right)\right]$$

$$t_b = \frac{2h \cos\alpha}{U}\left(1 - \frac{\alpha}{\alpha_x}\right) + \frac{5h}{U_m}\left(\frac{\alpha}{\alpha_x}\right)$$

α_x IS THE EXTREME VALUE OF α FOR A GIVEN SHOCK STRENGTH FOR WHICH REGULAR REFLECTION OCCURS

C_{df}, C_{dr} AND C_{db} ARE FRONT, TOP AND BACK SURFACE DRAG COEFFIENTS RESPECTIVELY

$P_d(t)$ = DYNAMIC PRESSURE

$$U_m = 422\sqrt{1+\xi^2}$$

Figure 32. Summary of theoretical predictions in the regular reflection region from Reference 8 1 - ?

TABLE VII

Comparison of Front-Surface Data with Theoretical Prediction

(1) Shot	(2) Nominal angle (deg)	(3) Height of burst (ft)	(4) p_m	(5) p_2 (measured)	(6) p_2 (calculated)	(7) $\frac{p_2 \text{ (measured)}}{p_m}$	(8) $\frac{p_2 \text{ (calculated)}}{p_m}$	(9) Column 8 minus Column 7	(10) Maximum pressure on gauge 1	(11) t_1/t_+
13	0	38	46.2	36.0	46.2	0.78	1.00	0.22	47	0.0955
13R	0	38	55.5	38.6	55.5	0.70	1.00	0.30	49	0.1163
12	0	64	13.2*	13.2	13.2	1.00	1.00	0	20	0.1115
14	0	90	10.9	9.4	9.4	0.86	0.86	0	9.7	0.1059
15	15	38	44.2	40.1	78.0	0.91	1.76	0.85	77	0.0814
16	15	64	12.9	13.0	19.0	1.01	1.46	0.45	19	0.0786
17	30	38	33.3	39.8	67.0	1.20	2.01	0.81	65	0.0946**
18	30	64	9.3	12.1	14.7	1.30	1.58	0.28	16	0.0708
20	30	90	5.6	8.1	8.3	1.45	1.48	0.03	10	0.0626
19	45	38	20.6	35.0	47.4	1.70	2.30	0.60	49	0.0736
21	45	64	7.0	10.8	12.2	1.54	1.74	0.20	12	0.0488†
23	45	90	4.5	6.5	7.1	1.44	1.58	0.14	8	0.0630
27	$66^{\circ}20'$	64	3.4	6.6	7.3	1.94	2.15	0.21	10.5	0.0249

*Only one free-field pressure measurement obtained

**t_+ less than expected

†t_+ larger than expected

behind the reflected shock front as it moves out of the re-entrant corner results in measured values of p_2 as much as 50 percent smaller than those calculated. It appears as if the decay behind the shock is mainly dependent upon the shock strength, since the values for t_1/t_+ do not vary much for a given angle.

Theoretical considerations indicate that the average pressure on the top surface rises linearly to a pressure, p_4, at a time (t_4) when the incident wave has traversed the top surface. Subsequently the pressure reaches a maximum equal to the free-stream overpressure plus a drag contribution at a time equal to $t_4 + t_1$. In these HE experiments, the peak average pressure on the top surface occurred at a time equal to t_4; and although subsequent maxima occurred in the average pressure-time curves, they were associated with the arrival of the reflected wave at the top surface and always smaller in magnitude than p_4. Table VIII compares measured and calculated values of p_4. Column 9 shows that the agreement is quite good and well within the scatter to be expected on this experiment.

As in the case of the top surface, the peak average pressure on the rear surface is theoretically considered to be a function of dynamic pressure as well as of overpressure. Since no dynamic pressures were measured, comparison between calculated and observed values is not warranted. However, a comparison of the time that maximum average pressure occurs on the back face (t_b) from observation and theoretical calculations is made in Table IX. The agreement between observed and calculated values is somewhat better than for the top pressure.

TABLE VIII

Comparison of Top-Surface Data with Theoretical Prediction

(18-foot target)

(1) Shot	(2) Nominal angle (deg)	(3) Height of burst (ft)	(4) Peak over-pressure	(5) p_4 (measured)	(6) p_4 (calculated)	(7) $\frac{p_4 \text{ (measured)}}{p_m}$	(8) $\frac{p_4 \text{ (calculated)}}{p_m}$	(9) Column 8 minus Column 7	(10) t_4/t_+
15	15	38	44.2	42.0	39.8	0.95	0.90	-0.05	0.0205
16	15	64	12.9	11.3	11.3	0.88	0.88	0.00	0.0318
17	30	38	33.3	21.9	26.6	0.66	0.80	0.14	0.0682*
18	30	64	9.3	7.2	7.8	0.77	0.84	0.07	0.0492
20	30	90	5.6	4.8	4.4	0.86	0.79	-0.07	0.0461
19	45	38	20.6	11.7	16.2	0.57	0.79	0.22	0.0465
21	45	64	7.0	4.3	5.3	0.61	0.76	0.15	0.0573**
23	45	90	4.5	3.2	3.4	0.71	0.76	0.05	0.0560
27	$66^{o}20'$	64	3.4	3.1	2.9	0.91	0.85	-0.06	0.0878

*t_+ less than expected

**t_+ larger than expected

TABLE IX

Comparison of Measured and Calculated Values for t_b

(18-foot targets)

Shot	Zenith angle (deg)	Burst height (ft)	t_b calculated (msec)	t_b measured (msec)	Percent difference between calculated and measured values of t_b
15	15	38	2.51	3.15	-25.5
16	15	64	4.23	4.00	+5.5
17	30	38	4.30	4.10	+4.9
18	30	64	5.43	4.95	+8.8
20	30	90	5.90	4.20	+28.8
19	45	38	- - *	4.07	- -
21	45	64	6.64	6.05	+8.9
23	45	90	6.88	6.30	+8.4
27	$66^{o}20'$	38	- - *	5.80	- -

*Calculation of t_b has no meaning since the theoretical value of α_x associated with the calculated shock strength is less than the zenith angle. α_x is the extreme value of α for a given shock strength for which regular reflection occurs.

CH V -- BLAST LOADING OF TARGET SURFACES IN THE LOW MACH-STEM REGION

Scope

Thirteen targets were located at horizontal distances from ground zero such that the Mach stem had formed before the blast wave arrived at the target. Three situations were planned for each target length, so that at the targets the stem height would be less than the target height in one case, slightly greater than the target height in another, and several times higher than the target height in the third. The data from these shots were used in the same manner as that described in Chapter IV for the regular reflection region. Average pressure-time curves and space-time-of-arrival plots were constructed, and the usual extrapolations were made for the front and top surfaces.

Mach-Stem Height

Two data sources were available for determining the Mach-stem height on some shots: (1) the Mach-stem data described in Chapter III determines the path of the triple point; (2) for those cases where the Mach-stem height was less than the target height, space-time-of-arrival plots could be used. The agreement between the Mach-stem heights shown in Figure 11 and those determined from the space-time-of-arrival plots show about the same dispersion, with two exceptions, as the agreement between different shots used to construct Figure 11. Mach-stem heights from both sources are tabulated in Table X. Of the two exceptions, only shot Z-26 is listed in Table X. The other exception, shot Z-27, was the only target in the low Mach region using a burst height of 64 feet. Data in Chapter III for a 64-foot height of burst indicates that the stem height at 142 feet from ground zero should have been about 1 foot. However, because of the small angle between the shock front and the front surface (20 degrees), a Mach stem is difficult to determine from the space-time-of-arrival plot for shot Z-27. It can be said only that if a Mach stem did exist, it was less than 1 foot high. For this reason, the 18-foot target on shot Z-27 has been included among data for the regular reflection region.

TABLE X

Summary of Data for Targets Located in the Low Mach-Stem Region
(height of burst is 38 feet)

Shot No.	Target (ft)	Horizontal distance from GZ in feet	Mach-stem height in feet		Ratio of Mach-stem height to target height	p_2/p_m	p_r/p_m	p_2/p_r	p_4/p_m	p_b/p_m
			From space-of-time-arrival plots	From Mach-stem height data						
Z-15	2	66	1.17	0.73	0.36	1.92	2.68	0.716	0.65	0.65
Z-17	2	92		3.32	1.61	2.43	2.50	0.972	0.71	0.68
Z-19	2	142		>10	>5.0	2.22	2.28	0.974	0.97	0.74
Z-9	4	66	0.65	0.73	0.36	2.18	2.59	0.842	0.70	0.70
Z-9R	4	66	0.79	0.73	0.36	2.01	2.69	0.747	0.68	1.06
Z-10R	4	92		3.32	1.61	2.30	2.37	0.970	0.88	0.58
Z-10RR	4	92		3.32	1.61	2.29	2.50	0.916	0.78	0.63
Z-11R	4	142		>10	>5.0	2.19	2.24	0.977	0.93	0.68
Z-22	18	66	0.75	0.73	0.36	1.90	2.63	0.722	0.70	0.42
Z-26	18	80	0.92	1.96	0.98	1.99	2.55	0.780	0.69	0.32
Z-24	18	92		3.32	1.61	2.14	2.48	0.863	0.76	0.40
Z-25	18	142		>10	>5.0	2.15	2.26	0.951	0.86	0.46

Mach-stem height data were collected, as indicated in Chapter III, out to a horizontal distance of about 107 feet for the 38-foot burst height. At this range the Mach-stem height was about 5 feet. The most distant targets for this burst height were 142 feet from ground zero, and it is estimated that the height of the Mach stem was greater than 10 feet at this point.

Target Surface Loading

The average pressure-time loading was studied in the same manner as for the regular reflection region. The results of this analysis are shown in Table X. The notation is the same as used before, p_2 is the peak pressure on the front surface, p_4 is the peak pressure on the top surface, and p_b is the peak pressure on the rear surface. The quantity p_r is the calculated reflected pressure resulting from normal incidence of p, the measured peak overpressures. It was calculated from the expression

$$p_r = 2p\left(\frac{4p + 7P_o}{p + 7P_o}\right)$$

where P_o is the ambient pressure.

Examination of the data in column 8 of Table X indicates that when the Mach stem is about 0.4 times the target height, the peak average pressure on the front surface is about three-quarters of that which would be expected if p were normally reflected. Columns 8 and 9 indicate the influence of Mach-stem formation on the front and top respectively. Generally, as one would expect, the pressure on the front approaches the peak reflected pressure and on the top, the peak free-field pressure.

Column 11 summarizes the effect of Mach-stem height on the back surface. No effect of Mach-stem height is apparent in these data.

Samples of the average pressure-time plots for targets in this region are included in Appendix A.

CH VI -- DURATION EFFECTS

Since it is known that the duration of positive pressure on the front surface of a target can be less than the duration of the positive phase for the incident blast wave in the Mach region, pulse durations on the front surface were determined experimentally to evaluate this effect in the regular reflection region.

The positive phase duration for the free-field blast wave was found on each shot by averaging the durations from the three ground baffle gauges. The duration of the positive pressure on the front surface was found by averaging the duration of the five pressure gauges on that surface of the target. A second pressure rise, commonly termed "Pete", near the end of positive phase occurs frequently in the blast wave resulting from HE detonations (see Reference 11). Consequently, the pressure time records for individual gauges were smoothed through "Pete" to zero pressure, and a corrected pressure duration (t_+) which excluded the durations of "Pete" was determined. For each target, ratios of the positive pressure duration on the front surface to the duration of the incident blast wave (t_f/t_+) along with $\frac{Ut_+}{h}$ were computed. (U is the velocity determined from the space-time of arrival plots associated with the apparent angle, t_+ is the corrected positive phase duration, t_f is the corrected positive phase duration on the front surface, and h is the target height.) For the 2-foot target, $\frac{Ut_+}{L/2}$ was calculated, L being the length of the target. These data are summarized in Tables XI and XII for targets in regular reflection and Mach regions respectively. Also presented in Tables XI and XII are the ratios of corrected durations of the back-surface positive pressure to the positive pressure in the incident wave (t_r/t_+).

The data for all targets in the Mach region when the height of the stem exceeds the target height are shown in Figure 33, along with data from other HE studies in this region. The data from other studies are the same data points identified in Figure 1. Examination of Figure 33 shows about the same trend observed in previous HE diffraction studies in the Mach region as one would expect. There is no discernible difference due to variation in target length and the low Mach-stem heights used in this series of shots. None of the values from this series fell as low (~ 0.6) as those from the earlier tests, despite their being at comparable overpressures.

TABLE XI

Summary of Pulse Duration Data for the Regular Reflection Region

Shot	Nominal angle (deg)	Height of burst (ft)	Target (ft)	t_f/t_+	t_r/t_+	* Ut_+/h	$\frac{t_f - t_1}{t_+}$
13	0	38	18	1.00	1.01	10.08	0.91
13R	0	38	18	1.07	1.02	8.09	0.95
12	0	64	18	1.21	1.19	8.77	1.09
14	0	90	18	1.14	1.14	9.17	1.04
1	0	38	4	1.90	0.97	10.86	0.82
2	0	64	4	1.98	1.02	10.83	0.89
22	0	38	2	1.00	0.99	17.56	0.88
18	0	64	2	1.03	1.12	19.52	0.93
23	0	90	2	1.12	1.06	18.06	1.01
15	15	38	18	0.77	0.92	11.93	0.69
16	15	64	18	0.96	1.02	11.46	0.88
3R	15	38	4	1.00	1.07	8.67	0.89
4	15	64	4	1.03	0.98	9.72	0.93
27	15	64	4	1.03	1.09	9.73	0.93
24	15	38	2	1.00	0.98	22.80	0.91
21	15	64	2	0.96	1.02	24.74	0.89
17	30	38	18	0.92	1.08	8.54	0.83
18	30	64	18	0.87	1.06	10.83	0.79
20	30	90	18	0.80	0.89	12.82	0.73
5	30	38	4	0.98	1.11	9.56	0.89
6R	30	64	4	0.86	1.01	11.12	0.78
25	30	38	2	1.02	1.08	17.73	0.93
12	30	64	2	0.88	0.91	39.06	0.84
14	30	90	2	1.00	1.02	19.66	0.91
19	45	38	18	0.82	1.15	8.86	0.74
21	45	64	18	0.81	0.99	13.28	0.76
23	45	90	18	0.91	0.99	10.53	0.85
7R	45	38	4	0.74	0.91	10.79	0.68
8	45	64	4	0.89	0.90	13.16	0.83
13	45	38	2	0.96	1.12	17.90	0.89
13R	45	38	2	0.96	1.17	19.08	0.87
16	45	64	2	1.05	1.12	21.67	0.99
20	45	90	2	0.92	1.05	26.73	0.87
27	$66^{\circ}20'$	64	18	0.89	1.02	10.07	0.86

*$\frac{Ut_+}{L/2}$ for 2-foot target

TABLE XII

Summary of Pulse Duration Data for Low Mach and Mach Region

Shot	Nominal angle (deg)	Mach-stem height	Height of burst (ft)	Target (ft)	t_f/t_+	t_r/t_+	$*Ut_+/h$
22	60		38	18	0.73	0.83	16.53
9	60		38	4	0.92	0.97	8.86
9R	60		38	4	1.00	1.09	9.26
15	60		38	2	1.07	1.23	15.08
26	64°40'		38	18	0.81	1.00	11.24
24	67°30'		38	18	0.88	0.89	11.40
10R	67°30'		38	4	0.75	0.95	13.45
10RR	67°30'		38	4	0.82	0.90	12.28
17	67°30'		38	2	0.97	1.00	22.30
25	75		38	18	0.81	0.96	12.30
11R	75		38	4	0.75	0.92	16.07
19	75		38	2	0.98	1.06	23.42

*$\frac{Ut_+}{L/2}$ for 2-foot target

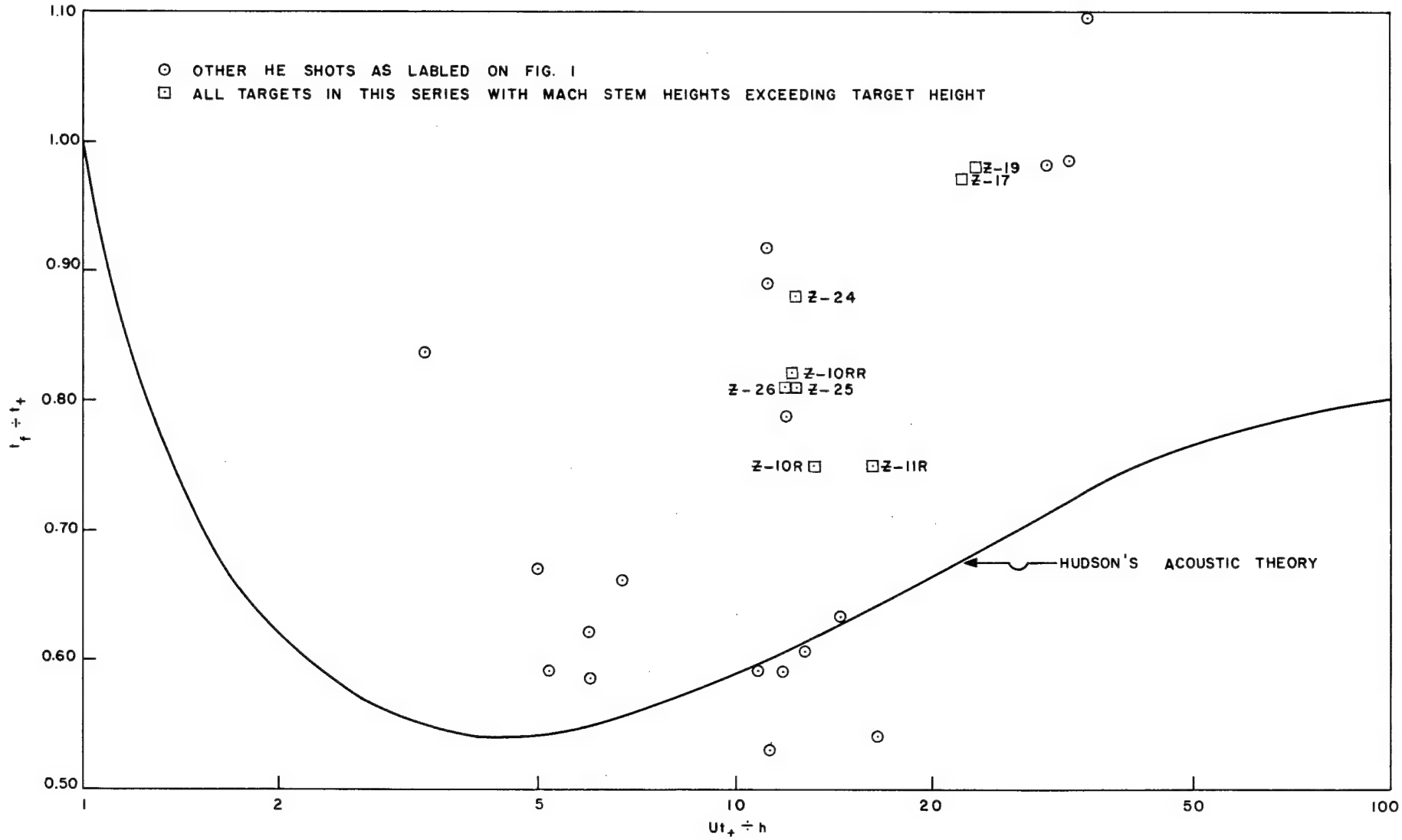

Figure 33. Duration effects in the Mach region

The shortening of the front-surface positive-pressure duration in the regular reflection region was examined in a manner similar to that used for the Mach region. Figure 34 shows the ratio t_f/t_+ plotted as a function of Ut_+/h for those targets in the regular reflection region. Examination of Figure 34 indicates that the duration of the positive pressure on the front surface is shortened in much the same manner as it is for Mach reflection but by a lesser amount. Since t_f was determined by averaging the positive durations of the five gauges on the front surface, $\frac{t_f - t_1}{t_+}$ is perhaps a more reasonable parameter than t_f/t_+ with which to investigate pulse shortening in the regular reflection region. This is true, since it would be expected that an individual gauge would record the ground reflected wave duration, shortened if applicable, plus some portion of the incident wave duration depending on the distance from the gauge position to the re-entrant corner. If it is assumed that the reflected wave has a constant duration during the transit time up the front surface of the target, then the duration of the reflected wave would be approximately equal to $t_f - t_1$. Figure 35 shows the ratio $(t_f - t_1)/t_+$ as a function of Ut_+/h. Here the amount of duration shortening is more in keeping with that in the Mach region.

Although there is considerable scatter in the data presented in Figures 34 and 35, it appears that shortening may also be related to the zenith angle. This dependence upon zenith angle is more apparent if the data are rearranged as shown in Table XIII. Here the data are divided into two groups. One group averages the values of Ut_+/h and $(t_f - t_1)/t_+$ for each nominal zenith angle for all 4- and 18-foot targets. The second group shows these values for the 2-foot targets. This is reasonable since the value of Ut_+/h for 4-foot and 18-foot targets is generally about 10 ± 2, whereas for the 2-foot targets the value of $\frac{Ut_+}{L/2}$ is generally more than twice that value. Examination of the 4- and 18-foot target data in Table XIII shows that although Ut_+/h (average) is increasing slightly with the zenith angle, the ratio $t_f - t_1/t_+$ (average) decreases. Hence, it is apparent that within the range of the spacial distribution of the shock wave (Ut_+) occurring in these tests, the shortening of positive pressure duration on the front face is dependent also on the zenith angle. The data for the 2-foot target shows little dependence of duration shortening on zenith angle. This is not unexpected, since for a cube, horizontal flow around the ends is more important relative to flow over the top, and horizontal flow is less sensitive to the effect of a change in zenith angle.

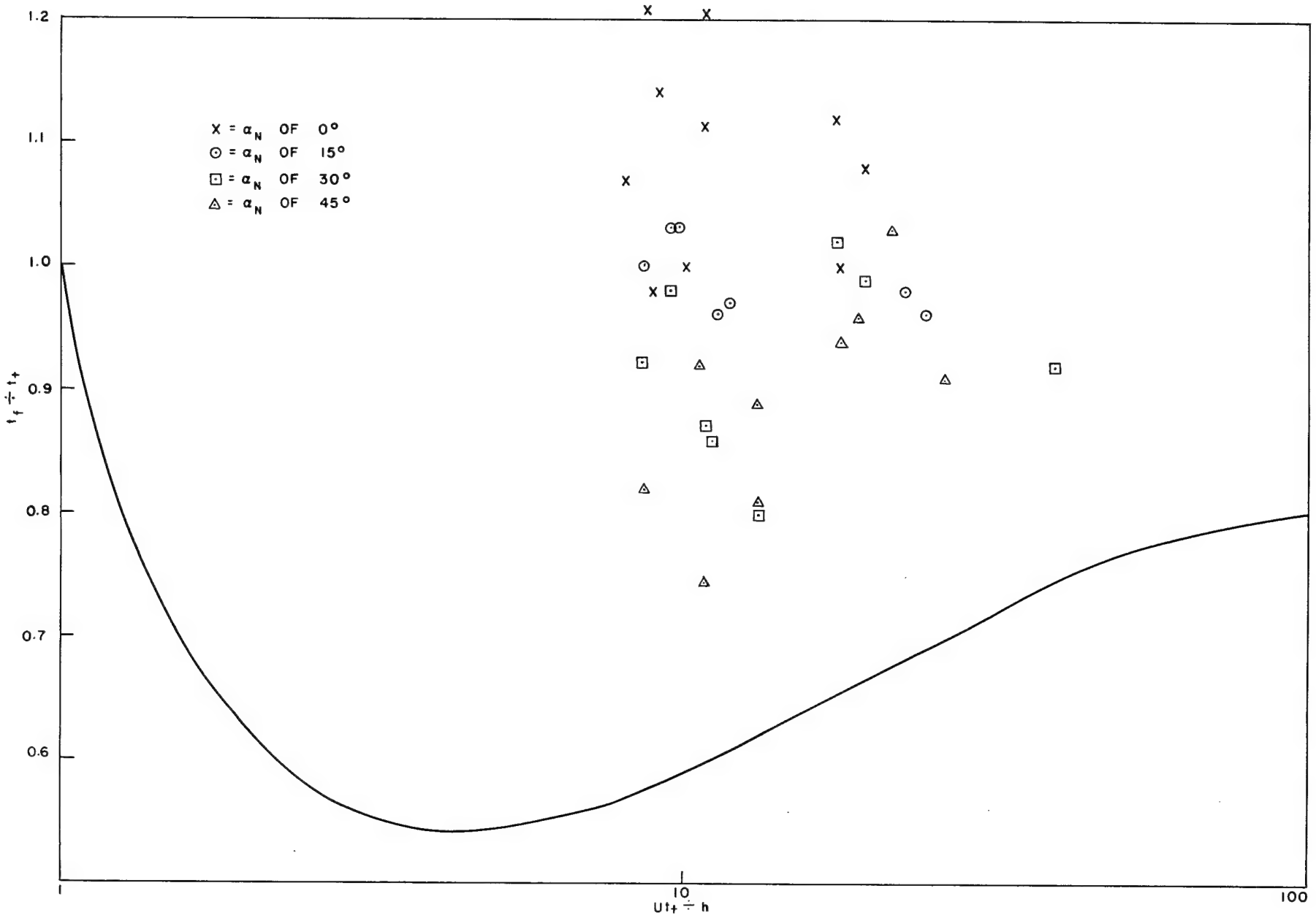

Figure 34. Duration effects in the regular reflection region

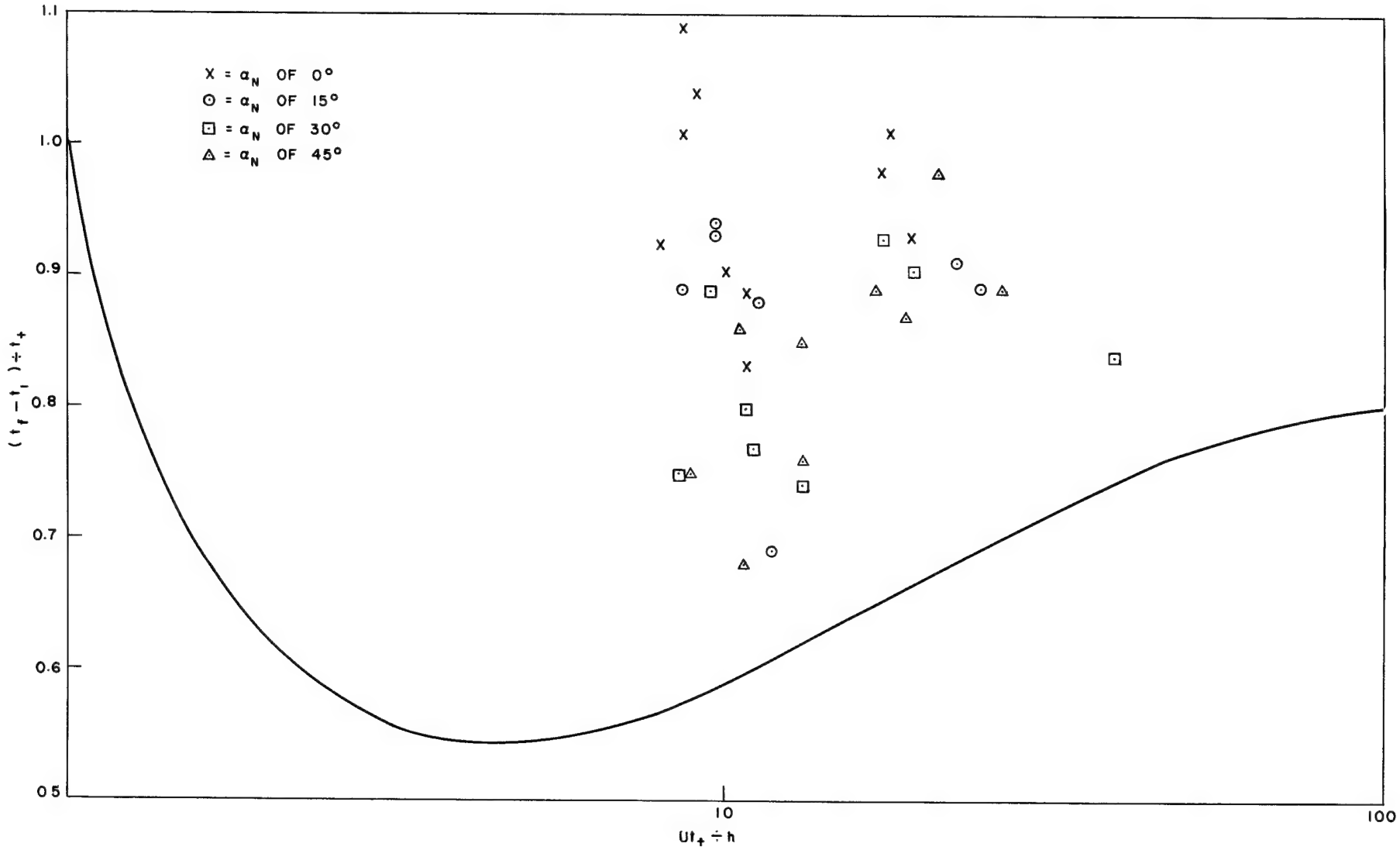

Figure 35. Relationship between $(t_f - t_1)/t_+$ and Ut_+/h

TABLE XIII

Effect of Zenith Angle on Front Surface Duration

Nominal zenith angle (deg)	Averaged 18- and 4-foot data		Averaged 2-foot data	
	Ut_+/h	$t_f - t_1/t_+$	$Ut_+/L/2$	$t_f - t_1/t_+$
0	9.63	0.95	18.47	0.94
15	10.30	0.86	23.77	0.90
30	10.57	0.80	25.48	0.89
45	11.32	0.77	21.44	0.91

CH VII -- END EFFECTS

The 4-foot targets on shots Z-1 through Z-11R were instrumented with a band of pressure-time gauges near the end of the target. This arrangement provided pressure-loading data for comparison with that obtained near the centerline of the targets. The end gauge band is described in Chapter II. Only two gauges were placed on the front surface in the end band, and these were located 4 and 20 inches from the re-entrant corner, as were gauges 1 and 4 of the centerline gauge band. Six gauges were used on each of the top and back surfaces in the end band. They were spaced as those of the centerline band.

The data from the end gauge band were used to construct average pressure-time plots for the various surfaces in the manner described in Chapter IV for the centerline band. From these plots, peak average pressures on the front (p_2'), top (p_4'), and back (p_b') surfaces were determined as before. Total impulse for the positive phase was determined for both the end and centerline gauge band on all surfaces. To measure the difference between the average pressure-time pulse near the target end and that on the centerline, ratios of maximum average pressure and positive-phase total impulse on the centerline gauge band to the same values on the end gauge band were computed. Table XIV summarizes these computations. (In Table XIV the symbols I_f, I_t, and I_b are the positive-phase total impulses on the centerline front, top, and back surfaces respectively; the primed terms are for the end band.)

With the exception of shots Z-4 and Z-9, no significant variations from unity in the ratios p_2/p_2' and I_f/I_f' occur in these data. One shot Z-4, gauges at positions 16 (end band) and 1 (center band) produced almost identical pressure-time curves. However, the pressure recorded at position 4 (center band) was roughly double that of position 17 (end band) throughout most of the positive phase. The shapes of the pressure-time curves for position 4 is similar to that of position 17. Although a re-examination of the gauge records offered no explanation for this difference, a calibration error appears likely.

Neither peak average pressure nor total positive-phase impulse on the top surface vary much between end and center gauges for the targets at which Mach-stem heights were larger than target height (shots Z-10R, 10RR, and 11R). For targets in the regular reflection region,

TABLE XIV

Summary of End-Effects Data

Shot	Zenith angle (deg)	Height of Mach-stem target height	p_2/p'_2	I_f/I'_f	p_4/p'_4	I_t/I'_t	p_b/p'_b	I_b/I'_b
1	0	0	0.94	0.90	0.94	0.97	0.85	1.02
2	0	0	--*	--*	1.12	0.96	0.89	0.96
3R	15	0	1.10	1.09	1.16	1.19	0.99	1.25
4	15	0	1.33	1.32	0.93**	0.78**	0.88	0.96
5	30	0	0.99	1.15†	0.87	0.94	1.19	1.18
6R	30	0	0.98	0.97	1.22	1.05	1.03	1.01
7R-	45	0	0.93	0.93	1.24	1.23	1.53	1.35
8	45	0	0.97	0.83	0.98	1.08	1.29	1.33
9	60	0.65	1.40	1.24	1.21	1.48	2.32*	0.97
9R	60	0.79	--*	--*	1.06	1.06	2.89	2.82
10R	67.5	1.6	1.05	1.23	1.01	1.19	0.91	1.47
10RR	67.5	1.6	1.03	1.03	1.07	1.00	1.42	1.29
11R	75	710	1.01	0.94	1.09	0.96	1.47	1.30

*One of two gauges on front-surface end band failed

**One centerline top-surface gauge appears erratic

†The only significant difference between end and center average pressure-time plate occurs near the end positive phase.

however, the ratios of p_4/p'_4 and I_t/I'_t vary considerably from unity, but no trend is apparent in the variations.

On shots Z-9 and Z-9R, where the Mach stem existed but was not as high as the target, higher pressures were experienced on the center than the ends, but not to the same degree for the two shots. Although I_t/I'_t for shot Z-9 equaled 1.48, much of the higher pressure on the center occurred near the end of the positive phase. Ten milliseconds after the blast wave appeared at the top surface, the ratio of center impulse to end impulse was only 1.27.

Analysis of the ratios p_b/b'_b and I_b/I'_b for zenith angles of 30 degrees and less indicates that the average pressure-time pulses for the back-surface end and center bands are nearly identical for shots Z-1, Z-2, Z-4, and Z-6. The average pulses for center and end back surface on shots Z-3 and Z-5 are identical only to the approximate time of occurrence of P_b For the targets with a zenith angle of 45 degrees and for all targets in the low Mach-stem or high Mach-stem regions, the shape of the average pressure-time curves on the end band is significantly different from those at the center of the target. Figures 36 through 40 compare the back-surface average pressure-time relationship for the end and center gauge bands of targets at 45 degrees and beyond.

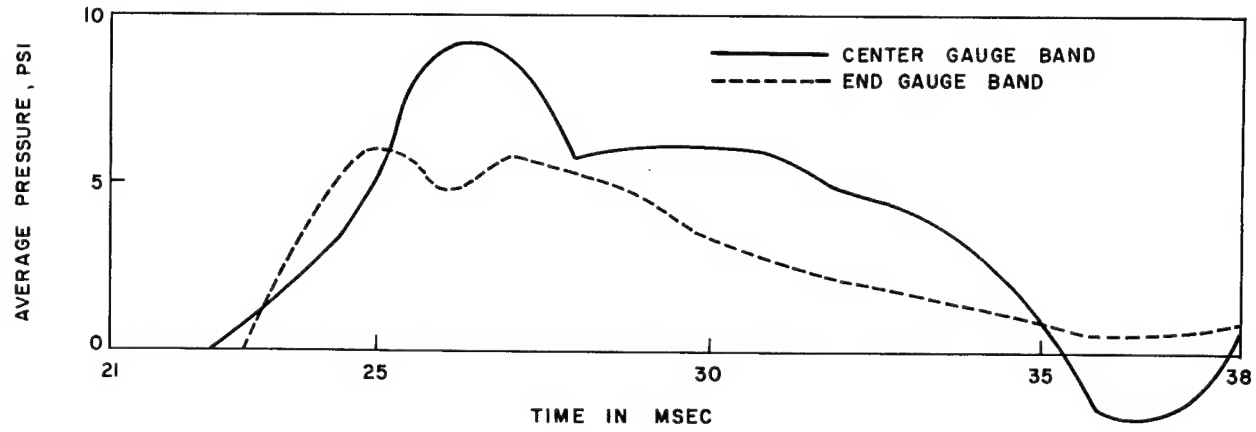

Figure 36. Comparison of back-surface average pressure-time relationships for end and center gauge bands on shot Z-7, α = 45 degrees

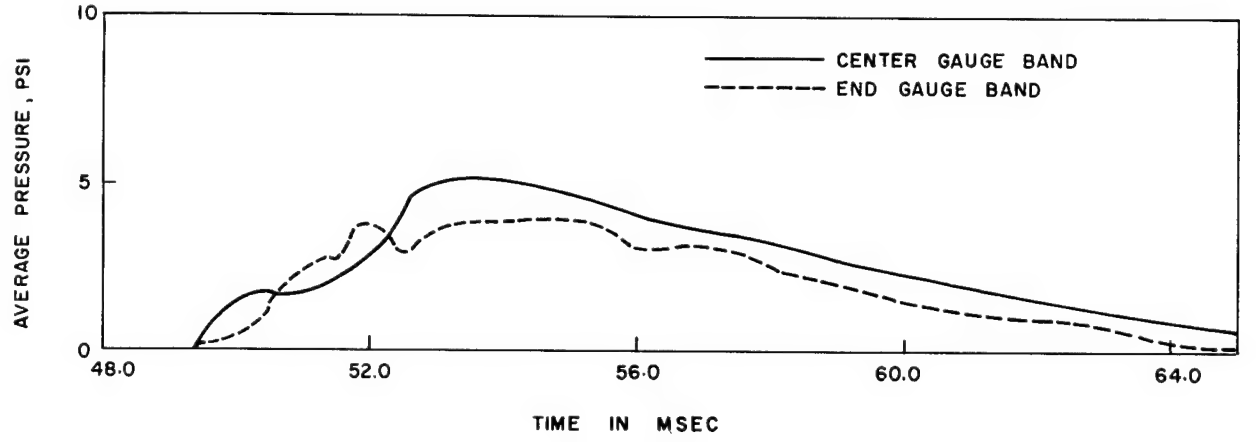

Figure 37. Comparison of back-surface average pressure-time relationships for end and center gauge bands on shot Z-8, α = 45 degrees

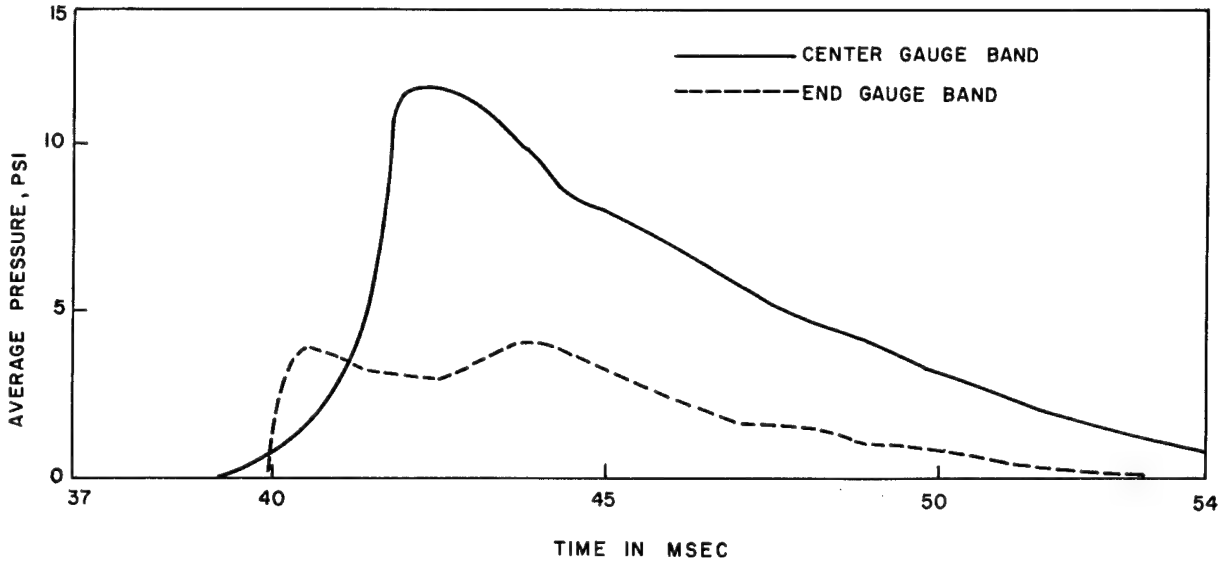

Figure 38. Comparison of back-surface average pressure-time relationships for end and center gauge bands on shot 9R, $h_m/h = 0.79$

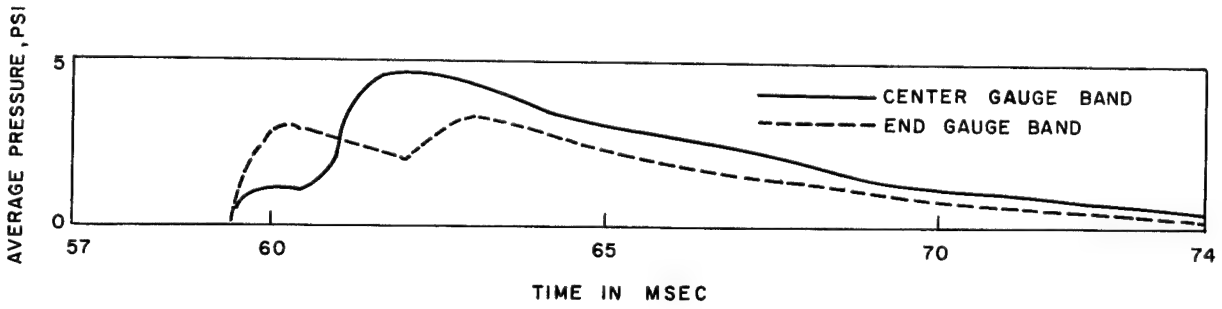

Figure 39. Comparison of back-surface average pressure-time relationships for end and center gauge bands on shot 10RR, $h_m/h = 1.6$

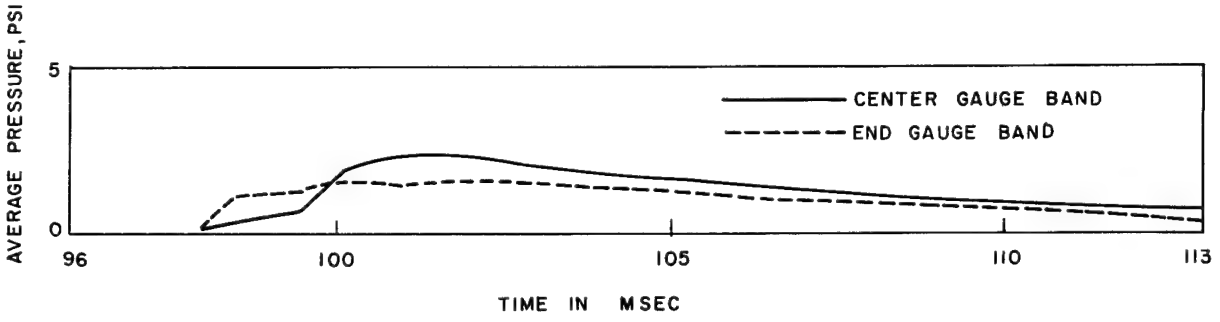

Figure 40. Comparison of back-surface average pressure-time relationships for end and center gauge bands on shot 11R, $h_m/h = 710$

CH VIII -- DISCUSSION

Regular Reflection Region

It has been previously mentioned that this experiment probably approaches the lower limits of practical interest, since scaling the targets to nuclear burst results in equivalence to a 7-story structure for a 20-kt weapon. However, the variation from theoretical considerations is probably well worth establishing at this lower limit. Further, the data presented are directly applicable for multistory structures over the range of conditions of the experiment, i.e., variable angles, pressures, Mach-stem heights and structure length.

The experiment was not sufficiently extensive in scope to determine at what values of t_1/t_+ the variation from theoretical prediction of front-surface loading becomes worthy of consideration, but results do indicate that for zenith angles greater than 30 degrees and for the lower values of shock strength used in this experiment, the variation from theory is not significant. However for angles less than 30 degrees, the difference between theory and experiment is significant for all values of shock strength tested, and this difference increases with increasing shock strength. The data for front-surface loading at a nominal zenith angle of 0 degree do not show the variation from theory to the extent that is apparent in the 15- and 30-degree data. This is reasonable, since 0 degree is perhaps the easiest condition to describe theoretically in the regular reflection region. However, the scatter of the data for a nominal angle of 0 degree with a height of burst of 38 feet is excessive; it resulted from the inability of the gauges to record the high pressures at ground zero for this lowest height of burst used. The average pressure-time curves presented in Appendix A employ the 38-foot height-of-burst data, since the maximum difference between extrapolated and recorded values occur here. Even these differences are not excessive except for the 0-degree zenith angle.

The data indicate (Figure 15) that the 4-foot target experiences lower front-surface pressure ratios (p_2/p_m) than the 18-foot target which is essentially two-dimensional, but this difference does not exceed 5 percent except for small angles. However, because diffraction about the ends does not permit a high front pressure, the lowness of the front-surface pressure ratio on the 2-foot target is clear throughout the regular reflection region.

The dispersion of data describing the shortening of the front-surface positive-pressure duration in the regular reflection region is comparable to that for the low Mach and high Mach regions. The relationship between t_f/t_+ or $\frac{t_f - t_1}{t_+}$ and Ut_+/h in this region is similar to that found by previous experimenters in the Mach region. Despite the dispersion, the data indicate that the shortening of the front-surface positive pressure is dependent also upon the zenith angle. The dispersion, however, prevents quantitative description of the amount of the effect.

Except for those targets at $\alpha = 45^o$, no serious variation from the predicted values of p_+ for the 18-foot target was found. At 45 degrees, however, the variation was 27.8 percent for the largest value of shock strength used.

Unlike the front surface, no difference between the top-surface pressure ratios for the 18- and 4-foot targets was noted. The 2-foot target experienced p_4/p values significantly less than those for the 18-foot targets. The observation concerning the scatter of the front-surface data at $\alpha = 0^o$ is also applicable for the top surface. Indeed, the value of P_4/p should be 1.00 for this condition if one disregards the decay in shock strength through a distance equal to the structure height.

Examination of the average pressure pulse for the back surface indicate that the maximum average pressure on this surface is extremely dependent on target length especially for larger zenith angles. The data for $\alpha = 0$ on the rear surface suffers from the gauge-response difficulty mentioned previously for front and top surfaces. Shot Z-21 appears to be anomalous for the rear surface mentioned above. Although the data for the 2- and 4-foot targets are not as consistent as desirable, there is still enough consistency to infer large variations from the 18-foot or two-dimensional target. The slow response of the gauges probably introduces little serious error on the rear-surface measurements, except for small angles, since the rise time of the average pressure on the rear surface is fairly long.

Although the time of maximum average pressure on the rear face of the 18-foot targets is in good agreement with theoretical predictions, Figures 25 through 28 indicate that this time, t_b, is also extremely dependent on target length.

Low Mach-Stem Region

In this experiment four targets were located so that the height of the Mach stem was less than the target heights. When the height of the Mach stem was about 0.4 times the target height, the observed p_2 was about three-fourths of that which would be expected if the peak overpressure were normally reflected. No significant effect of target length was apparent for these targets. Similarly, the value of p_4/p varied only from 0.65 to 0.70, despite

the fact that all three target lengths were represented in this group. The average pressure on the rear surface is of course dependent upon target length. The 2- and 4-foot targets have nearly similar p_b/p_m values, but these are 50 percent higher than those for the 18-foot target.

In those cases where the Mach-stem height exceeded the height of the target, the Mach stem height was determined from the data presented in Chapter III. From those data, the Mach-stem height is known only to about $\pm$0.5 foot. In the region where the Mach stem as determined from Chapter III was employed, no real discrepancy is apparent in p_2/p_r where the stem height greatly exceeded the target height, despite different target lengths. There are minor variations in p_2/p_r, but these are more probably a function of the variation in Mach-stem height (a range from about 0.6 to 1.6 feet higher than the target). The values of p_4/p_m illustrate the transition between where the stem is lower than the target height and where the stem is much higher than the target height; i.e., from about 0.7 p_m to nearly 1.0 p_m respectively.

Impulse

An examination of the net translational impulse should summarize the extent of the zenith angle on the blast loading of a structure. Figure 41 shows the variations of the net translational total impulse ($I_f - I_b$) versus apparent zenith angle for targets of each length. Because of differences in overpressure due to differences in heights of burst for random pressure variations, the plot has been normalized by dividing by the total incident impulse which was an average of the impulses of the three incident pressure gauges. The net translational impulse for a variety of structure lengths and zenith angles can thus be interpolated from the figure.

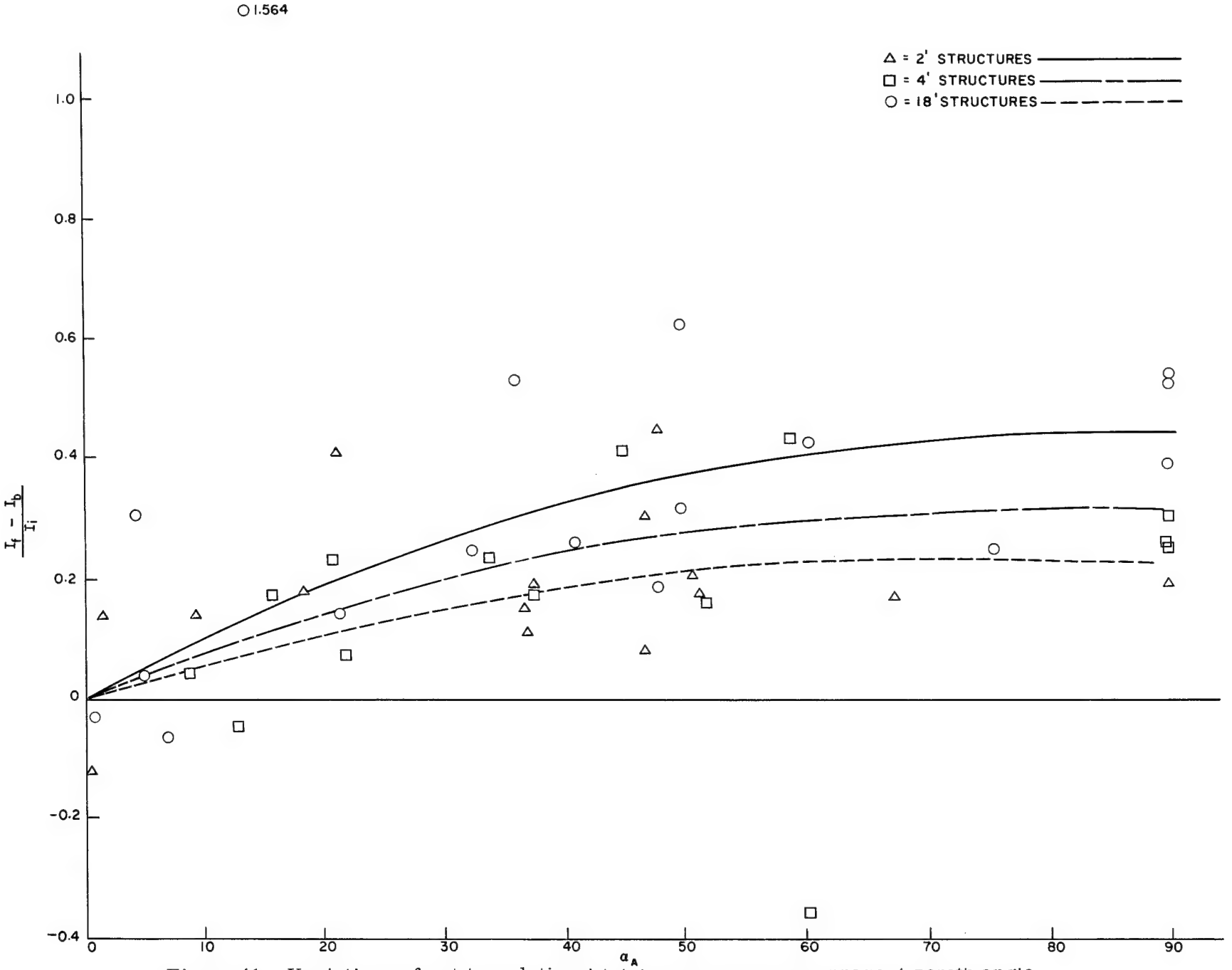

Figure 41. Variations of net translational total impulse versus apparent zenith angle

CH IX -- CONCLUSIONS AND RECOMMENDATIONS

The data presented herein indicate, within the scope of the parameters investigated, in what ranges of zenith angle and shock strength deviations from theoretical prediction are significant for the front and top pressure ratios. Further, these data are applicable to multi-story structures over a wide range of conditions. Specifically it may be concluded that:

1. Front-surface peak average pressures predicted from theory may be overestimated by nearly 50 percent for small angle and strong shocks. However, the variation between theory and these data decreases with increasing angles and/or decreasing shock strengths. This variation is insignificant for the larger zenith angles and weaker shocks.

2. Top-surface peak average pressures as measured do not significantly vary from predictions except for strong shocks and/or large zenith angles.

3. Predicted times for the occurrence of maximum average pressure on the rear face are in good agreement with measured times on the two-dimensional targets, but both this time and the peak average pressure are dependent upon target length for three-dimensional targets.

4. Shortening of the positive-phase duration on the front face in the regular reflection region occurs in a manner similar to the shortening observed in the Mach reflection region. This shortening is dependent upon zenith angle and the ratio Ut_+/h.

5. Peak average pressure on the front surface in the region where the Mach-stem height is more than about 0.41 times the target height is essentially independent of target length. However, peak average pressure on the top surface remains a function of Mach-stem height, at least up to Mach-stem height 1.6 times the target heights.

It is recommended that no continuation of this work be considered unless time resolution and gauge response is adequate to provide scaling to a 1-story structure subjected to blast from a 300-kt weapon. While larger yields are probable, it is unlikely they will have heights of burst sufficient to make zenith angle a significant variable.

LIST OF REFERENCES

1. The U.S. Strategic Bombing Survey, The Effects of the Atomic Bomb on Hiroshima, Japan, 3 Volumes, May 1947.

2. Ad Hoc Analytical Services, Phase Report No. III, Task VI: Study of Blast Effects in Regular Reflection Region, Armour Research Foundation Repor+ ARF No. MO 44, 4 May 1954.

3. Weiderman, A. H., and Schiffman, T. H., Experimental Observations of Regular Reflection Loadings on Three Dimensional Blocks, Armour Research Foundation, ARF No. MO 69 (Final Test Report No. 6), January 4, 1956.

4. Tzantos, G. T., Schiffman, T. H., and Weiderman, A. H., Basic Loading on the M.I.T. Multi-Story Structures in the Regular Reflection Region, Armour Research Foundation, ARF No. MO 69 (Final Test Report No. 4) March 22, 1956.

5. Hudson, C. C., Duration Shortening of a Peaked Shock in Normal Reflection at a Rigid Wall, Sandia Corporation Technical Memorandum TM 174-53(51), November 3, 1958.

6. Shreve, J. D., Pressure-Distance-Height Study of 250-16 TNT Spheres, Operation TUMBLER WT-520, March 13, 1953.

7. Vortman, L. J., and Shreve, J. D., The Effect of Height of Explosion on Blast Parameters, Sandia Corporation SC-3858(TR), June 20, 1956.

8. Vulgan, E. J., The Wiancko Pressure Transducer (An Evaluation with Suggested Modifications) Sandia Corporation Technical Memorandum TM 11-56(51), November 8, 1955.

9. Hudson, C. C., Blast Diffraction End Effects I, Sandia Corporation AFSWP 461, August 24, 1954.

10. Bryant, E. J., Eherhard, R. A., and Kingery, C. H., Mach Reflection Over Hard-Dirt and Dry Sand, Ballistic Research Laboratories Report BRL-809, July 1952.

11. Curtis, W., Free Air Blast Measurements on Spherical Pentolite, Ballistic Research Laboratory, BRL MR No. 544, July 1951.

APPENDIX A

SAMPLE AVERAGE PRESSURE-TIME CURVES

Sample plots of the average pressure-time curves are shown in Figures A-1 through A-8. The plots were constructed by measuring the average pressure on a given surface from pressure profiles for each target surface at successive time intervals. The resulting plots give the average pressure acting on a surface as a function of time.

The curves presented in this appendix represent the 18-foot target at each zenith angle used. All plots are for height of burst of 38 feet. This height of burst was chosen because here the difference between recorded maximum pressure values and extrapolations is greatest and because all targets experiencing Mach reflection at larger zenith angles used the 38-foot height of burst. Thus Figures A-1 through A-8 show the average pressure-time relationships for each surface on the target and for the free-field overpressure for each value of zenith angle.

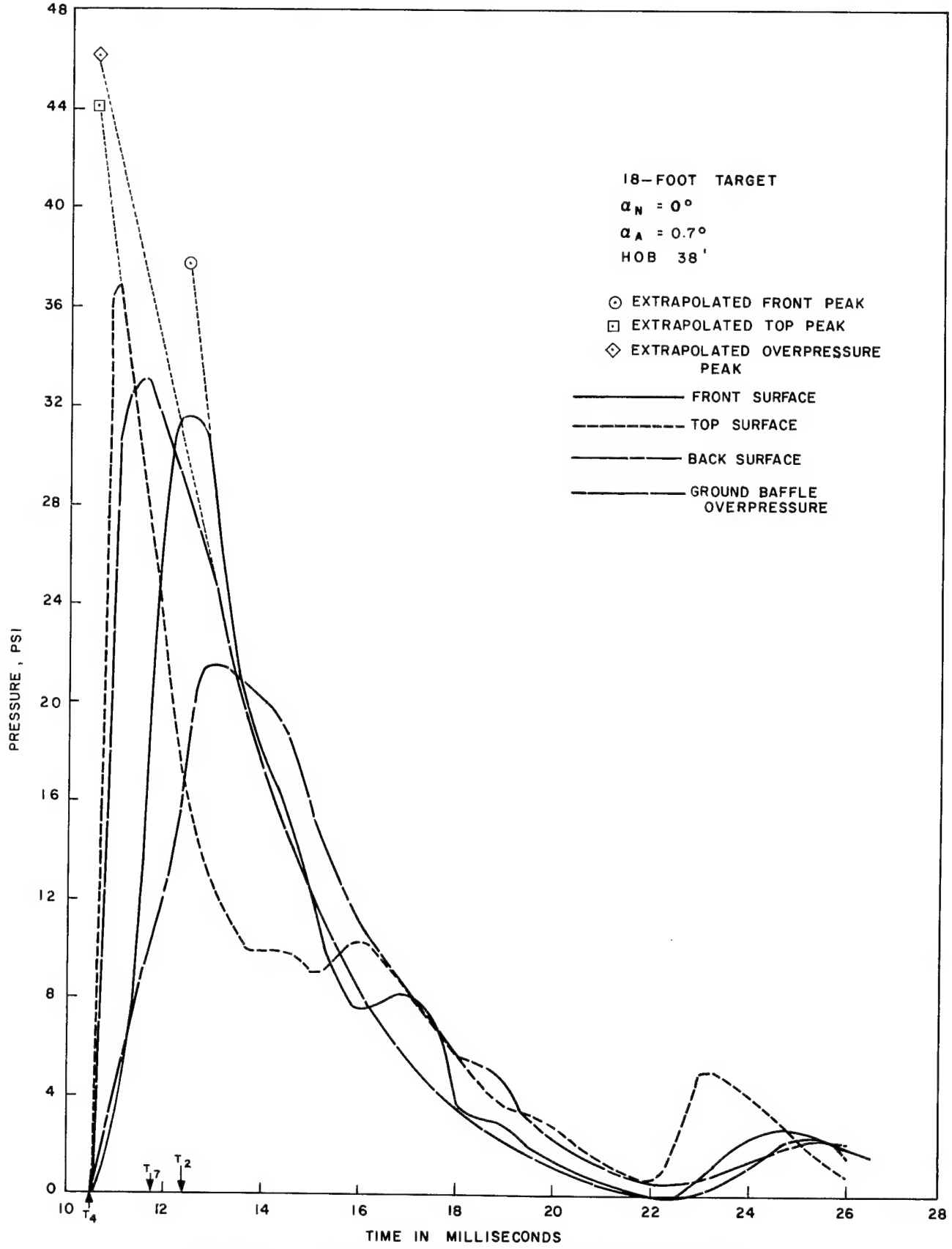

Figure A-1. Average pressure-time plot for shot Z-13

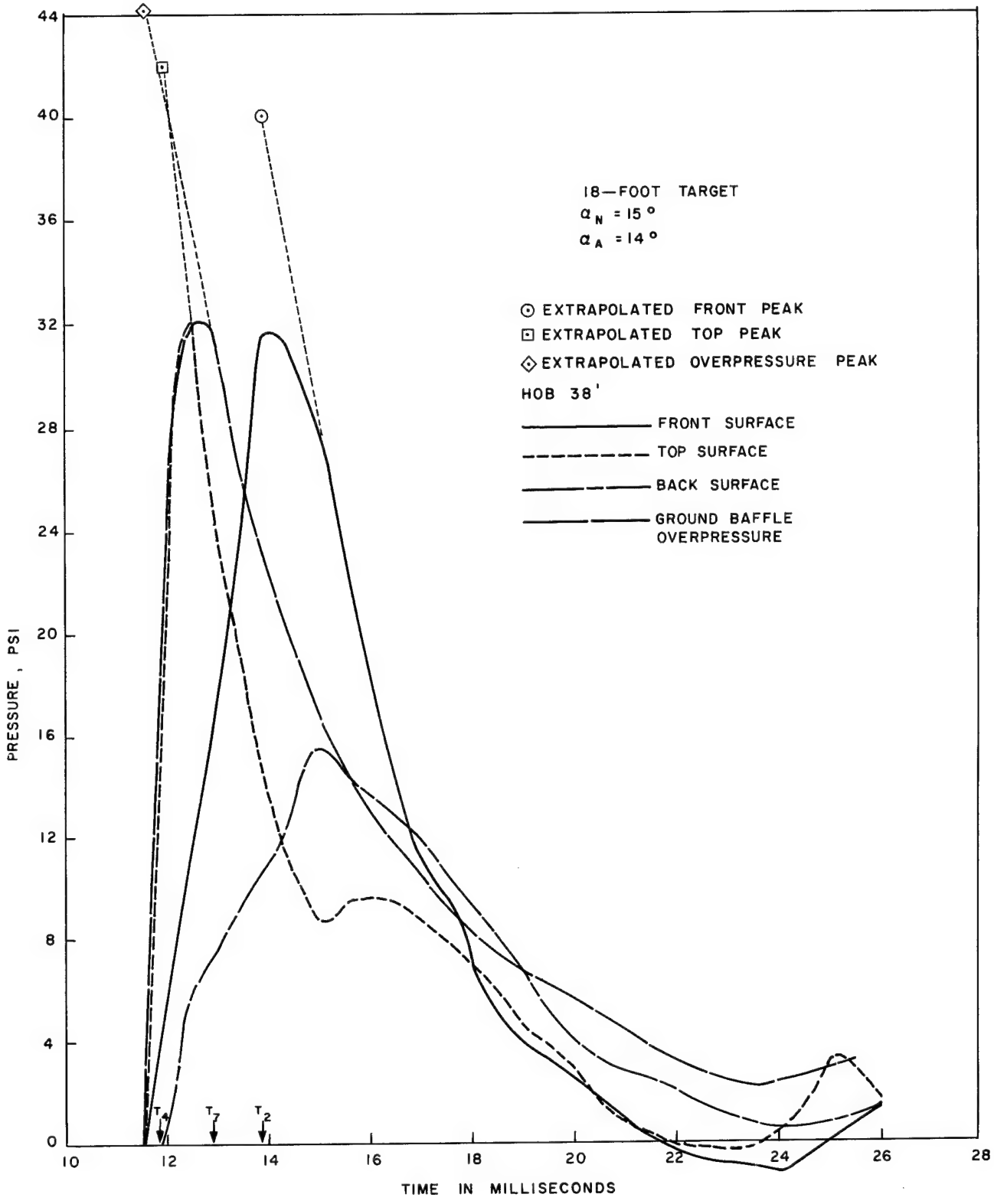

Figure A-2. Average pressure-time plot for shot Z-15

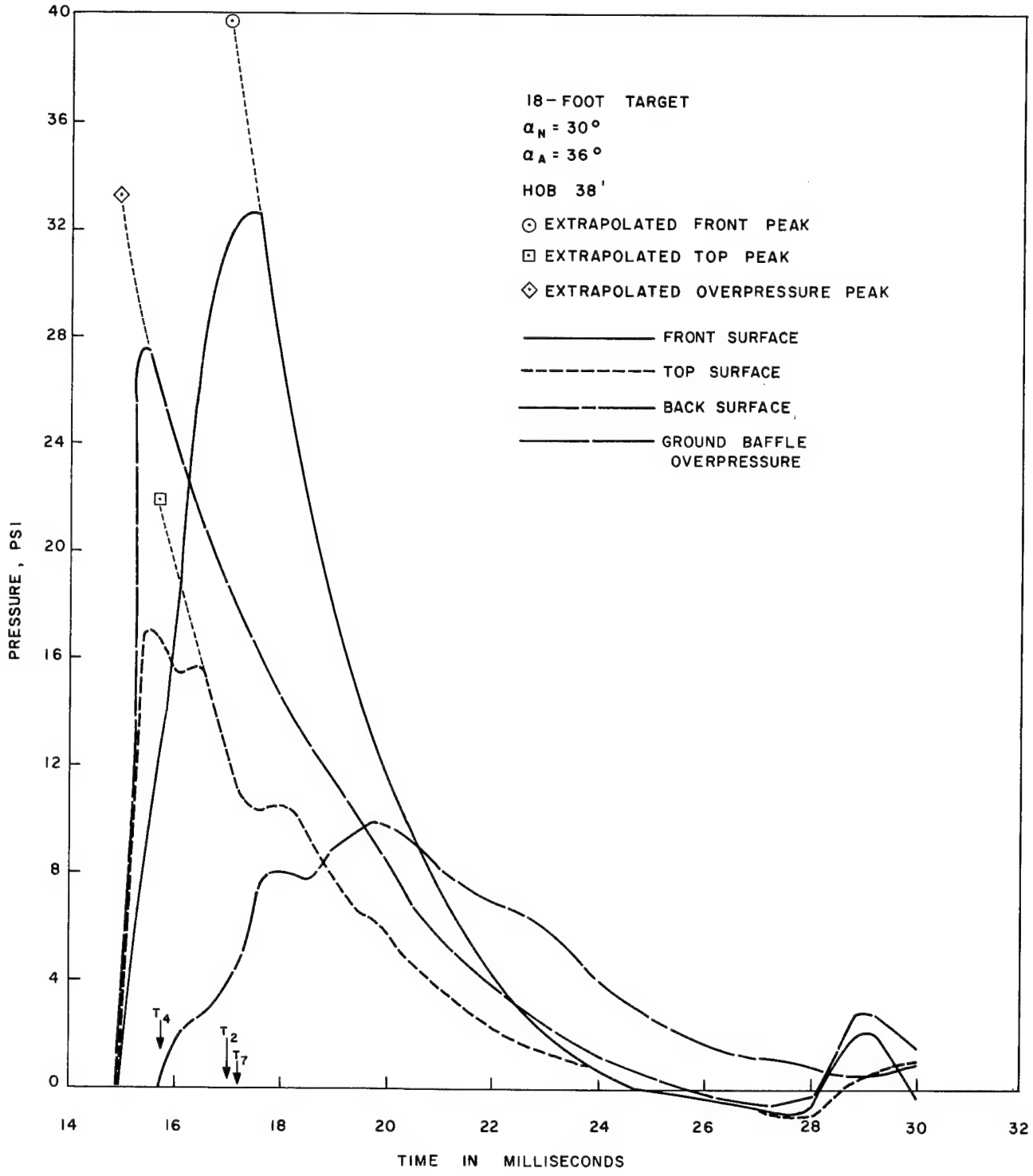

Figure A-3. Average pressure-time plot for shot Z-17

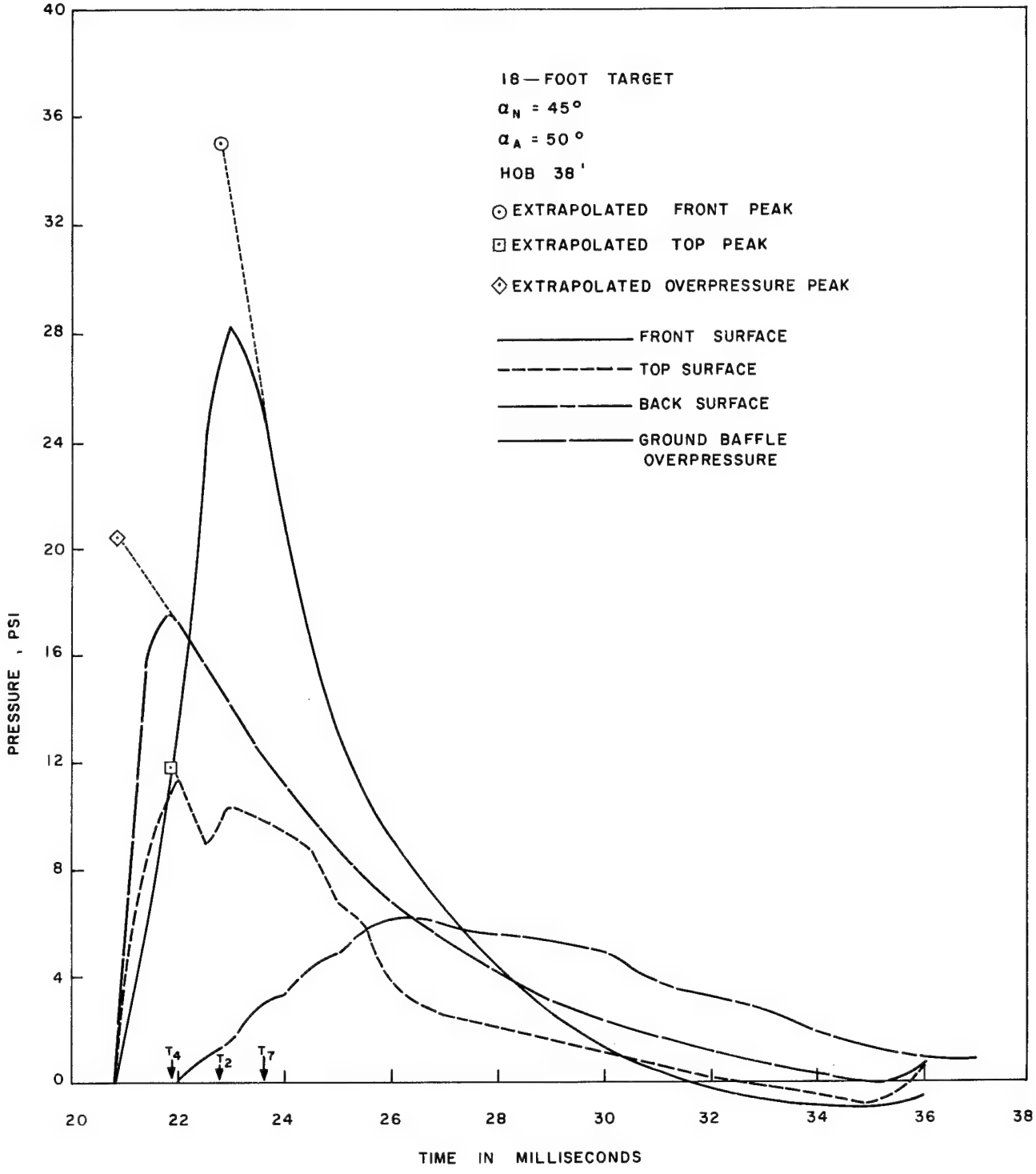

Figure A-4. Average pressure-time plot for shot Z-19

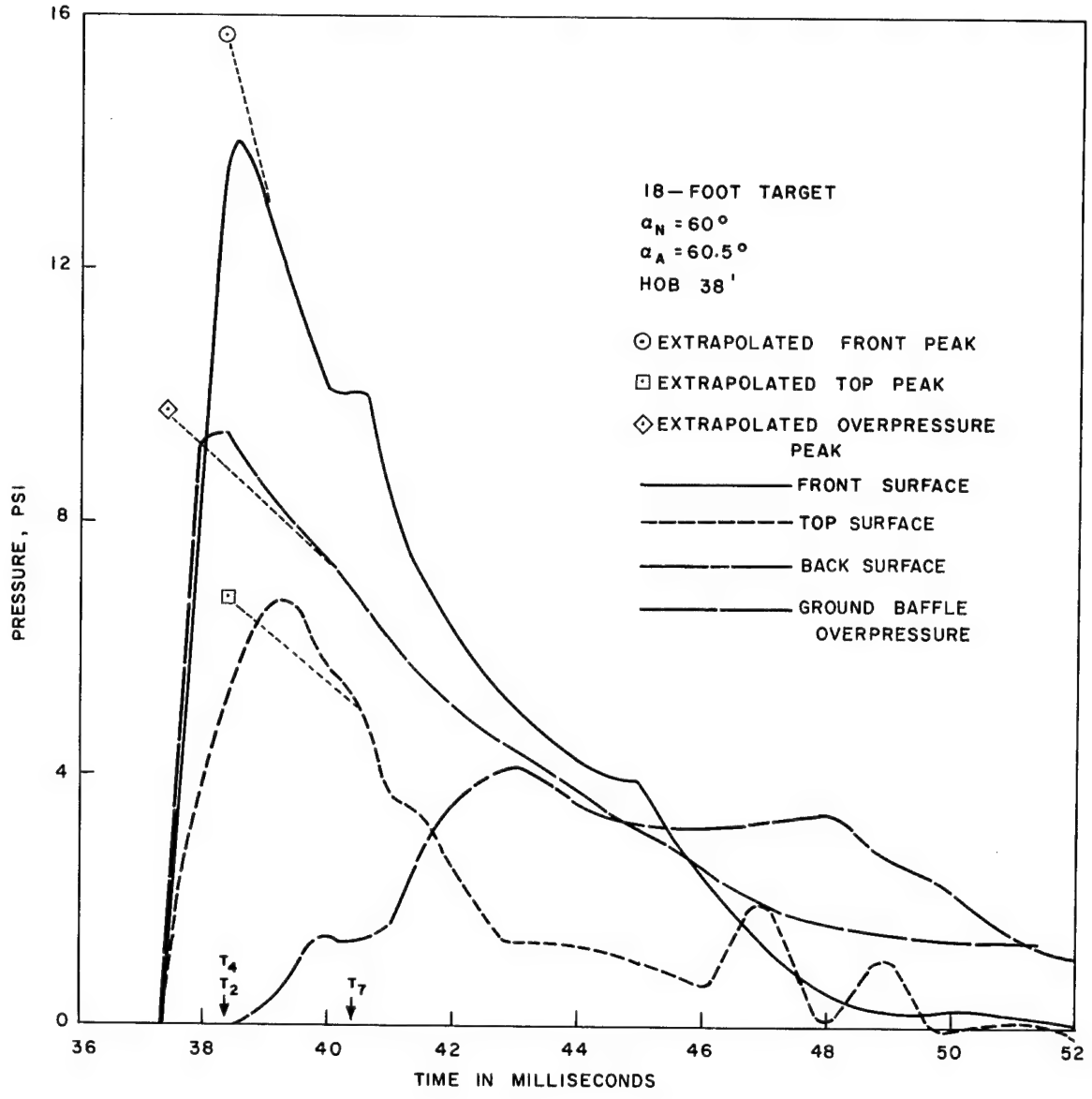

Figure A-5. Average pressure-time plot for shot Z-22

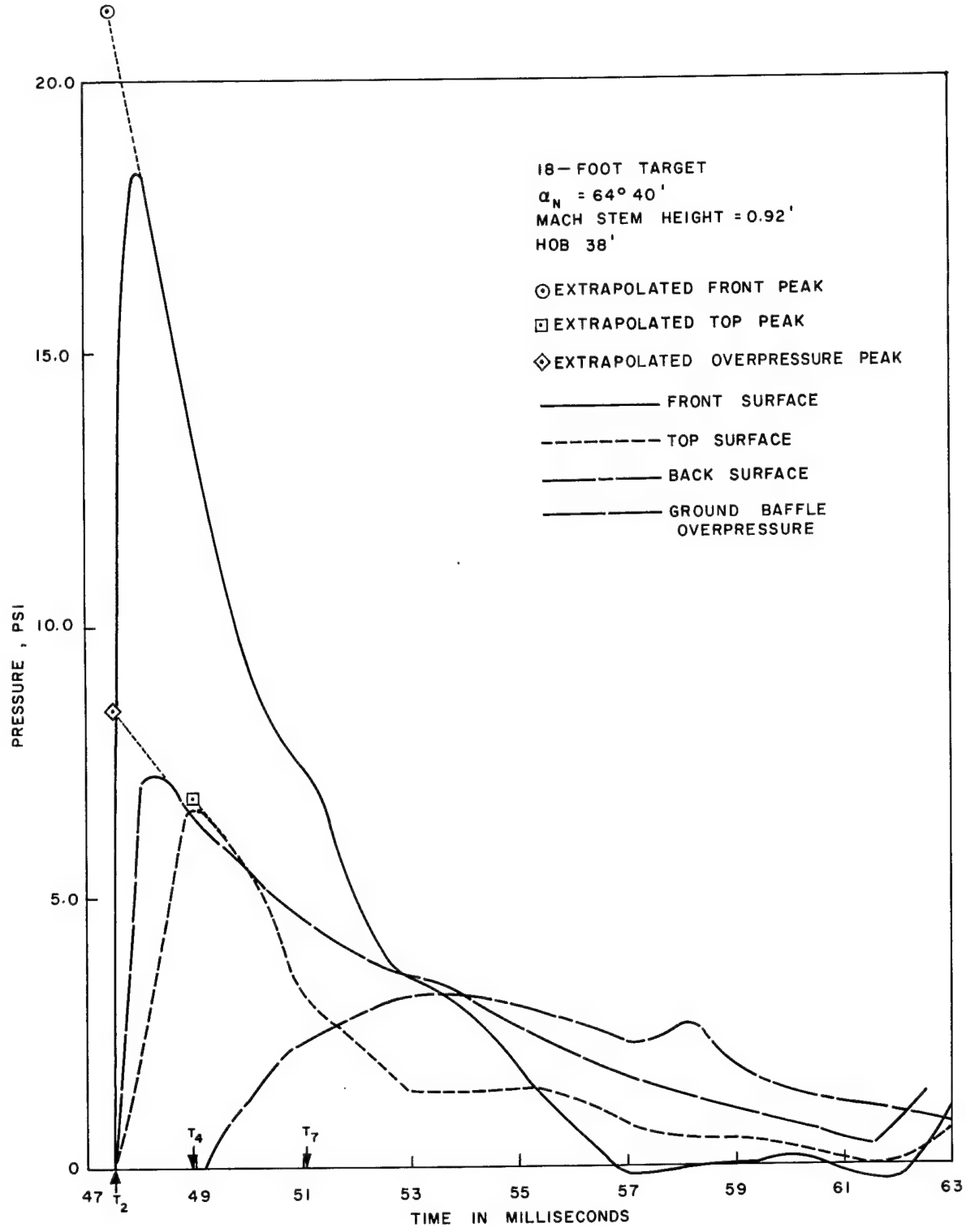

Figure A-6. Average pressure-time plot for shot Z-26

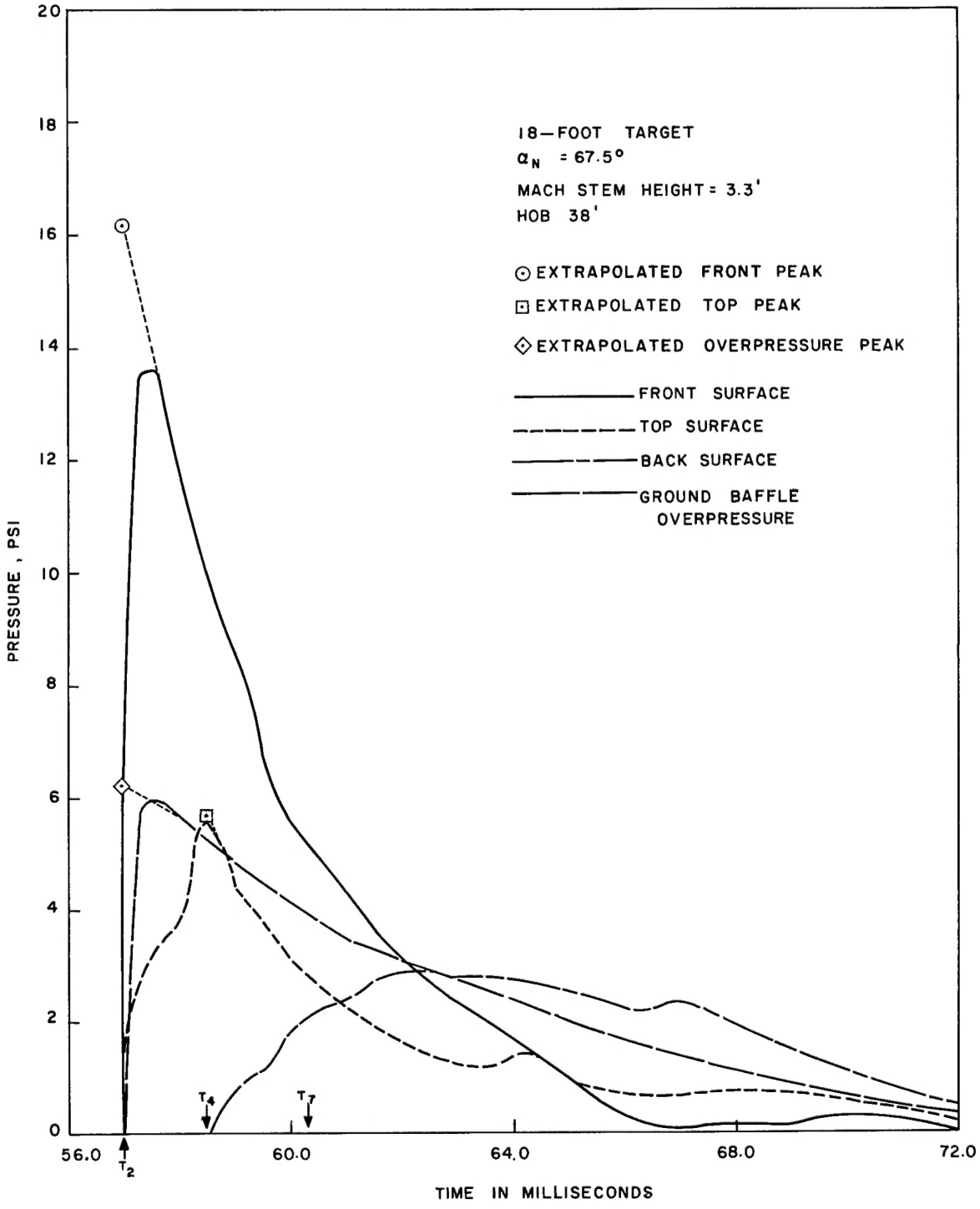

Figure A-7. Average pressure-time plot for shot Z-24

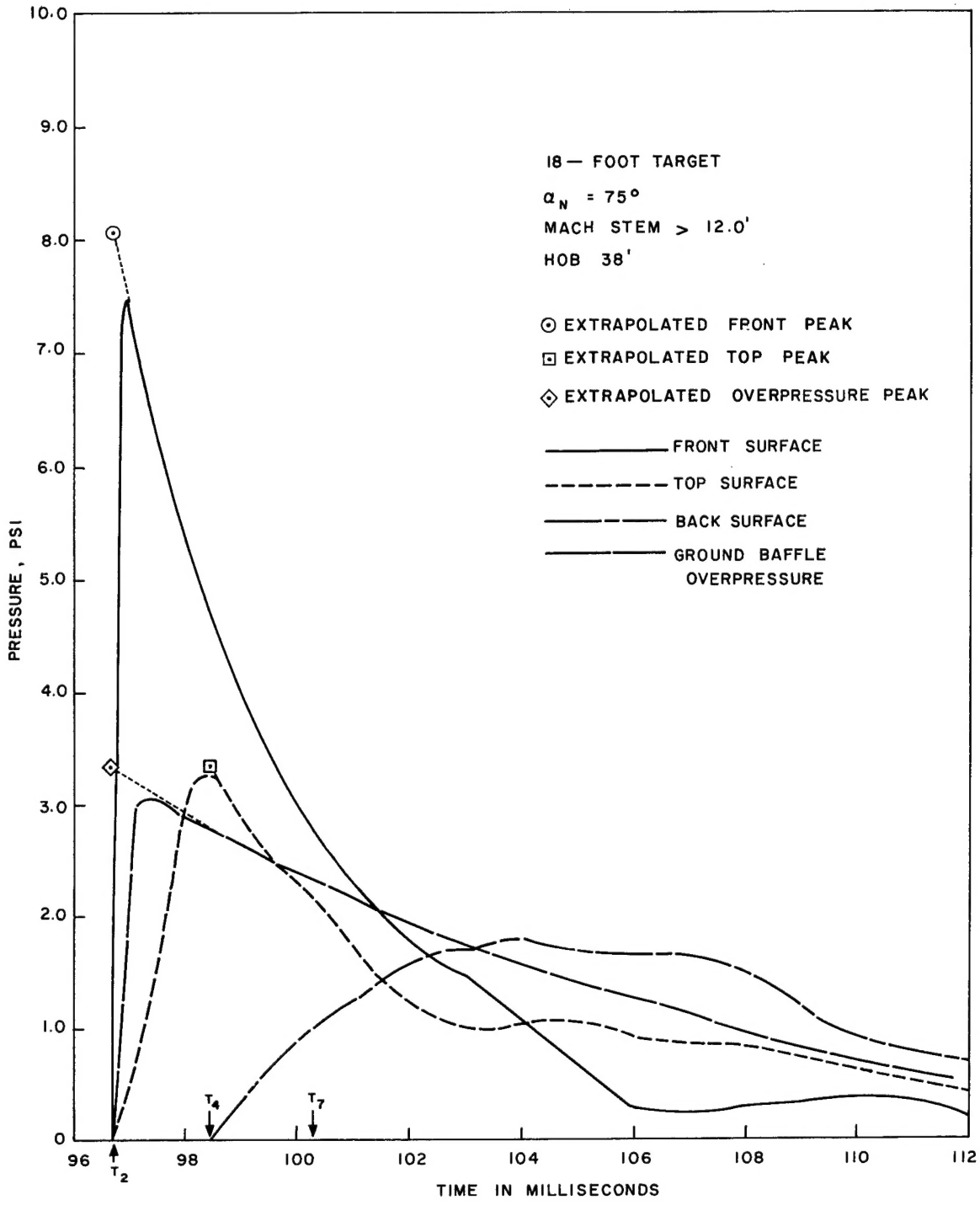

Figure A-8. Average pressure-time plot for shot Z-25

INITIAL DISTRIBUTION

Federal Civil Defense Adminstration, Washington, D. C. (25)
Director Civil Effects Test Group, Washington, D. C. (4)
Office of Technical Services, Washington 25, D. C. (75)
Chicago Midway Laboratories, Chicago, Illinois, Attn: Dr. Severin Raynor
Armour Research Foundation, Chicago, Illinois, Attn: Dr. S. J. Fraenkel
American Machine & Foundry Co., Chicago, Illinois
Dr. F. T. Mavis, Dean, College of Engineering, University of Maryland, College Park, Maryland
Dr. Elio D'Appolonia, Pittsburgh, Pennsylvania
Dr. Thomas E. Stelson, Head, Dept. of Civil Engineering, Carnegie Institute of Technology, Pittsburgh, Pennsylvania
U. S. N. Ordnance Laboratory, White Oak, Silver Spring, Maryland
Attn: Mr. G. K. Hartmann
Stanford Institute of Technology, Menlo Park, California, Attn: Mr. R. B. Vaile
Commanding General, Aberdeen Proving Ground, Aberdeen, Maryland, Attn: Director, Ballistics Research Laboratory
Los Alamos Scientific Laboratory, Los Alamos, New Mexico, Attn: Report Librarian (for Dr. A. C. Graves, J-Division)
Chief, Classified Technical Library, Technical Information Service, Washington, D. C.
Attn: Jean O'Leary (for Dr. Paul C. Fine)
Chief, Classified Technical Library, Technical Information Service, Washington, D. C.
Attn: Jean O'Leary
Chief, AFSWP, Washington, D. C. (110)
Forrestal Research Center Library, Aeronautical Sciences Building, Princeton University, Princeton, New Jersey, Attn: Maurice H. Smith, Librarian
(for Dr. Walker Bleankey)
K. F. Hertford, Manager, ALO
Massachusetts Institute of Technology, Cambridge, Massachusetts,
Attn: Dr. Robert J. Hansen
The University of Michigan, Ann Arbor, Michigan, Attn: Dr. B. Johnston
The University of Illinois, Urbana, Illinois, Attn: Dr. N. M. Newmark
Manager, ALO, USAEC, Albuquerque, New Mexico (for Mr. S. B. Smith, Holmes & Narver, Inc.)
R. L. Corsbie, DBM
R. L. Corsbie, DBM (for H. L. Bowman)
Brig. Gen. A. D. Starbird, AEC/DMA
J. E. Reeves, ALOTO
G. W. Johnson, LRL
G. Pelsor, LRL
J. P. Molnar, 1
R. W. Henderson, 1000
T. F. Lonz, 4561-1 (20)
W. F. Carstens, 4723
G. A. Fowler, 5000
C. F. Quate, 5100 (2)
M. L. Merritt, 5110
T. B. Cook, 5111
J. D. Shreve, 5112 (6)
L. J. Vortman, 5112-1
C. D. Broyles, 5113
R. A. Bice, 5200
D. B. Shuster, 5230
R. E. Poole, 8000
R. E. Dewhurst, 8233

M-3679 (Ed. 22) AEC Category
EFFECTS OF ATOMIC WEAPONS

DISTRIBUTION

Bettis Plant (WAPD) (2)
Brookhaven National Laboratory
Chicago Operations Office
Combustion Engineering, Inc.
duPont Company, Aiken (2)
General Electric Company (ANPD)
General Electric Company, Richland
Holmes and Narver, Inc.
Knolls Atomic Power Laboratory
Lovelace Foundation
Mound Laboratory
National Lead Company of Ohio
Office of the Surgeon General
Phillips Petroleum Company (NRTS) (2)
Public Health Service
Reynolds Electrical and Engineering Company, Inc.
Union Carbide Nuclear Company (ORGDP) (2)
Union Carbide Nuclear Company (ORNL) (3)
UCLA Medical Research Laboratory
University of Rochester (2)
Technical Information Service Extension (25)